Durham University

Durham E-Theses

E.P.R. lineshapes in maser materials

Kirkby, C. J.

How to cite:

Kirkby, C. J. (1967) *E.P.R. lineshapes in maser materials*, Durham theses, Durham University. Available at Durham E-Theses Online: http://etheses.dur.ac.uk/8538/

Use policy

The full-text may be used and/or reproduced, and given to third parties in any format or medium, without prior permission or charge, for personal research or study, educational, or not-for-profit purposes provided that:

- a full bibliographic reference is made to the original source
- a link is made to the metadata record in Durham E-Theses
- the full-text is not changed in any way

The full-text must not be sold in any format or medium without the formal permission of the copyright holders.

Please consult the full Durham E-Theses policy for further details.

Academic Support Office, The Palatine Centre, Durham University, Stockton Road, Durham, DH1 3LE
e-mail: e-theses.admin@durham.ac.uk Tel: +44 0191 334 6107
http://etheses.dur.ac.uk

E.P.R. Lineshapes in Maser Materials

by

C.J. Kirkby, B.Sc. (Dunelm)

A thesis submitted in candidature for the degree of

Doctor of Philosophy

Faculty of Science
University of Durham

September, 1967

DURHAM UNIVERSITY SCIENCE 1968 LIBRARY

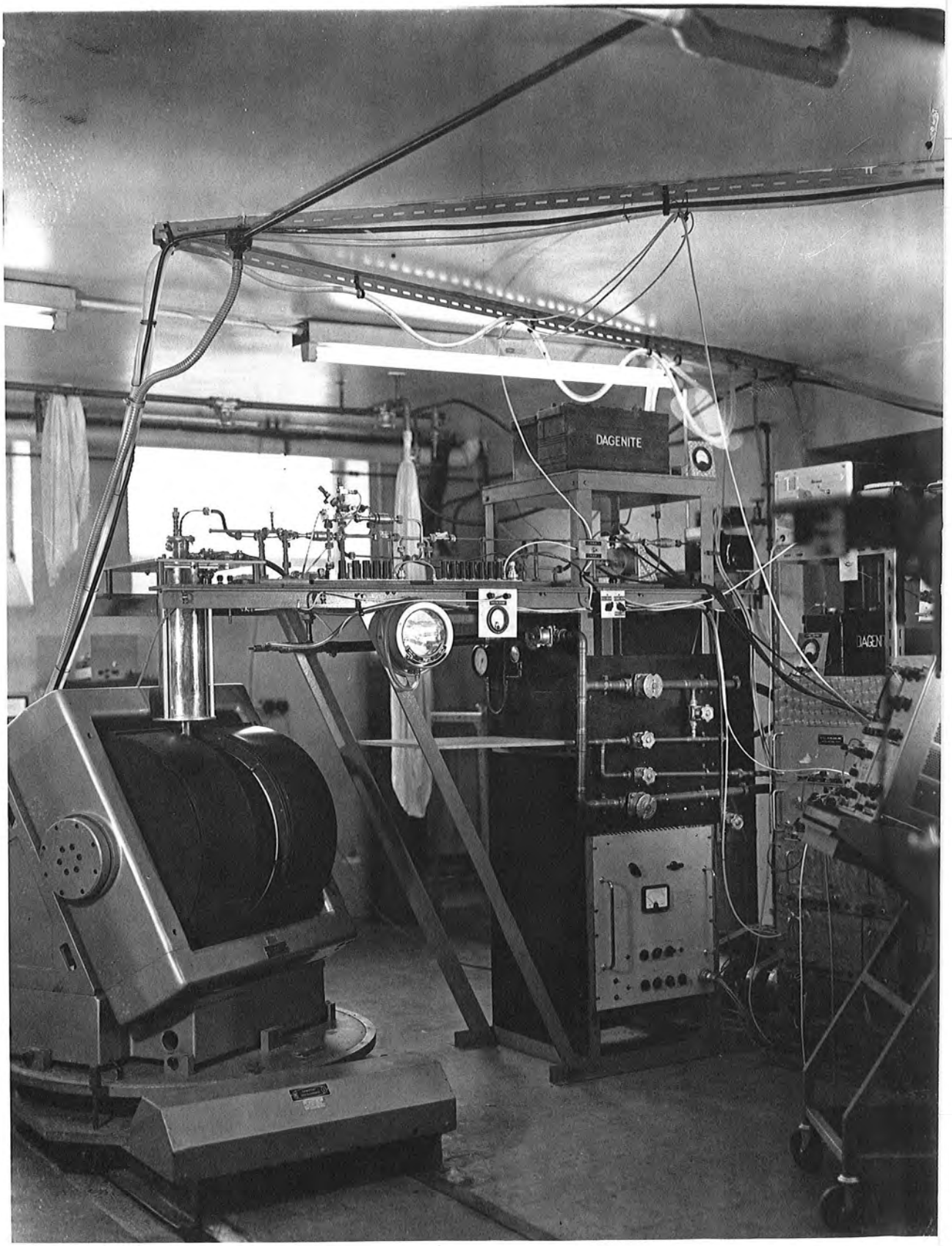
DAGENITE

ABSTRACT

Using a 35 Gc/sec spectrometer, E.P.R. linewidths have been measured in a number of synthetic ruby specimens grown by various means. In addition, measurements of both linewidth and relaxation time have been made on a number of specimens of calcium tungstate doped with neodymium.

Using a mathematical treatment of the second moment, the homogeneously broadened ruby line has been resolved into concentration-dependent and concentration-independent components. The observed constant nature of the former suggests that the effective concentration of paramagnetic centres is not indicative of the true chemical concentration.

Analysis of the inhomogeneous ruby line results in broadening components representative of axial misorientation and strain. A moderate correlation is obtained between misorientation figures derived from x-ray and e.p.r. measurements, and a similar correlation exists between strain and spin-lattice relaxation times. There appear to be no significant differences between the various types of flame-fusion material available.

Preliminary analysis suggests that the homogeneous line in calcium tungstate owes its width to processes similar to those occuring in ruby, but strain does not appear to be predominant

in the inhomogeneous broadening. Relaxation times in this material exhibit concentration and orientation dependence and a temperature dependence has been fitted empirically in the Direct and Raman regions.

ACKNOWLEDGEMENTS

I would like to express my thanks to the following organisations and individuals, without whose assistance the present work could not have been completed. For financial assistance I am indebted to the Admiralty C.V.D. and the Science Research Council (formerly D.S.I.R.), and to the Thermal Syndicate Ltd. of Wallsend for their constant co-operation in supplying ruby specimens. For their never-failing help and encouragement, I would like to thank Professor D.A. Wright, my supervisor Dr. J.S. Thorp, Drs. L. Clark and D.A. Curtis and all members of the staff of the Department of Applied Physics, in particular Mrs. R.A. Morant who brought the "variance" technique to my notice. Thanks are also due to the research students within the Department, in particular G. Brown and Dr. D.R. Mason, for ideas, advice and many helpful discussions, and to the technical staff led by Mr. F. Spence, for ably converting ideas into "hardware". For the typing and duplication of this thesis I am indebted to Mrs. J. Nichols and Mr. G. Brown.

C. J. Kirkby

CONTENTS

Abstract			(i)
Acknowledgments			(iii)
Contents			(iv)
Chapter 1		Introduction	
	1.1	The Solid State Maser	1
	1.2	Paramagnetic Energy Levels and the Spin-Hamiltonian	2
	1.3	Electron Paramagnetic Resonance	6
	1.4	Absorption Lineshapes	8
	1.5	Factors Affecting Choice of a Maser Material	11
	1.6	Practical Maser Materials	14
	1.7	The Present Work	17
Chapter 2		The Crystalline Properties of Synthetic Ruby	
	2.1	The Material	18
	2.2	X-Ray Investigation Techniques	26
	2.3	Ruby Misorientation Results	36
	2.4	The Distribution of Chromium	42
	2.5	Conclusions	
Chapter 3		The Q-Band Spectrometer and Associated Techniques	
	3.1	The Spectrometer System	46
	3.2	Absorption Display and Measurement Techniques	54
	3.3	Cryogenic Techniques	60

Chapter 4	E.P.R. Linewidths in Ruby I Homogeneous Broadening	
4.1	Homogeneous Broadening Mechanisms	62
4.2	Theory of Homogeneously Broadened Lines	65
4.3	E.P.R. Linewidths in Ruby	70
4.4	Experimental Results in Ruby	74
Chapter 5	E.P.R. Linewidths in Ruby II Inhomogeneous Broadening	
5.1	Inhomogeneous Broadening Mechanisms	85
5.2	Experimental Linewidth Results	93
5.3	Analysis of Linewidth Results	96
5.4	Discussion of Ruby Results	100
5.5	Artificial Degradation of Crystal Quality	108
Chapter 6	E.P.R. Linewidths in Neodymium Scheelite	
6.1	Crystal Structure	110
6.2	Paramagnetic Resonance in Calcium Tungstate	113
6.3	Homogeneous Broadening	115
6.4	Inhomogeneous Broadening	119
6.5	Conclusion	123
Chapter 7	Spin-Lattice Relaxation Measurements	
7.1	Relaxation Processes	125
7.2	Experimental Results: I Ruby	128
7.3	Experimental Results: II Nd:$CaWO_4$	130
Appendix 1	Reprint of Paper Published in B.J.A.P.	135
Appendix 2	Ruby Line Broadening Components	141
Appendix 3	Ruby Eigenvectors at Q-Band	145
References		149

Chapter 1

INTRODUCTION

1.1 THE SOLID STATE MASER

The word "Maser" was first coined by Gordon, Zeiger and Townes (1954) as an acronym for "Microwave Amplification by the Stimulated Emission of Radiation". This term describes the action of a device first proposed by Weber(1953), who realised that the inversion of the populations of a system of quantum energy levels could provide a means of amplification of an r.f. signal. The basis of such a device was the phenomenon of stimulated emission, postulated many years previously by Einstein (1917). By considering a quantum system as a harmonic oscillator, Einstein showed that incident radiation of the appropriate frequency could stimulate downwards as well as upwards transitions, with equal probabilities, and that the energy transfer would be in phase with the incident wave. Whether nett power was absorbed or emitted depended on whether the population of the lower level was greater or less than that of the upper level. In normal conditions of thermal equilibrium the former situation always obtains. Weber's system demanded a means of inverting the population from the thermal equilibrium condition, and the maser of Gordon et al. achieved this by physical separation of ammonia molecules in

different energy states, operating at a frequency of 23.87 Gc/sec.

An alternative scheme for obtaining inversion was proposed by Basov and Prokhorov (1955) involving the use of a three-level system and an additional source of r.f. power. This idea was derived independently by Bloembergen (1956) who extended the principle in his proposal for a continuously operating three-level maser utilising the paramagnetic energy levels in a solid. Figure 1.1 is a representation of such a system, incorporating some notation to be used subsequently. The first operating maser of the Bloembergen type was built by Scovil, Feher and Seidel (1957) and as a result of research it was found that Bloembergen's proposal was correct in detail. The first proposal for obtaining maser action in the optical region was made by Schawlow and Townes (1958) and stimulated emission in this region was first achieved by Maiman (1960).

1.2 PARAMAGNETIC ENERGY LEVELS AND THE SPIN-HAMILTONIAN

Bloembergen's proposal for a maser involved the use of the paramagnetic energy levels occuring in certain crystalline solids. Paramagnetism arises in certain ions, notably many members of the various transition groups, which posess unpaired electrons giving rise to magnetic dipole moments. The total angular

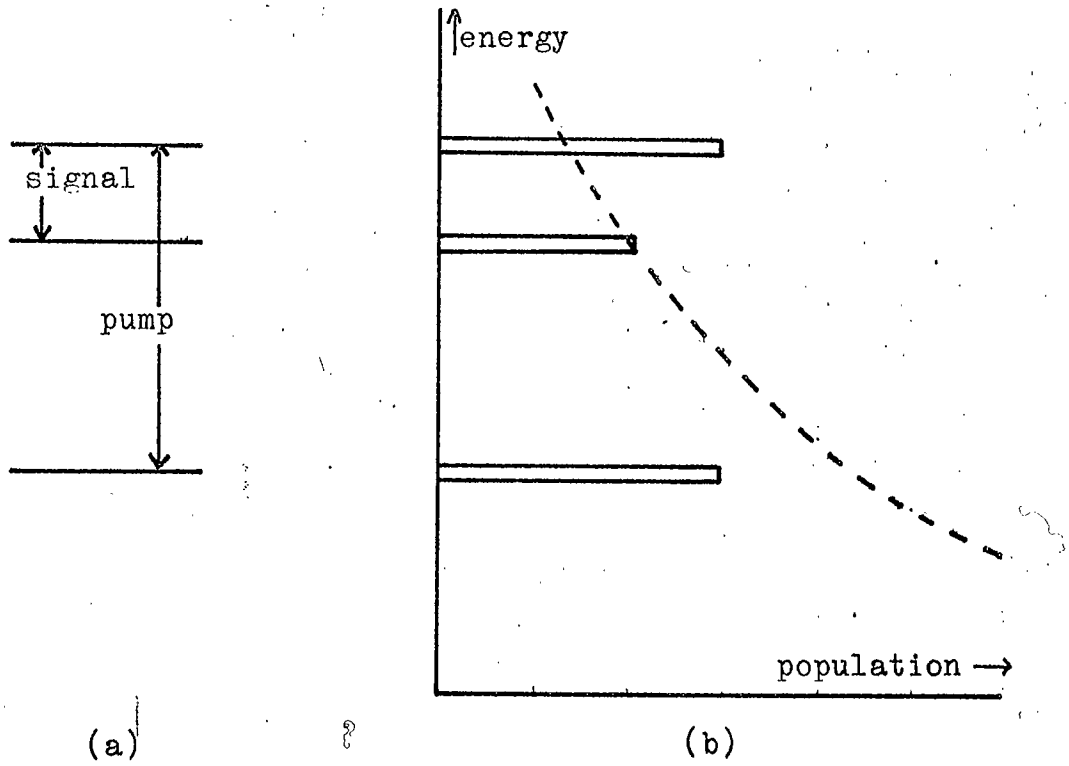

Figure 1.1
Three-Level Maser System

(a) Pump and Signal Frequencies
(b) Populations on Saturation of Pump Transition

momentum, J, results from the vector addition of the spin and orbital angular momenta, S and L respectively, and one result of quantum theory is that the ground state of a free ion posessing momentum J has a degeneracy of (2J + 1) in the absence of any applied field.

A paramagnetic ion situated in a crystalline environment is subjected to strong electric fields. As a result, some of the ground state degeneracy may be lifted, subject to the condition of Kramers' theorem (Kramers', 1930) that in the case of an ion posessing an odd number of electrons every level must retain even degeneracy. In many cases it is found that the paramagnetic energy levels are related to the spin of the free ion rather than to its total momentum. This is due to the breaking of the coupling between L and S by the crystal field. The energy levels are degenerate in S, and among elements of the iron group it is usually found that only the ground state levels are populated in normal conditions. The effects of orbital angular momentum are thereby effectively removed from the region of observation, this being known as quenching.

A concept commonly used is that of "effective spin", S', obtained by setting the number of energy levels observed in

the ground state equal to (2S + 1). When orbital motion is completely quenched then S' is equal to S, the true spin of the ion, and in the presence of a magnetic field alone the Zeeman splitting of the levels would be given by the relation:

$$E_m = Mg\beta H \qquad (1.1)$$

where β is the Bohr Magneton, i.e. the unit of magnetic moment, M is a magnetic quantum number covering the range +S' to -S' and g is a numerical constant which in the case of free ion is equal to the Lande g-factor, but in a crystalline environment indicates the degree of quenching of the orbital momentum.

The presence of crystal electric fields causes mixing of states, i.e. any particular energy level can no longer be described by a single quantum number. Thus in the case of an ion having an effective spin of 3/2 a particular energy state $|i\rangle$ must be represented by:

$$|i\rangle = a_i|+3/2\rangle + b_i|+1/2\rangle + c_i|-1/2\rangle + d_i|-3/2\rangle \qquad (1.2)$$

using the notation of Dirac (1947). The constants a_i etc., referred to as eigenvectors, obey the normalisation law:

$$|a_i|^2 + |b_i|^2 + |c_i|^2 + |d_i|^2 = 1 \qquad (1.3)$$

As the levels can no longer be represented by a unique value of

M it follows that the quantum selection rule, $\Delta M = 1$, breaks down, and under certain conditions the so-called forbidden transitions may be observed.

The Spin-Hamiltonian (Abragam and Price, 1951) is a concept which provides a concise description of the ground state energy levels, and in quantum-mechanical terms is an operator, $\mathcal{H}_s$, satisfying the eigenvalue equation:

$$\mathcal{H}_s |n\rangle = E_n |n\rangle \qquad (1.4)$$

where E_n represents the eigenvalue, i.e. the energy of the state $|n\rangle$. The form of the Hamiltonian depends on the system under consideration, but in many cases encountered in microwave spectroscopy a convenient representation is:

$$\mathcal{H}_s = g\beta \underline{H}.\underline{S}' + D\left[S_z'^2 - S'(S'+1)\right] + E(S_x'^2 - S_y'^2) \qquad (1.5)$$

The first term simply represents the orientational energy of a particular spin S' in the applied magnetic field, H. The second term has axial symmetry, and as the effective spin vector has length $S'(S'+1)$ and axial component S_z' this term is proportional to the transverse component of S' and can be interpreted as an electric quadrupole interaction between the ion and the lattice. The third term represents an additional non-axial anisotropy and

can be regarded as being due to an electric moment of higher order. The constants D and E are related to the crystal-field splitting of the ground state, and in an axially symmetric system of $S' = 3/2$ E=0, and the zero-field splitting equals 2D. If the paramagnetic ions posess resultant nuclear magnetic moments additional terms must be included in the Spin-Hamiltonian to take account of this.

1.3 ELECTRON PARAMAGNETIC RESONANCE

To describe the dynamic behaviour of a system of interacting paramagnetic particles, Bloch (1946) proposed a set of phenomenological equations. These introduced the concepts of transverse and longitudinal relaxation times, T_2 and T_1 respectively, and described how the magnetisation of the system is perturbed from the thermal equilibrium state by the application of r.f. power. It is sufficient here to quote the equations without reference to their derivation and further to neglect the details of their solution. The rate of change of the magnetisation of the system is given by:

$$\begin{aligned} dM_x/dt &= -\gamma(M_y H_z - M_z H_y) - M_x/T_2 \\ dM_y/dt &= -\gamma(M_z H_x - M_x H_z) - M_y/T_2 \\ dM_z/dt &= -\gamma(M_x H_y - M_y H_x) - (M_z - M_o)/T_1 \end{aligned} \qquad (1.6)$$

where $\gamma = g\beta\mu_o/\hbar$, M_o is the equilibrium magnetisation and $\underline{H}$ is the applied magnetic field. By making appropriate substitutions (Siegman, 1964, p.186) it is possible to derive an expression for the dynamic susceptibility, χ, having the form:

$$\chi = \chi' + j\chi'' = -T_2 f_o \chi_o \left[\frac{-T_2 \Delta f}{1 + T_2^2 \Delta f^2} + j \frac{1}{1 + T_2^2 \Delta f^2} \right] \quad (1.7)$$

where χ_o is the static susceptibility, $f_o = \gamma H_o$ and $\Delta f = f - f_o$. χ is now a function of f, the frequency of the r.f. field. The components χ' and χ'' can be readily identified from Eq. 1.7. The expression for χ'' has the mathematical form commonly known as Lorentzian, having a width between halfpower points equal to $2T_2$. The r.f. power absorbed by the magnetic system can be shown to be (Siegman, p.30):

$$P = -f\mu_o \chi'' H^2 \quad (1.8)$$

in which the imaginary component of the susceptibility gives the power absorption a frequency dependence. The real part, χ', represents a reactive effect causing a shift in frequency while χ'' causes a change in the Q-factor of the system.

The real and imaginary components of the complex susceptibility are related by the Kramers-Kronig relations (Kronig, 1936) which are specialised examples of transfer functions

occuring in network theory, and which can be written as:

$$\chi''(f) = -\frac{1}{\pi}\int_{-\infty}^{+\infty} \frac{\chi'(r)}{(r-f)}\,dr$$

$$\chi'(f) - \chi'(\infty) = \frac{1}{\pi}\int_{-\infty}^{+\infty} \frac{\chi''(r)}{(r-f)}\,dr \qquad (1.9)$$

Figure 1.2 shows the variation of χ' and χ'' with frequency. χ'' will be seen to show a pronounced peak in the region of $\Delta f = 0$. The strong power absorption at this point is the phenomenon of paramagnetic resonance.

1.4 ABSORPTION LINESHAPES

Two mathematical functions are commonly used to represent the shapes of spectral lines, namely the Lorentzian and the Gaussian. The Lorentzian (Lorentz, 1915) has been encountered already as a result of the solution of the Bloch equations, and this function is the response of any lightly damped system of interacting particles posessing an exponential relaxation mechanism. The Gaussian or Error function is widely used to represent the distribution of errors (Gauss, 1873) and, in this context, the effects of random processes, despite the fact that there are some doubts as to its universal validity.

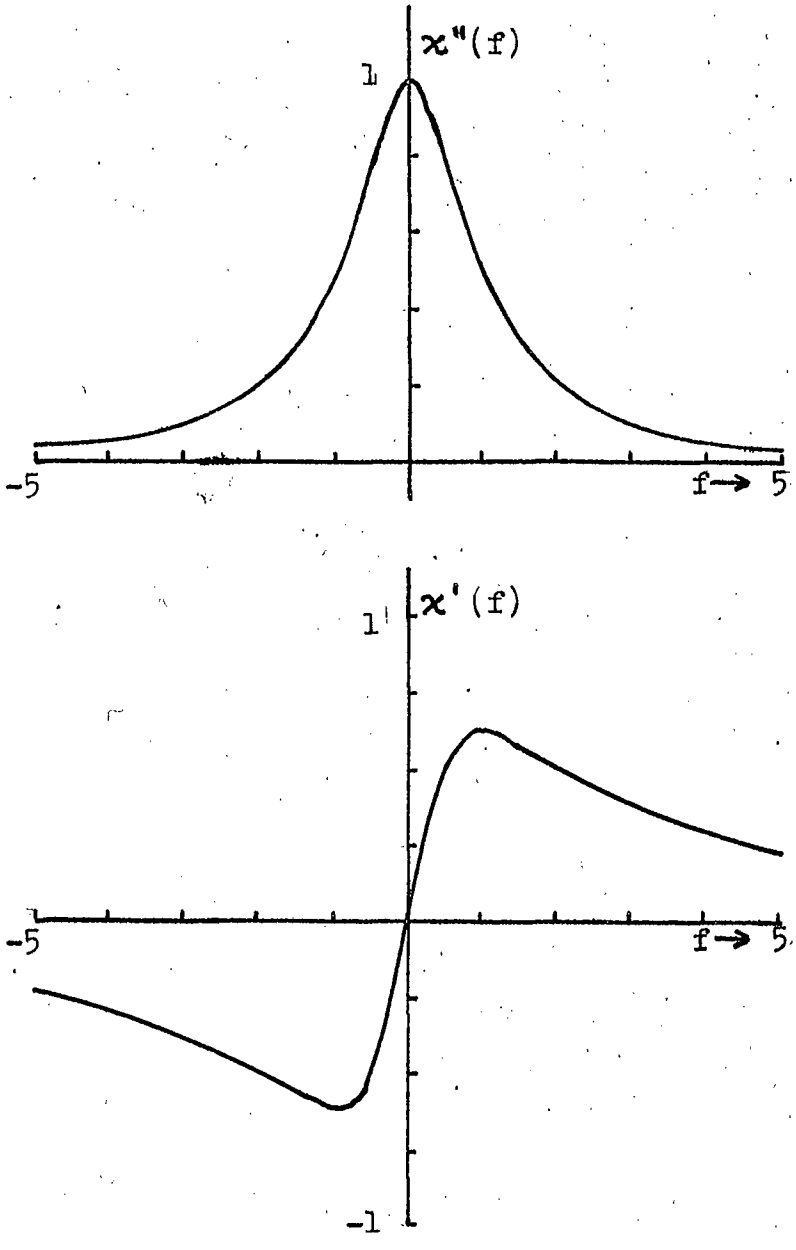

Figure 1.2
Normalised Real and Imaginary
Susceptibility as Functions of Frequency
(Frequency in arbitrary units)

The mathematical representations of these functions are:

$$\text{Lorentzian:} \quad L(x) = \frac{a}{\pi(a^2 + x^2)} \tag{1.10}$$

$$\text{Gaussian:} \quad G(x) = \frac{1}{b\sqrt{2\pi}} \exp(-x^2/2b^2) \tag{1.11}$$

where both functions are normalised to unit area. Figure 1.3 shows the functions L(x) and G(x). The differences in their forms is immediately apparent as the Lorentzian is sharper in the peak and has broader wings than does the Gaussian. With each absorption function there is a corresponding dispersive function connected by the Kramers-Kronig relations, Eq. 1.9. As the absorption component is the one commonly studied no further consideration of the dispersive functions will be made.

Two parameters commonly used to specify the width of an absorption line are the half-power width, $\Delta H_{\frac{1}{2}}$, and the width between points of inflection of the first derivative of the absorption, ΔH_{ms}. There has been a certain amount of confusion in the literature regarding the definition of $\Delta H_{\frac{1}{2}}$, as some workers use the term to represent the full width at half power while others use it for half of this value. In what follows $\Delta H_{\frac{1}{2}}$ refers to the full width, and both this and ΔH_{ms} are defined

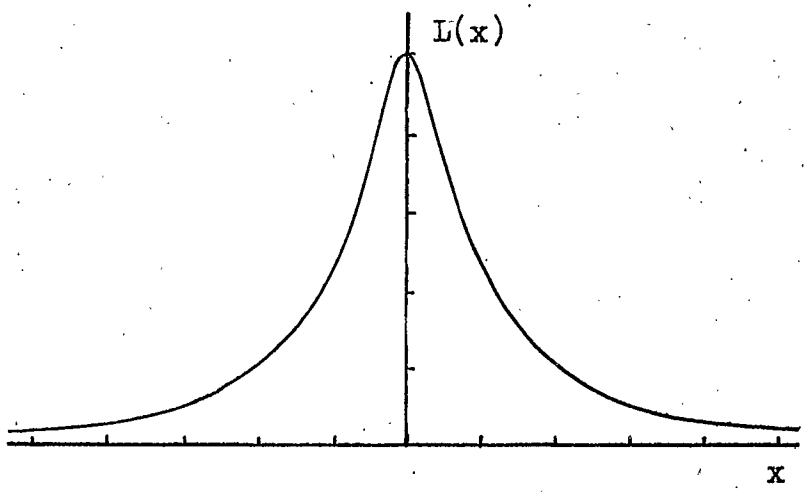

(a) Lorentzian

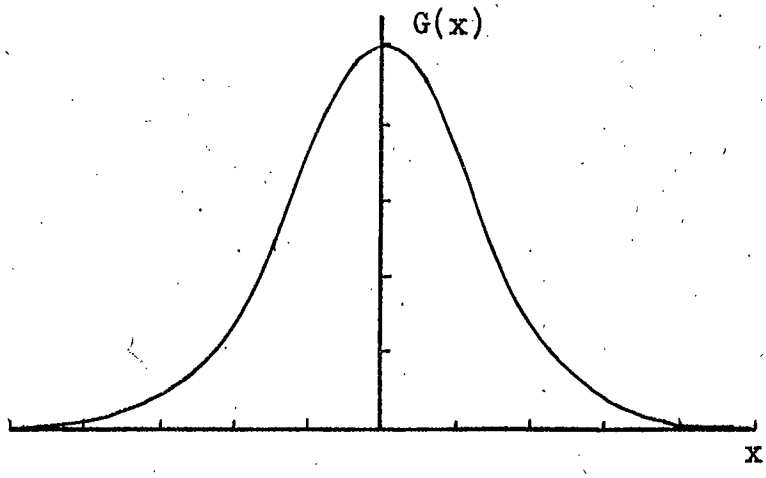

(b) Gaussian

Figure 1.3

Normalised Lineshape Functions

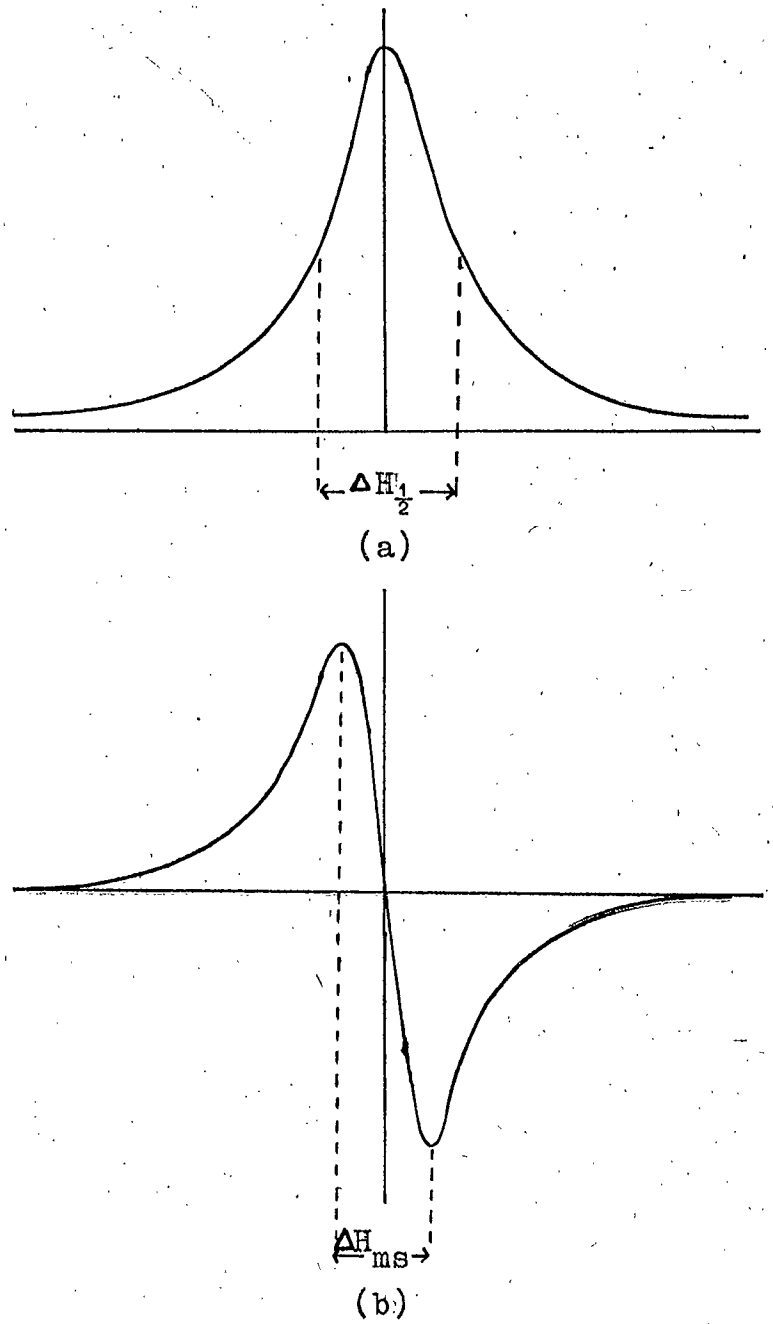

Figure 1.4
Definition of Linewidth Terms
(a) Half-Power Width $\Delta H_{\frac{1}{2}}$
(b) Derivative Peak-to-peak Width ΔH_{ms}

explicitly in Figure 1.4. Using these definitions the following relations hold for the functions as defined in Eqs. 1.10 and 1.11.

Lorentzian: $\Delta H_{\frac{1}{2}} = 2a$, $\Delta H_{ms} = 2a/\sqrt{3}$, $\Delta H_{\frac{1}{2}} = 1.732\ \Delta H_{ms}$ (1.12)

Gaussian : $\Delta H_{\frac{1}{2}} = 2\sqrt{2\log_e 2}.\ b$, $\Delta H_{ms} = 2b$, $\Delta H_{\frac{1}{2}} = 1.175\,\Delta H_{ms}$ (1.13)

The form of Eq. 1.11 is such that the parameter b is equal to the standard deviation of the Gaussian. However, owing to the divergent nature of the moments of the Lorentzian, of which more later, it is impossible to calculate a standard deviation for a function of this type unless the profile is truncated at some point.

When an absorption line is broadened by mechanisms giving independent Gaussian and Lorentzian contributions the resultant line is obtained (Mitchell and Zemansky, 1934) by convolution of the two broadening functions. Using the notation of Eqs. 1.10 and 1.11 this leads to the result:

$$Y(x) = \frac{a}{\pi b\sqrt{2\pi}} \int_{-\infty}^{+\infty} \frac{\exp(-y^2/2b^2)}{a^2 + (x - y)^2}\, dy \qquad (1.14)$$

This is known as the Voigt function and can only be evaluated numerically (Voigt, 1912). Tabulations of it, expressed in a somewhat different notation, having been given by Posener (1959).

1.5 FACTORS AFFECTING CHOICE OF A MASER MAERIAL

Howarth (1958) has made a detailed study of the physics of the three-level maser, and described the power emission of the device in terms of a magnetic Q-factor. As power is being emitted this has a negative value and for greatest emission must be as low as possible. He derived an expression for magnetic Q-factor having the form:

$$-\frac{1}{Q_m} = A.\frac{n_o W_s f_s}{(2S + 1)kTH_s^2} \qquad (1.15)$$

in which n_o is the density of active ions in the system, W_s is the probability of a transition at the signal frequency f_s, and H_s is the signal field strength. Various constants have been collected in the term A. The linewidth of the signal transition enters into Eq. 1.15 through the term W_s which is proportional to the effective spin-spin relaxation time, defined as the inverse of the linewidth. Howarth further showed that the gain-bandwidth product could be expressed in the form:

$$G.\ (\Delta f/f) = 2/Q_m \qquad (1.16)$$

or, in terms of linewidth, Δf_1:

$$G.\ (\Delta f/f) = B/\Delta f_1 \qquad (1.17)$$

Q_m depends inversely on the effective spin density, n_o, but this is limited as a means of improving Q_m because above a certain limit the linewidth begins to increase with spin density, as will be discussed subsequently. Below this limit a narrow line generally means better maser performance. If the lines are inhomogeneously broadened, causing only part of the spin population to be active, a sustantial loss of efficiency may occur. Thus a knowledge of the factors affecting line broadening is important in maser technology.

Rate equations for the three levels of the system can be set up, and their solution (Siegman, p.245) gives an expression for the inversion ratio of the signal transition under conditions of near saturation of the pump transition. Using the notation of Fig. 1.1 this takes the form:

$$I = \frac{f_p / f_s - (1 + T_i / T_s)}{1 + T_i / T_s} \qquad (1.18)$$

where the T's represent spin-lattice relaxtion times and the suffices p, s and i refer to pump, signal and idle transitions respectively. Here the inversion ratio, I, is defined as the ratio of the inverted population difference to the thermal equilibrium value. Eq. 1.18 shows that the inversion ratio, and consequently

the maser efficiency in terms of pump power, is dependent only on the ratio of the relaxation times. With a more exact analysis, the condition for non saturated operation, i.e. low signal operation, can be shown to be:

$$W_s << 1/T_s + 1/T_i \qquad (1.19)$$

Operation of a Bloembergen maser requires the use of a paramagnetic material providing at least three levels that are readily saturable, and whose splittings can be brought into the microwave region by the application of a suitable magnetic field. The number of levels should be as low as possible to keep the effective spin density high.The host lattice should provide a non-cubic environment for the paramagnetic ions as this causes the mixing of states necessary for the use of the forbidden $\Delta M = 2$ transitions, and the paramagnetic ions should occupy equivalent lattice sites. Both the paramagnetic ions and the ions of the lattice should have low nuclear magnetic moments in order to reduce the incidence of hyperfine interactions. The paramagnetic dilution should be sufficient to reduce spin-spin interactions to the point where saturation becomes practicable, but there must be sufficient spins to overcome cavity and coupling losses. Orbital momentum should be quenched in order to assist in assuring long

spin-lattice relaxtion times and so aid the saturation of the pump transition. The host lattice should be hard, robust and chemically stable. It should not suffer damage on cooling and should be susceptible to growth as large well formed single crystals.

1.6 PRACTICAL MASER MATERIALS

Subsequent chapters will describe work performed on two materials that have found wide use in the maser field, namely chromium: aluminium oxide (ruby), and neodymium: calcium tungstate. Ruby has found use both in the optical and the microwave regions, but for continuous operation Nd:$CaWO_4$ is available only in the optical region.

The first use of ruby as a maser material was reprted by Makhcv et al. (1958) and an assesment of its suitability for this purpose was made by Kikuchi et al. (1959). The parameters of the Spin-Hamiltonian are (Geusic, 1956):

$$g_{\parallel} = 1.984 \ , \quad g_{\perp} = 1.986 \ , \quad 2D = -0.3831 \text{ cm}^{-1}, \quad S' = 3/2$$

The crystal field causes splitting, with an orbital singlet, $^4A_2$, situated some 10,000 cm^{-1} below the triplet $^4F_2$. As the spin-orbit coupling is only 87 cm^{-1} (Bleaney and Stevens, 1953) orbital momentum is almost completely quenched. The combination of

trigonal field and spin-orbit coupling causes splitting of the ground state into two Kramers' doublets, and the negative sign of D indicates that the doublet $\pm 3/2$ lies lowest. The splitting of the ground state levels as a function of magnetic field, together with the observable transitions at 35 Gc/sec are shown in Figure 1.5 for orientations of 0° and 90°. The energy levels are labelled according to the convention adopted by Schulz-du Bois (1959), who assigned to each level a quantum number ranging from -3/2 to +3/2 in order of increasing energy. Owing to the mixing of states these quantum numbers have true physical significance only at 0°. At other orientations they merely provide convenient identification.

Laser action in Nd:$CaWO_4$ was first observed by Johnson and Nassau (1961), but unlike ruby the laser transition terminates on the first excited state, some 2,000 cm^{-1} above the ground state, thereby allowing of room-temperature c.w. operation. In common with other rare-earth ions, the crystal field is weak relative to the spin-orbit coupling and the states must be represented by J rather than S. In the calcium tungstate lattice the ground state is designated $^4I_{9/2}$ (Carlson and Dieke, 1958), giving S = 3/2, J = 9/2 and L = 5. There is strong crystal-field mixing of the J_z states within the ground J- manifold, resulting in a set of five Kramers' doublets situated at 0, 114, 161

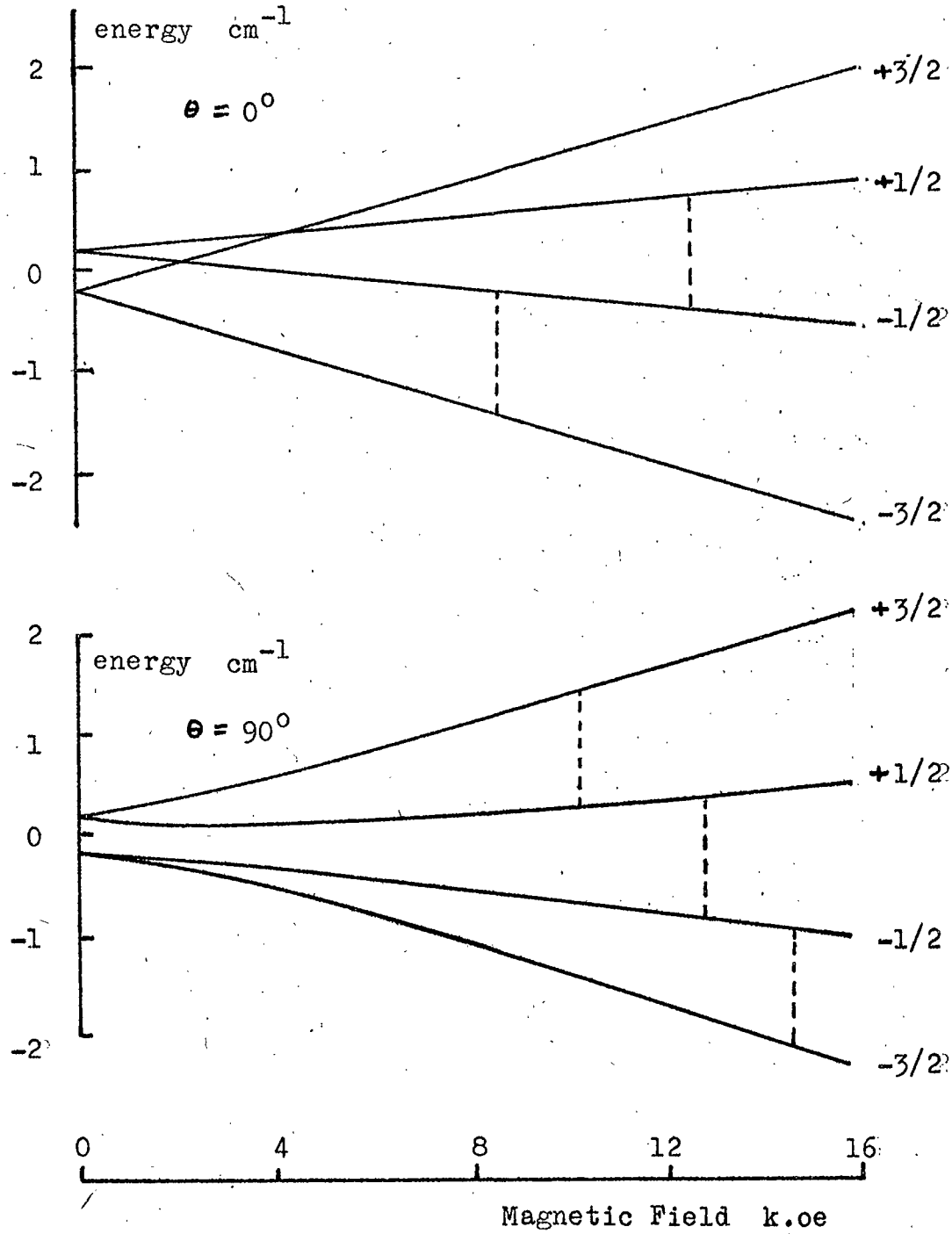

Figure 1.5

Ground Levels of Cr^{3+} Ion in Al_2O_3

230 and 471 cm^{-1} respectively (Johnson and Thomas, 1963). At helium temperature only the lowest of these is populated, and it is reported to have the form (Ranon, 1964):

$$|\pm a\rangle = 0.6828\,|\pm 9/2\rangle + 0.5407\,|\pm 1/2\rangle + 0.4916\,|\mp 7/2\rangle \quad (1.20)$$

where the quantum numbers refer to J_z. Paramagnetic resonance between these levels is represented by the Spin-Hamiltonian (Kask, 1963):

$$g_{\parallel} = 2.034\ , \quad g_{\perp} = 2.528\ , \quad S' = 1/2$$

in addition, two isotopes of neodymium, Nd^{143} and Nd^{145}, are present in an abundance of about 20%, and by virtue of their nuclear spin of 7/2 give rise to additional terms (Ranon, 1964):

$$^{143}A = 0.2129\ cm^{-1}\ , \quad ^{142}B = 0.2593\ cm^{-1}\ ,$$

$$^{145}A = 0.1317\ cm^{-1}\ , \quad ^{145}B = 0.1611\ cm^{-1}\ ,$$

which are included in the Spin-Hamiltonian of Eq. 1.5 as:

$$A.\ (S_z I_z) + B.\ (S_x I_x + S_y I_y)$$

Figure 1.6 shows the energy levels of $Nd:CaWO_4$, and on a larger scale the crystal field splitting of the ground-manifold.

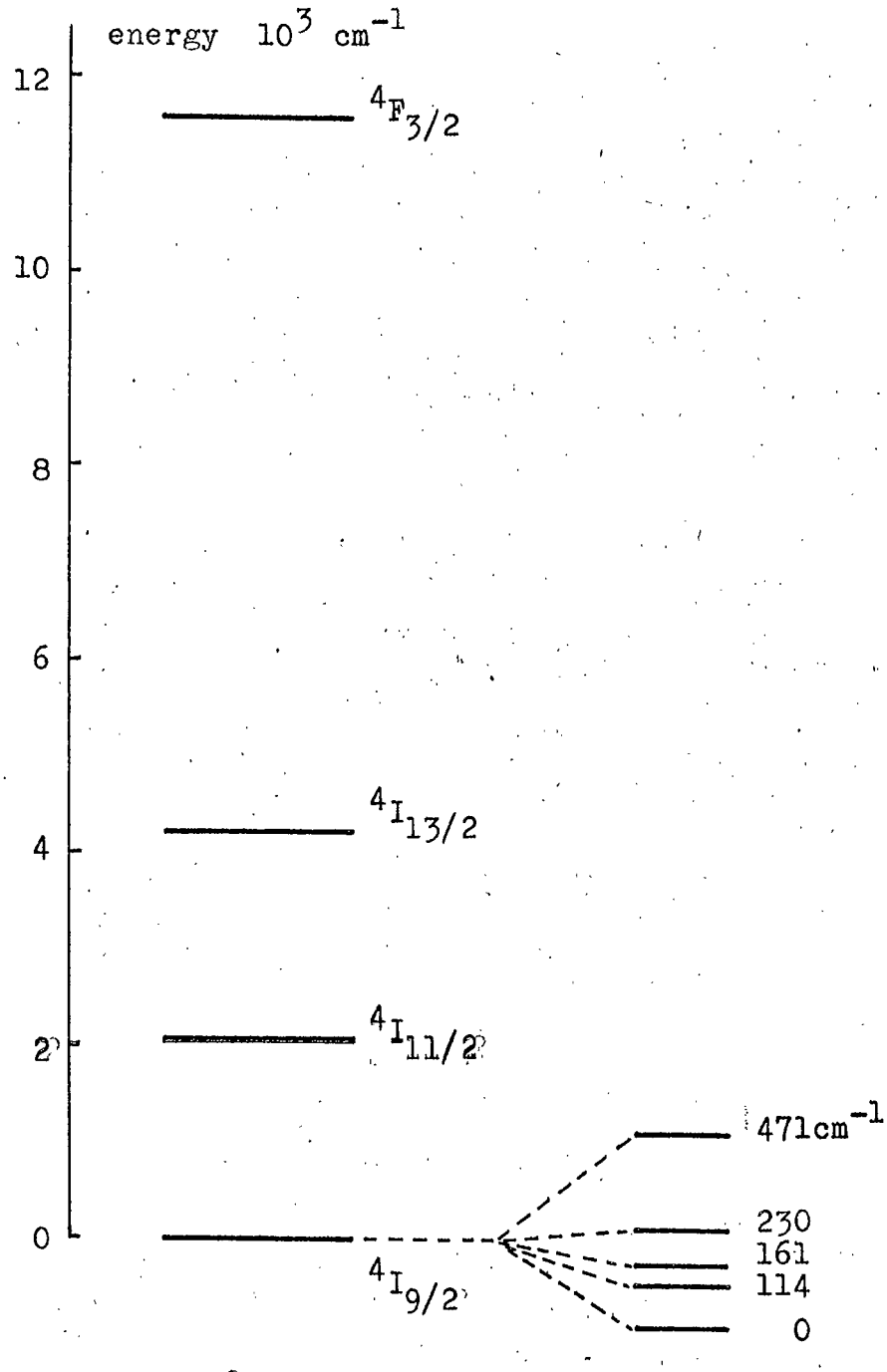

Figure 1.6

Energy Levels of Nd^{3+}:$CaWO_4$

(Ground-state splitting shown on larger scale)

1.7 THE PRESENT WORK

The work to be described here comprises an investigation of the e.p.r. linewidths in synthetic ruby, and of linewidths and spin-lattice relaxation times in Nd:$CaWO_4$, with the aim of investigating the effects of crystalline defects on these properties. Some indication has already been given of the importance of these properties in determining the behaviour of a maser material. To investigate crystal defects in ruby considerable use has been made of X-ray techniques, as will be described in the next chapter. In addition, optical absorption and electron microprobe analysis have been used. The factors affecting the broadening of e.p.r. absorptions in ruby will be discussed in detail, and this will be followed by a description and preliminary interpretation of measurements of linewidth and relaxation time in Nd:$CaWO_4$. Finally, the effects of crystal defects on relaxation times will be considered, and further evidence regarding the connection between relaxation and lattice strain will be presented.

Chapter 2

THE CRYSTALLINE PROPERTIES OF SYNTHETIC RUBY

2.1 THE MATERIAL

2.1.1 Growth Processes

The physical properties of corundum, the ruby host lattice, render its growth a somewhat difficult process. The melting point of the material, 2050°C (Scheuplein and Gibbs, 1960), means that quite sophisticated techniques have to be used to ensure the growth of boules of practical size. To date, four principal methods have been used commercially for the growth of corundum or ruby, these being the Verneuil, the Vapour Phase, the Czochralski and the Fluxed Melt processes.

The Verneuil process (Verneuil, 1904) was one of the first successful methods employed for the growth of corundum, and is still widely used commercially. Powdered aluminium oxide, containing in the case of ruby a small quantity of chromic oxide, is fed from a hopper into the growth furnace. Here, in an oxy-hydrogen flame, the powder is fused and the molten material is deposited on to a seed crystal. This is suitably located and oriented within the furnace and during growth of the boule it is slowly removed at such a rate that the deposition of fresh material always occurs at the same plane in the furnace. To keep the thermal stresses within the boule to a minimum, various

subsidiary heaters are used to reduce the thermal gradients in the region of the freshly grown material as far as possible. Despite these precautions, subsequent annealing of the boules is necessary to render them amenable to handling, and this is achieved by heating to nearly 2000 °C in a special furnace and then cooling slowly under carefully controlled conditions. The Verneuil process suffers from the disadvantage that the raw material is easily contaminated, and thus impurities are introduced into the boule during growth.

The Vapour Phase process is a modification of the Verneuil method, developed by the Thermal Syndicate Ltd. of Wallsend, Northumberland, who originally used it for the growth of high purity synthetic vitreous silica, (Jack and Stephenson, Unpublished). The starting materials are fed into the furnace as vapours rather than as solids, and this allows of a greater degree of control of the rate of feed. Usually halides of aluminium and chromium are employed as these materials can be easily produced in the vapour state as very pure compounds. The vapours react in an oxy-hydrogen flame and the corundum or ruby is deposited on the oriented seed as in the Verneuil process. An example of the reactions involved is:

$$2Al + 3Cl_2 = 2AlCl_3$$

$$2AlCl_3 + 3H_2O = 6HCl + Al_2O_3$$

The chromium halide is produced and deposited by a similar series of reactions and the gaseous by-products are swept away by the feed gas flow. Withdrawal of the boule is carried out as in the Verneuil process and the newly grown material is then annealed to reduce stresses.

As an alternative to growth on to a seed, crystals may be grown by pulling from a melt, and this forms the basis of the Czochralski method (Czochralski, 1904). An oriented seed crystal is placed in contact with a melt of the material contained in a suitable crucible, and is slowly withdrawn through a vertical negative temperature gradient. The design of the furnace is critical, particularly in view of the temperatures involved in the growth of corundum. Ruby as grown by this method is said to be more free from strain than material grown by either of the two "flame-fusion" methods described previously.

It is possible to grow ruby at a somewhat reduced temperature from a flux of a suitable solvent (Linares, 1965). Fluxes typically used are the metallic halides, but the method suffers from the disadvantage that the resulting crystals are often contaminated with impurities derived from the flux. In a flux of lead fluoride a growth temperature of around 1200°C is achieved, and the material is reported to be virtually free of strain, (Adams et al., 1966).

2.1.2 The Crystal Structure of Ruby

Chemically, ruby consists of corundum, Al_2O_3, in which some of the aluminium ions have been replaced during growth by trivalent chromium ions. The degree of substitution encountered in the material examined here was of the order of 0.1 % of chromium by weight. The growth methods aim to distribute the chromium evenly throughout the boule, but this topic will be discussed elsewhere.

Ruby crystallises in the rhombohedral system (Wyckoff, 1964), having three-fold symmetry, with three diad axes, the a-axes, symmetrically disposed about and perpendicular to the trigonal c-axis. Each aluminium ion in the corundum lattice is situated at the centre of a distorted octahedron of oxygen atoms. When substitution of chromium takes place, the site is shifted slightly along the body diagonal of this octahedron, and experiences crystal fields having both cubic and trigonal symmetry components. The unit cell contains two Al_2O_3 molecules, with the four positions of the Al ion being energetically equivalent, since they transform into one another by translation, or translation and inversion at the central ion (Sugano and Tanabe, 1958).

The ruby boules examined in the present investigation have been grown with their c-axes oriented at 0°, 60° and 90° to

the growth direction. 0° boules tend to show some external form of axial symmetry, but this is not evident in the 60° and 90° crystals which sometimes tend to exhibit a pronounced tabular habit. Most of the vapour phase material that has been examined has been grown in the 0° orientation, whereas the Verneuil boules have been grown exclusively in the 90° position. The two specimens of Czochralski ruby available were grown at an orientation of around 60°.

2.1.3 The Defect Structure of Ruby

Ruby grown by flame-fusion and pulling processes crystallises at 2050 $^{\circ}$C, and although every attempt is made to keep temperature gradients in the furnace to a minimum the newly grown material still experiences a longitudinal temperature gradient of around 6 $^{\circ}$C per mm. in the Vapour Phase process and about 20°C per mm in the Verneuil process (Jack and Stephenson, Unpublished). In addition, both the thermal conductivity and thermal expansion coefficients of corundum show anisotropy, the respective values being:

Thermal Expansion	$\parallel$ c-axis	6.582×10^{6} $^{\circ}C^{-1}$	(Sharma, 1951)
	$\perp$ c-axis	5.425×10^{6} $^{\circ}C^{-1}$	
Thermal Conduction	$\parallel$ c-axis	0.017 cal $^{\circ}C^{-1}$ cm^{-1} sec^{-1}	(Knapp, 1943)
	$\perp$ c-axis	0.015 cal $^{\circ}C^{-1}$ cm^{-1} sec^{-1}	

Consequently the newly grown material contains a large number of dislocations and is highly stressed. Many workers have investigated the distribution of dislocations in corundum, and two principal systems have been observed. The "Basal" system contains dislocations lying in the (0001) plane, and having Burger's vectors in the $\langle 11\bar{2}0 \rangle$ directions, while the "Prismatic" system consists of dislocations lying in the $\{11\bar{2}0\}$ planes with Burger's vectors in the $\langle 10\bar{1}0 \rangle$ directions (Stephens and Alford, 1964). Figure 2.1 shows the relative orientations of these systems. There is evidence (Curtis, 1964) that dislocations are propagated from the seed crystal during growth, but it appears that the addition of chromium to the lattice during growth is not responsible for the introduction of additional dislocations as Thilo et al. (1955) reported no alteration of the lattice constants up to 8 mole % Cr_2O_3.

By treatment with ortho-phosphoric acid under carefully controlled conditions Scheuplein and Gibbs showed that etching of dislocations occurs preferentially in certain well-defined orientations in space. One region about 5° in radius was found to be centered on the direction of the c-axis, (0001), and was due to dislocations of the prismatic system. Three further regions each about 20° in diameter, located at 120° intervals near the

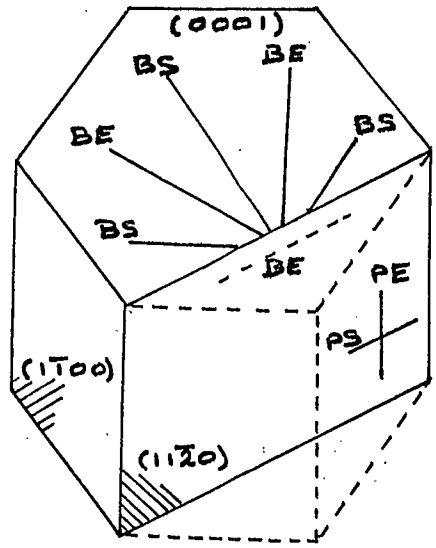

Figure 2.1

Illustration of Pure Edge and Screw Dislocations for Basal and Prismatic Systems

BE = Basal Edge
BS = Basal Screw
PE = Prismatic Edge
PS = Prismatic Screw

positions $\{20\bar{2}1\}$ and $\{10\bar{1}1\}$, were also observed. Bond and Harvey (1963) succeeded in decorating dislocations in sapphire, corundum doped with iron, by including 1% by weight of ZrO_2 in the growth mixture followed by annealing of the crystals for four hours at 1500 °C, and were able to observe directly that they lay predominently in the six $\langle 11\bar{2}0 \rangle$ directions. Subsequent annealing of the material causes dislocations of like sign to segregate and form plane walls perpendicular to the slip planes, i.e. lying mainly in the $\{1\bar{1}00\}$ planes. These walls form low-angle grain boundaries separating blocks of relatively undistorted material, and this process of polygonisation results in the formation of the mosaic structure investigated here. Kronberg (1955) simulated this by introducing dislocations into ruby rods by bending them at 1800 °C. On annealing at 2000 °C polygonisation occured. Stephens and Alford reported that annealing reduced the number of basal dislocations from 2.0×10^6 to about 2.0×10^5 cm^{-2}, while the density of dislocations lying in prism planes remained at around 3.0×10^{-5} cm^{-2}. Figure 2.2 is a stereographic projection of the corundum lattice showing the planes and directions referred to above.

The formation of a low-angle grain boundary, if considered in terms of the classical picture of an array of edge dislocations of like sign, results in both atomic misfit along

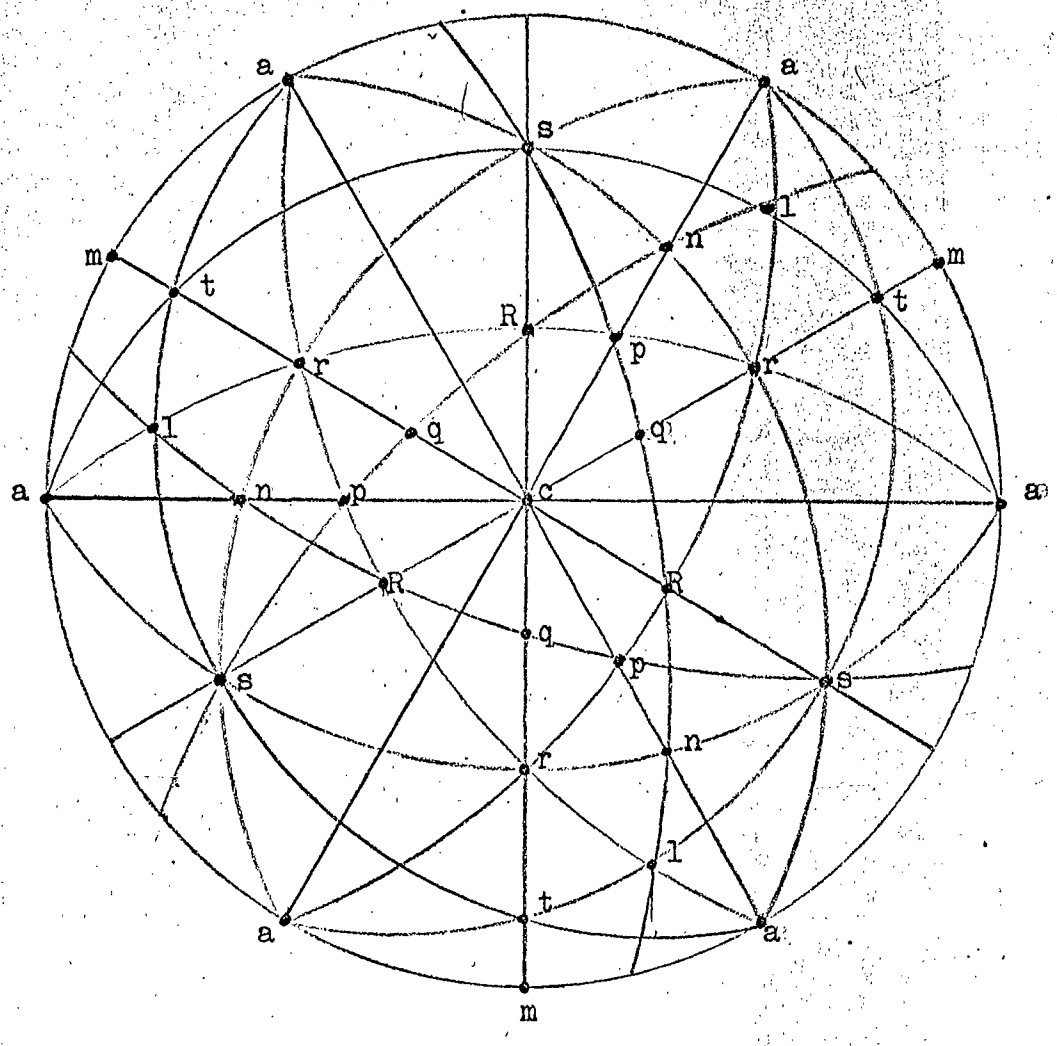

Figure 2.2

Stereographic Projection of Corundum Lattice
(Showing some of the principal zones)

The forms indicated are:

a: $\{11\bar{2}0\}$,	c: (0001),	l: $\{21\bar{3}1\}$,
m: $\{10\bar{1}0\}$,	n: $\{22\bar{4}3\}$,	p: $\{11\bar{2}3\}$,
q: $\{20\bar{2}5\}$,	r: $\{10\bar{1}1\}$,	R: $\{01\bar{1}2\}$,
	s: $\{02\bar{2}1\}$,	

the boundary and deformation of the surrounding region extending over many atomic spacings. The angle of misorientation is given by :

$$\theta = \underline{b}/D \qquad (2.1)$$

where $\underline{b}$ is the Burger's vector and D is the dislocation separation (Read, 1953). For misorientations greater than about 15 minutes of arc it is impossible to resolve individual dislocations in a grain boundary. The values of $\underline{b}$ for corundum are 8.22 A.U. for the prismatic system and 4.75 A.U. for the basal system (Scheuplein and Gibbs, 1960).

Likhachev (1961) discussed the formation of thermal strain at grain boundaries in polycrystalline materials, and presented results for all thirty-two crystal classes. The amount of strain depends upon the degree of perfection of the crystal texture, and this is allowed for in the theory. Likhachev considers the stresses acting on a crystallite having anisotropic thermal expansion coefficients, surrounded by the rigid medium whose thermal expansion coefficients differ from that of the crystallite by factors dependent upon the degree of perfection of the texture of the sample as a whole. Calculations have been performed using the formula appropriate to the case of trigonal symmetry, together with the appropriate crystallographic constants for ruby. It is

estimated that in cooling from 2000 ^{o}C to room temperature a system posessing no preferential orientation would experience strains of the order of 10^{-2}. This figure will be reduced as a result of the near parallel orientation of the crystallites, and the actual strain existing in an annealed boule may be two or more orders of magnitude less than this.

2.2 X-RAY INVESTIGATION TECHNIQUES

2.2.1 The back-Reflection Laue Method

Extensive use has been made of the Laue technique for the investigation of crystalline defects in ruby, as well as for the orientation of as-grown boules in preparation for cutting. The basis of the method is that the single crystal specimen has incident upon it the "white" unfiltered radiation emanating from the x-ray tube. Each set of lattice planes within the crystal then selects radiation of the particular wavelength satisfying the Bragg relation :

$$n\lambda = 2d.\sin\theta \qquad (2.2)$$

and diffracts this coherently. In most of the work to be described, the back reflection modification of the method was used, as this gave increased resolution and reasonable exposure times. In the back-reflection method the diffracted beam does not have to traverse a great thickness of material before reaching the film, and this

gives a picture of a localised region near the surface rather than a vague average through a considerable thickness of material. This method is not as accurate as some of the other more sophisticated methods of studying crystal texture, but it has the advantage of being simple to carry out, and no special preparation of the surface under examination is required.

The x-ray exposures were made using a home-made camera and a Philips type PW1008 x-ray generator fitted with a tube containing a copper target. Unfiltered radiation from this tube was used for all the exposures. The camera could be fitted with collimators of various sizes, and the one most commonly used gave exposure times of about one hour. This exposure time was used for most of the work, as was a standard film-specimen distance of 3 cm. Increasing this distance would have increased resolution but the exposure time would have been increased considerably as a result. The specimen was mounted on a goniometer allowing of various degrees of rotation and translation. The exposures were made on flat film, Ilford Industrial Type G. and processing was under approximately constant conditions, with a development time of 4 minutes in Ilford X-Ray Developer.

The defect structure of the ruby lattice was investigated by means of measurements of two parameters that could be derived

from back-reflection Laue photographs. These are the "mosaic misorientation" i.e. the angular misorientation between neighbouring crystallites, and the "c-axis misorientation", which is a measure of the way in which the direction of the crystallographic c-axis varies over the extent of the specimen.

2.2.2 Mosaic Misorientation

The formation of mosaic structure in corundum as a result of the annealing of material containing dislocations has been described above. The presence of this structure is revealed in the observation of a broadening or even splitting of the diffraction spots in a back-reflection photograph. This splitting occurs when the x-ray beam illuminates a region of the specimen in which there are crystallites oriented in different directions, resulting in two or more spots instead of the one which would be expected from perfect material. Figure 2.3 shows typical photographs from relatively good material and material exhibiting a great deal of mosaic structure.

Cosideration of the relative orientations of the dislocation systems and the lattice shows that observations of mosaic structure on the (0001) plane reveal polygonisation connected with the basal system of dislocations, as shown in Figure 2.4. Prismatic dislocation systems would be revealed by

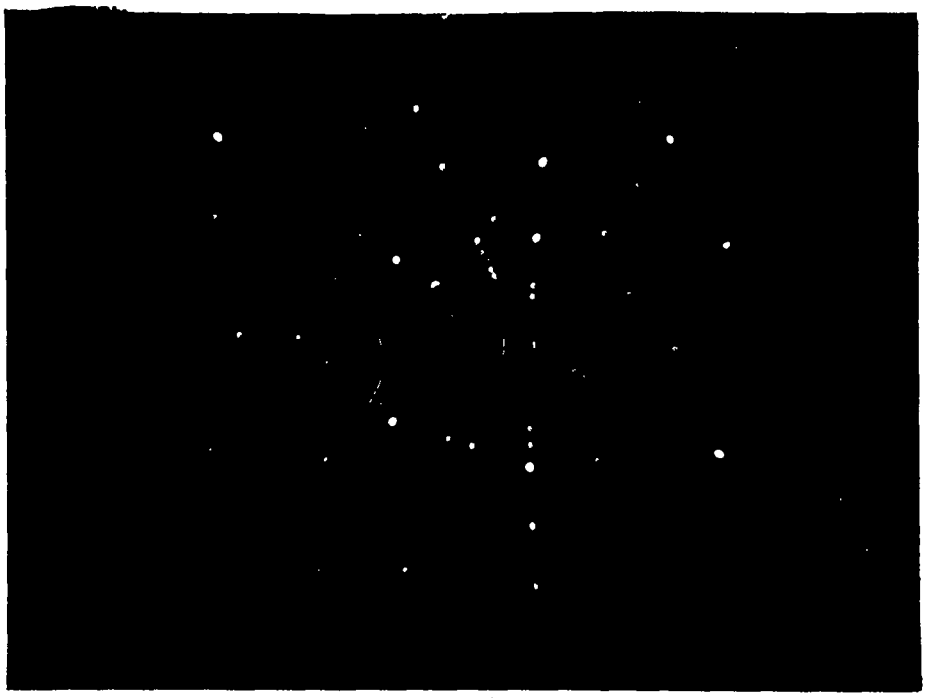

(a)

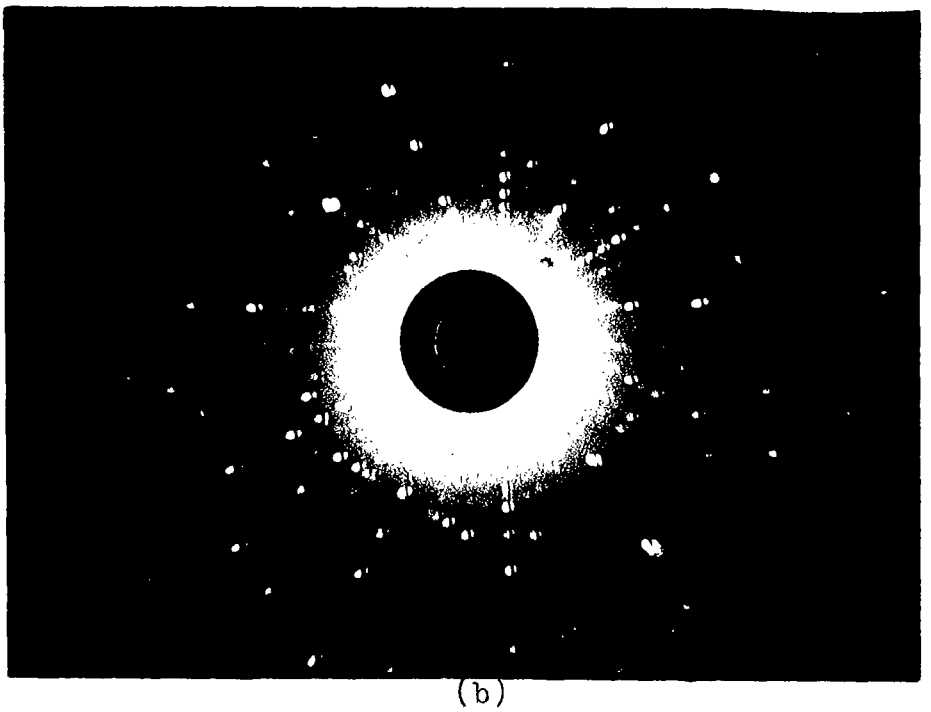

(b)

Figure 2.3

X-Ray Photographs

(a) Good Material

(b) Bad Material

investigating the $\{11\bar{2}0\}$ planes, i.e. planes perpendicular to the diad axes. Most of the present work has been devoted to an investigation of the basal slip system, and the corresponding orientations of the c-axis directions. Prismatic slip only affects the a-axes, and consquently only the azimuthal angle, of the coordinate system for paramagnetic resonance and these variations have not first order effect on the resonance spectrum of ruby.

From a measurement of the broadening or splitting of the spots, and knowing the dimensions of the x-ray camera, it is possible to deduce the angular misorientation within the region illuminated by the x-ray beam. Further, from a knowledge of the area of the illuminated region, and the number of components that each diffraction spot is split into, it is possible to gain an estimate of the sizes of the crystallites. Owing to the limited depth of penetration of the x-rays, only the region immediately adjacent to the surface could be investigated by this technique. Curtis showed that the means used to prepare the ruby surface did not affect the crystallite structure in any detectable way, and consequently the information obtained at the surface can be considered representative ofthe bulk material.

The diffraction spot resulting from "good" material has a finite size governed by the physical dimensions of the

camera system. Curtis considered only splitting of the spots into separate components, but did not examine the cases in which mosaic caused unresolvable broadening of the spots. Unless this effect is considered, the limit of resolution of the method is about 20 minutes of arc, this being the approximate angular diameter of a typical diffraction spot. Detailed analysis of diffraction spot profiles requires techniques superior to those available when the bulk of the work was performed. A photodensitometer has since become available, and this point may well repay further investigation.

2.2.3 C-Axis Misorientation

If the local direction of the c-axis in ruby is examined as a function of position within the boule it is found that there may exist a variation in orientation. At each point within the specimen there may be observed mosaic misorientation, but between different regions of investigation there may exist misorientations of the local c-axis direction, and figures of up to 3^{o} of arc have been observed.

Estimates of the magnitude of the c-axis misorientation present have been made by taking x-ray photographs at different locations on the specimen on the same film. To assist in identification of the different images produced, a metal disc from which two 60^{o} sectors had been removed was used to mask the

film, with the result that three photographs could be obtained on each film. From the pattern of spots on the film the zone lines had to be reconstructed in order to locate the positions of the spots corresponding to the reflections from the (0001) planes, which were obscured by the collimator. Sufficient of the pattern appeared in each 60° sector to permit of this, and once the positions of the (0001) spots had been located it was possible to calculate the misorientations from a knowledge of the camera geometry. The theory of this calculation was given by Curtis. The accuracy of this method was limited by the accuracy with which the zone-lines could be reconstructed, and to assist in this the specimen was aligned with the (0001) face as nearly as possible perpendicular to the incident beam of x-rays, which ensured that the zone-lines were straight lines. Where each spot was split into several components as a result of the presence of mosaic structure an estimate was made of the position of the centre of the system. This estimation would lead to still further inaccuracies, and it was estimated that values under about 30 minutes of arc were order of magnitude approximations only.

2.2.4 The Distribution of the Misorientations

In the simple case of the imperfect material, the specimen is viewed as consisting of many perfect crystallites

arranged in a mosaic form. For the purposes of this model the following assumptions are made.

a) The formation of the mosaic is such that, when drawn from a common origin in space, the unit vectors along the c-axes of the microcrystals lie within an axially symmetric cone. In the cases of ruby and calcium tungstate this assumption is justified by the axial symmetry of the respective lattices.

b) The unit vectors are distributed symmetrically about the axis of the cone, and the angular deviations of the individual unit vectors from the cone axis may be described in terms of a suitable distribution with a standard deviation σ_b. The cone axis is taken to represent the effective c-axis of the imperfect crystal, and the aperture of the cone is the greatest misorientation present in the crystal. In the perfect crystal this is equal to zero.

Measurements of c-axis and mosaic misorientations performed as described above are then, in effect, measurements upon the same distribution of crystallite orientations, the only difference being in the distances separating the points of observation. A mathematical treatment of the relationship between the observed misorientations and the original orientation distribution will now be outlined.

Consider the situation already assumed, in which the axial distribution of crystallite orientations is symmetric, and the radial distribution is represented by the function F(r). Figure 2.5 represents this distribution pictorially, with the normal to the circle at O representing the predominant c-axis direction and the circle representing the boundary of the permitted orientations. If this circle has a radius equal to a, then the chord PS drawn through the two points R and R' has a length $2a.\cos\Theta$, where Θ is defined by the positions of R, R' and O, as shown in the figure.

The probability of observing the orientation represented by the point R is simply that given by the radial distribution function F(r) evaluated at this point. This is also the local value of G(r'), the distribution function observed along the chord PS. Then:

$$G(r') = F(r) = F\left[(r'^2 + a^2\sin^2 O)^{\frac{1}{2}}\right] \qquad (2.3)$$

The radial distribution function is frequently assumed to have a Gaussian form, represented by:

$$F(r) = \frac{1}{b\sqrt{2\pi}} \exp\left(-r^2 / 2b^2\right) \qquad (2.4)$$

where b is the standard deviation of the distribution. Inserting

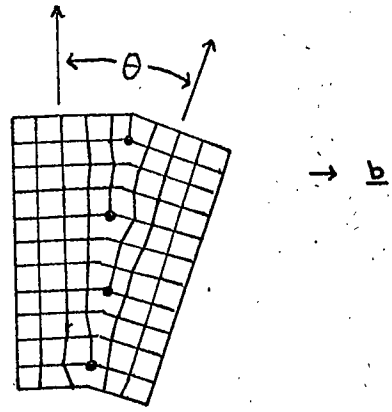

Figure 2.4
Formation of Low Angle Grain
Boundary by Set of Edge Dislocations

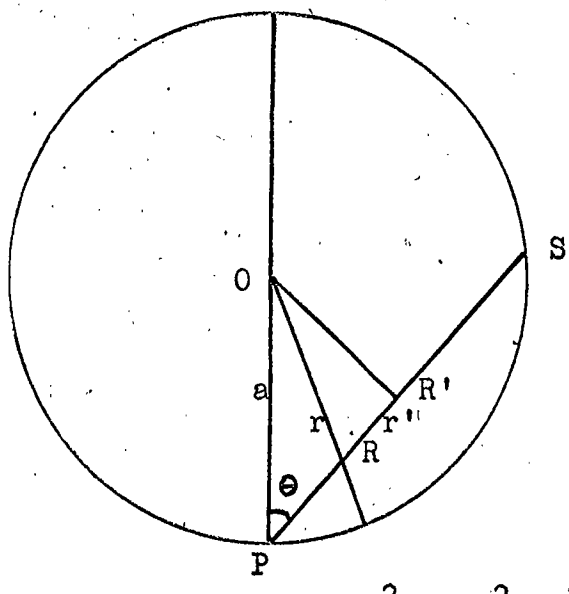

$$r^2 = r'^2 + a^2 \sin^2 \theta$$

Figure 2.5
Illustration of Theory of
Misorientation Distribution

this expression into Eq. 2.3 leads to the result:

$$G(r') = \frac{1}{b\sqrt{2\pi}} \exp - \left[(r'^2 + a^2 \sin^2\theta)/2b^2 \right] = F(r).\exp\ (-a^2 \sin^2\theta\ /2b^2) \qquad (2.5)$$

which represents a Gaussian, of reduced amplitude, but posessing the same standard deviation, b , as the radial distribution function.

Consider now two crystallites with a relative misorientation z, and absolute orientations relative to the predominant c-axis direction of x_1 and x_2 respectively, where $(x_1 - x_2) = z$, forming part of a system whose distribution function may be represented by f(x). Then the probability of observing a misorientation z may be represented by ;

$$Y(z) = \int_{-\infty}^{+\infty} f(x_1).\ f(x_1 - z)dx \qquad (2.6)$$

Assuming for the sake of mathematical convenience that f(x) is again a Gaussian function (c.f. Eq. 2.4) it can be shown that this integral leads to the result

$$Y(z) = \frac{1}{b\sqrt{\pi}} \exp\ (-z^2/2b^2) = \frac{1}{\sqrt{2}}\ f(z) \qquad (2.7)$$

which is a Gaussian, having the same standard deviation, b, as the fundamental distribution of orientations. The author is indebted to D.R. Mason for assistance in deriving the result

of Eq. 2.7.

Combining the results of Eqs. 2.5 and 2.7 it can be seen that the distribution of misorientations observed along any chord of Fig. 2.5 can be represented by :

$$Y'(r', \Theta) = \frac{1}{\sqrt{2}} \exp(-a^2 \sin^2 \theta / 2b^2). F(r) \qquad (2.8)$$

To obtain the overall distribution of misorientations in space as observed in the system represented by Fig. 2.5 it is necessary to integrate over all values of θ, i.e. :

$$Y''(r') = \int_{-\pi/2}^{+\pi/2} \frac{1}{\sqrt{2}} \exp(-a^2 \sin^2 \theta / 2b^2) F(r). d\theta \qquad (2.9)$$

which results in :

$$Y''(r') = \frac{\pi}{\sqrt{2}} (1 - a^2 / 4b^2 + 3a^2 / 16b^2 - \ldots) F(r) \qquad (2.10)$$

Thus if the original distribution of orientation was Gaussian then the observed distribution of misorientations between the crystallites will also be Gaussian, having the same standard deviation as the original. A similar argument holds for any other function that is self-reproducing (Hughes and MacDonald, 1961).

2.3 RUBY MISORIENTATION RESULTS

Rubies grown by the Vapour Phase, Verneuil and Czochralski methods have been subjected to an extensive analysis by x-ray methods, and mosaic and c-axis measurements have been made as already described. Vapour Phase and Verneuil material was made available through the kind cooperation of the Thermal Syndicate Ltd., and the samples of Czochralski material were obtained from the Linde Corporation.

Table 2.1 summarises the experimental results, each of which, in most cases, was obtained from at least ten, and often considerably more, measurements. Figures are quoted for the mean mosaic and c-axis misorientations, for the standard deviation of each of these quantities and the standard deviation of the whole set of misorientation figures obtained for each specimen. In addition, indication is made of the growth method and orientation, and of the chromium concentration. The standard deviation results from each specimen were subjected to a statistical test (Moroney, 1956, p. 234), and it was found that with few exceptions there was no significant difference in the figures for mosaic and c-axis misorientation, indicating that the two sets of results were representative of the same distribution of orientations. The results obtained will be discussed with reference to the chromium concentration, the growth

conditions and the distribution of the observed misorientations.

Ruby	Growth	Conc^{n}.	Mean Mosaic	St.Dev. Mosaic	Mean C-axis	St.Dev. C-axis	St.Dev. Total
2B	V.P. 0°	0.002	39'	20'	83'	25'	25'
467	"	0.013	33'	23'	67'	26'	28'
G2B	"	0.032	16'	14'	54'	23'	22'
G2A	"	0.032	41'	59'	83'	42'	57'
312B	"	0.041	28'	20'	102'	31'	30'
312C	"	0.041	24'	19'	56'	31'	28'
344	"	0.047	18'	14'	48'	24'	20'
337A	"	0.052	5'	10'	41'	18'	16'
337C	"	0.052	8'	13'	54'	25'	22'
319G	"	0.080	3'	2'	56'	27'	23'
354	"	0.20	23'	7'	65'	41'	31'
252	V.P.90°	0.015	3'	6'	96'	39'	32'
374	Ver.90°	0.016	5'				
367	"	0.034	25'	22'	49'	28'	27'
H1	"	0.037	5'	0'	69'	36'	34'
628	"	0.044	5'				
458	"	0.052	18'	21'	58'	32'	31'
L1	Cz.60°	0.042	0'	0'	66'	4'	4'
L2	"	0.045	(0')	(0')	(0')	(0')	(0')

Table 2.1

Summary of X-ray Results

2.3.1 Misorientation and Chromium Concentration

Table 2.1 shows that there is no obvious dependence of any of the observed quantities on the chromium concentration. Reference has already been made to the fact that quite large quantities of chromium can be substituted into the corundum lattice before any alteration of the lattice constants is observed, and the figure of 8% reported by Thilo and his collaborators is two orders of magnitude greater than the concentration in any specimen examined here. The chromium ion, having a radius (Goldschmidt, 1920) of 0.55 A.U. replaces an aluminium ion of radius 0.45 A.U. and as the nearest neighbour oxygen atoms are at least 2.0 A.U. distant the distortion caused by a single substitution is relatively small, and insufficient actually to induce new dislocations in the material. However, as will be discussed later, there is evidence (Thorp et al. 1964) to suggest that during growth and annealing impurity ions, in this case chromium, do tend to segregate in the regions of greatest dislocation density.

2.3.2 Misorientation and Growth

Table 2.1 indicates the relative incidence of ruby growth method and orientation, and it will be seen that only the Vapour Phase process was represented by material grown in more

than one orientation.

In general the 90° specimens exhibit a somewhat lower mean mosaic misorientation, an average of 11' of arc, than do the 0° samples with their average of 21'. The two samples of Czochralski material appear to be better than either of the other two types in this respect. However misorientation still exists in the Czochralski ruby, as is evidenced by the c-axis misorientation figures, which show little dependence on growth conditions. The chief factor of difference between the various types of material would thus appear to be in the size of the mosaic blocks, and in the 0° material this appears to be in some cases appreciably less than the area illuminated by the incident x-ray beam.

A qualitative explanation for the dependence of mosaic structure on growth orientation can be given in terms of the dislocation systems in ruby, the anisotropic thermal conductivity and expansion coefficients, and the temperature gradients set up during and subsequent to growth (Curtis and Thorp, 1965). Removal of the newly grown crystal from the flame region during flame fusion growth will lead to a small temperature gradient radially in the boule and a somewhat greater one along its growth axis. In the 0° position the growth axis coincides with the c-axis, which is the axis of maximum thermal expansion

and thermal conduction coefficients, and the large thermal stresses set up along the c-axis will lead to the conditions conducive to the formation of dislocations of the basal system. In the 90° orientation the stresses along the c-axis, now no longer the growth axis, are somewhat reduced, and the incidence of basal dislocations may be less. As already explained, misorientations of the c-axis directions are caused entirely by dislocations of the basal system, and consquently the mean misorientation observed might reasonably be expected to be less in the 90° case.

It will be noticed that 60° material has been omitted from this discussion. No flame fusion material grown in this orientation has been available, and insufficient information concerning the technology of the Linde Czochralski process has been available to allow of a true comparison. However, if the samples of Czochralski available here were truly typical of this material, then crystallographically it is superior to the average flame fusion ruby.

2.3.3 The Observed Misorientation Distribution

For mathematical convenience the model of a Gaussian distribution of orientations was assumed earlier, and a similar assumption has been made by other workers (Shaltiel and Low, 1961; Wenzel and Kim, 1966). However, no experimental verification of

this appears to have been made in the literature and in order to test this experimentally, about fifty measurements of mosaic and c-axis misorientation were made on Ruby 344. As already indicated, the distribution of observed misorientations should indicate the nature of the underlying distribution of orientations.

Figure 2.6 shows a histogram of the misorientation results, (in order to have more data to work on, the results for mosaic and c-axis were combined) together with curves representing Lorentzian and Gaussian functions enclosing the same area and having the same standard deviation as the data represented by the histogram. The class-interval of the histogram was taken as 20', which as well as being the standard deviation of the distribution was approximately the order of magnitude of the accuracy of the measurements. Comparison of the observed results with the two theoretical curves revealed a pronounced trend towards a distribution of Lorentzian form. This result can be explained qualitatively in terms of a simple system of resonant particles. If each particle is randomly oriented within the limits specified in the earlier assumptions, then the response of the system might reasonably be expected to be Gaussian. If the system is restrained by some form of damping, in this case the restraints on orientation imposed crystallographically, then on theoretical grounds a Lorentzian

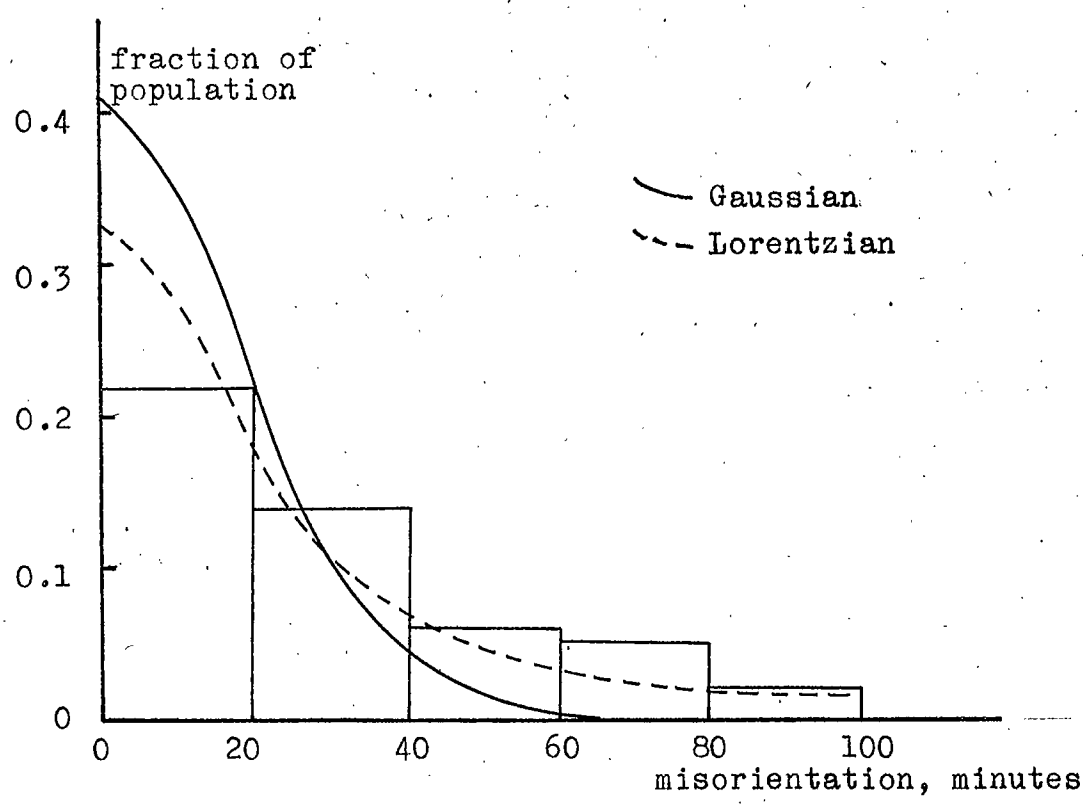

Figure 2.6
Distribution of Misorientations

distribution of orientations would be expected.

2.4 DISTRIBUTION OF CHROMIUM

2.4.1 Chromium Distribution and Growth

As will be seen subsequently, paramagnetic processes in ruby are to a certain extent dependent on chromium concentration, and the macroscopic behaviour may be influenced by gradients and inhomogeneities in composition. Precautions are taken to ensure homogeneity of doping during growth of flame fusion ruby, but in practice it is found that these are not always successful.

The situation existing at the growth region is somewhat complex, and distribution and diffusion of additive ions have to be considered. Sil'nichenko and Gritsenko (1965) have shown that the "take-up" of chromium in ruby is of the order of 0.3 and similar figures for the distribution of gadolinium and samarium in calcium tungstate were observed by Nassau and Broyer (1962). The problem of the distribution of dopant ions within the lattice is one of ionic diffusion. Van Bueren (1960) points out that grain boundaries are regions of enhanced lattice disorder and may thus provide easy diffusion paths during growth.

A certain amount of evidence is available to suggest that concentration inhomogeneities do exist in ruby grown by current techniques. Dodson (1962), using a chemical analysis technique

requiring samples of 50 mg., observed heterogeneity on a semi-microscopic scale, and by combining the results of a similar analysis with those of x-ray and etching investigations Thorp et al. (1964) showed a correlation between chromium concentration, misorientation and dislocation density. Dils et al. (1962) used electron probe microanalysis and observed not only local inhomogeneities, over distances of the order of 100 microns, but also a general decrease in concentration from the centre of the boule to the edge, a trend opposite to that reported by Thorp et al.

2.4.2 Examination of Concentration Inhomogeneities

Optical analysis of chromium concentration has been carried out using the method described by Dodd et al. (1963). The basis of this is the Beer-Lambert law of optical absorption, which states that the absorption at a particular frequency is given by:

$$I/I_o = \exp(-\mu cd) \qquad (2.11)$$

where c is the concentration of absorbing centres, d is the light path length in the specimen and μ is the absorption coefficient for the particular frequency. Owing to the way in which optical absorptions are caused this method measures only substitutional chromium, whereas chemical methods include interstitial ions as well. The absorption spectrum of ruby in the visible region consists

of two broad bands, centred on 4100 and 5600 A.U., the relative intensities of which are dependent on the orientation of the E-vector of the radiation relative to the c-axis. The spectrum in the perpendicular position is shown in Figure 2.7, this being the orientation used in these measurements.

Optical absorption measurements were made using a Hilger and Watts monochromator, Type D285, together with a tungsten filament source and a photomultiplier detector. Measurements of bulk concentration gave results within the limits of accuracy of those obtained by spectrographic analysis (Mostyn, private communication) and from this it was deduced that all the chromium was substititional. To measure concentrations over small regions of the specimens a beam 0.07 mm in diameter was used, and the specimen was traversed across this by means of a micrometer arrangement. Figure 2.8 shows the result of an investigation of this nature performed on a slice, 1.5 mm thick, of a Vapour Phase ruby having a bulk concentration of 0.2 %, and it can be seen that the maximum inhomogeneity is about 10%. Curtis (1964) estimated the grains to have dimensions of between 10^{-1} and 10^{-2} cm and thus in traversing a thickness of 1.5 mm the beam is passing through tens of grains. In consequence, any small scale inhomogeneities will tend to become averaged out by this technique.

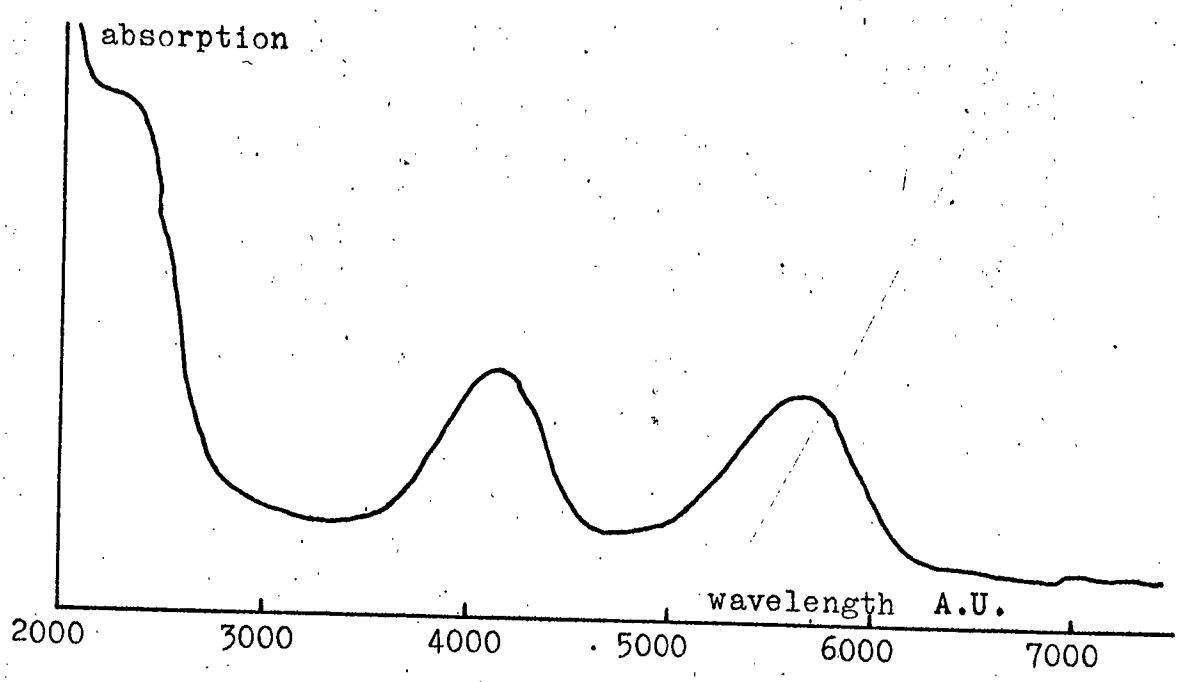

Figure 2.7
Optical Absorption Spectrum of Ruby

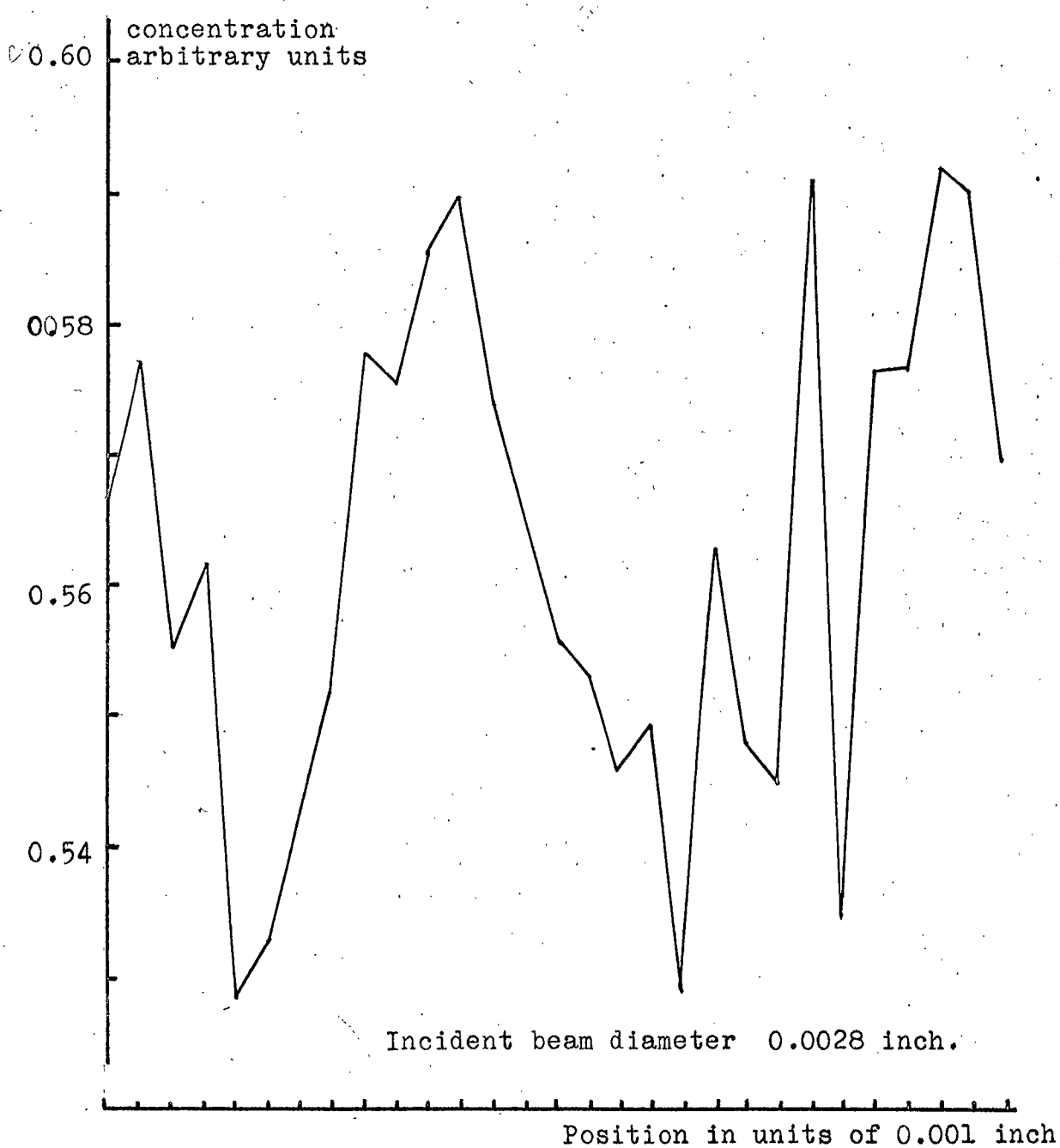

Figure 2.8

Variation of Chromium Concentration
(Vapour Phase Ruby, 0.2 % Cr)

A somewhat thinner specimen of a lower concentration ruby was prepared, but owing to the considerably reduced absorption it was difficult to observe any local effects.

One specimen of Verneuil ruby was examined by electron probe microanalysis, by courtesy of the Geology Department, University of Durham. Measurements were made at approximately 1 mm intervals, investigating a volume which was estimated to be a hemisphere about 1/40 mm in diameter. At the concentration levels existing in the specimen, chromium proved to be a difficult element to detect, with a signal about twice the noise level. However, some evidence of inhomogeneity was detected, with a concentration decrease of about 30 % over the first 5 mm from the edge of the specimen with a fairly constant value in the central region. Unfortunately, no absolute values of concentration could be obtained by this method.

2.5 CONCLUSIONS

In general, ruby grown at elevated temperatures is not crystallographically perfect, and relatively large misorientations between different regions of the specimens have been observed. Vapour Phase and Verneuil material appears to be very similar, and the factor affecting the quality of flame-fusion ruby appears to be growth orientation. Ruby grown by the Czochralski method appears to be superior to the best flame-fusion material.

Chapter 3

THE Q-BAND SPECTROMETER AND ASSOCIATED TECHNIQUES

3.1 THE SPECTROMETER SYSTEM

The e.p.r. spectrometer used during the course of the work described here was a magic-tee bridge instrument with facilities for broad-line e.p.r. display and pulse-saturation relaxation-time measurement. The spectrometer was basically that described by Mason (1966) with the addition of synchrodyne detection at 160 kc/sec (Curtis, 1964) and certain detail modifications giving improved sensitivity and operational convenience. A block diagram of the apparatus is shown in Figure 4.1 and a photograph of the experimental arrangement appears as the Frontispiece.

3.1.1 The Magic-tee Bridge Spectrometer

The microwave spectrometer was of the conventional bridge type, modified by the addition of a superhet detection system using a single klystron to provide both signal and local oscillator sources (Brown et al, 1965). The signal power source was an E.M.I. reflex klystron, type R5146, providing about 20 mW over a frequency range 34.0 - 35.5 Gc/sec. This was mounted in an oil bath, an arrangement giving very good frequency stability, and its heater was driven from a battery to reduce 50 c/sec noise. The klystron was isolated from the rest of the spectrometer by a ferrite isolator, Microwave Instruments type WQ286, followed

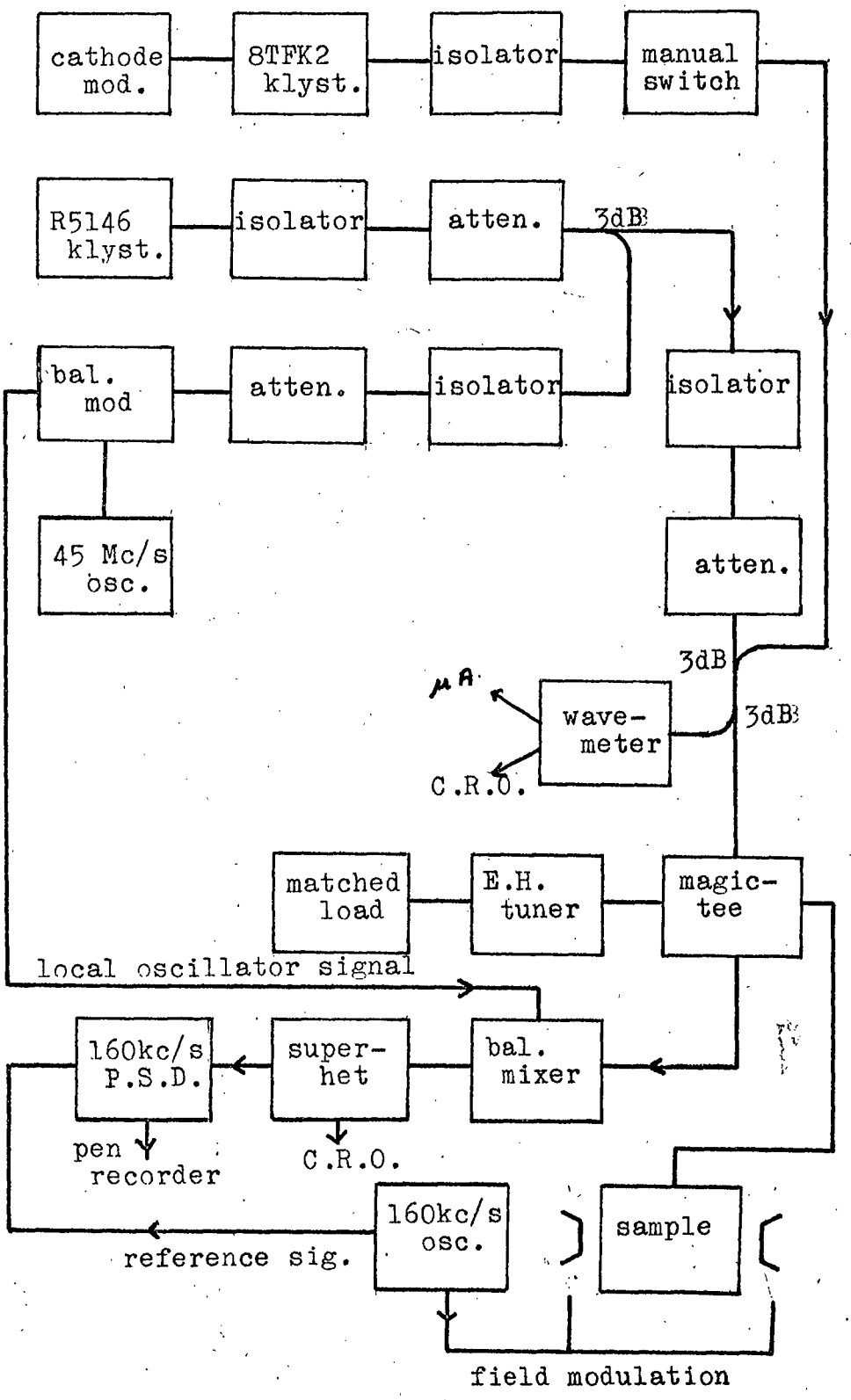

Figure 3.1

Block Diagram of Spectrometer

by an attenuator. Measurement of frequency was accomplished by means of a combined transmission-absorption wavemeter, Mid-Century type MC 22/2A, operating in the absorption mode. Power for the local oscillator was split off at a 3dB coupler, followed by a further isolator in each arm to reduce interaction effects. The bridge element was a magic-tee, Microwave Instruments type WQ 308, and the matching arm of the bridge comprised an E-H tuner, Mid-Century type MC 22/13D, and a matched load. The specimens were generally cut to fit the cross-section of the wave-guide, 0.280" x 0.140", with a length of about 1 cm, and were mounted on a short-circuiting plunger terminating a length of thin-walled (0.012") stainless steel waveguide connected directly to the magic-tee. The usual orientation was with the c-axis in the plane of rotation of the magnetic field, enabling polar angle, θ, to be determined directly. Figure 4.2 indicates the coordinate system appropriate to this situation.

For measurement of relaxation times by the pulse saturation method saturating pulses were obtained from an Elliott water cooled drift-tube klystron, type 8TFK2, providing about 20 Watts at frequencies in the region of 35 Gc/sec. This was powered by an Elliott power unit, type PKU1, modified by the addition of a modulation unit, type 668, supplying a modulated

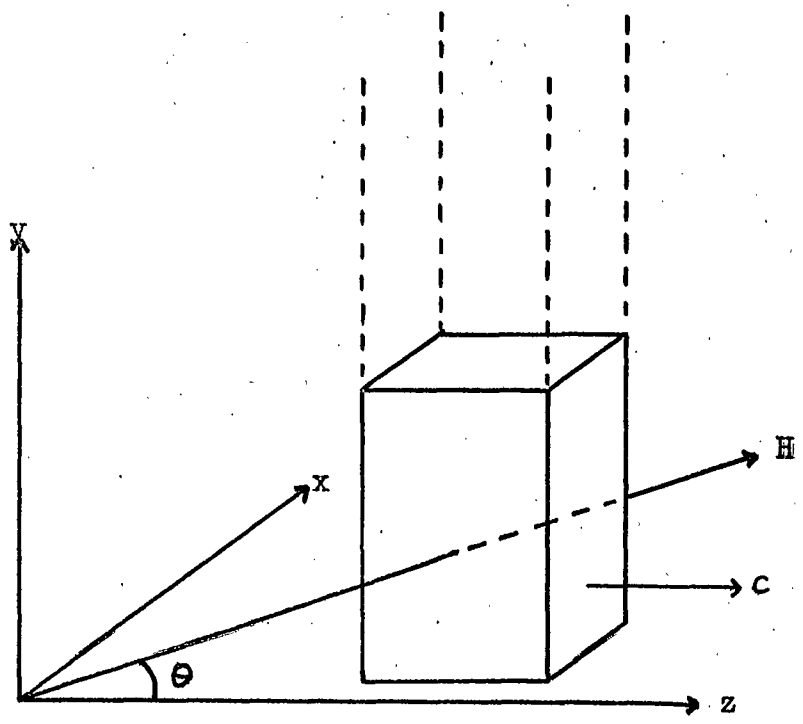

Figure 3.2

Coordinate System for Specimen Orientation
Magnetic Field, H, Rotates in XZ-Plane

potential to the cathode of the valve. The pulse length was variable from 30 μsec to 600 msec with a repetition rate ranging from 0.15 c/sec to 1 kc/sec. The E.M.I. klystron was used to monitor the recovery of the spin system following the saturating pulse, (c.f. Sec. 3.2.4) and the two klystrons were brought into frequency coincidence using the transmission-absorption wavemeter. Once the wavemeter had been set to the frequency of the monitor klystron the power valve was tuned until pulses were observed at the transmission mode output. The two frequencies were then nearly identical.

3.1.2 The Single Klystron Superhet

The normal operation of a microwave superhet requires the use of two klystrons, one each for signal and local oscillator sources. These must be tuned such that the difference in their frequencies falls within the passband of the I.F. amplifier, which from noise considerations (Strum, 1953) is typically chosen to be around 50 Mc/sec. At frequencies in the region of 35 Gc/sec such fineness of control becomes difficult.

The superhet of Brown et al. overcomes this difficulty by deriving the local oscillator power directly ftom the signal power source by means of amplitude modulation of the latter to produce two sidebands spaced from the carrier by frequencies

equal to the I.F. This process was carried out at a crystal diode operated in the transmission mode and driven at 45 Mc/sec. As long as the modulation frequency remains constant, drift of the klystron frequency is relatively unimportant. In the original design the whole of the power was modulated, with the result that both sidebands entered the cavity. This arrangement attracted a certain degree of criticism, partly due to misinterpretation of the original description, and Buckmaster and Dering (1966) stated that the presence of the sidebands in the cavity degraded the sensitivity of the system by 13 dB. The apparatus was subsequently modified to eliminate this and an increase in sensitivity was obtained. From observations on a ruby specimen of known concentration an estimated minimum detection level of around 10^{16} spins/oersted was obtained. In the modified arrangement the modulation was performed in a balanced modulator, consisting essentially of a hybrid-tee, the H-arms of which contain opposite polarity diodes, G.E.C. types VX3136 and VX3171, driven in phase at 45 Mc/sec by an Advance signal generator, type E.2. Only the two sidebands then appear at the E-arm, the carrier being eliminated entirely by the action of the tee, and these are applied to the local oscillator input of the superhet mixer. The signal returning from the cavity is applied to the other input. The crystals operate in the low-

signal square-law region and thus the superhet output is proportional to the power returning from the bridge. The I.F. amplifier consists of eleven stagger-tuned amplification stages followed by a detector. Originally its bandwidth was 10 Mc/sec, a figure appropriate for use with a separate local oscillator, but this was reduced to about 3 Mc/sec with a consequent increase in gain.

3.1.3 The Low-Q Cavity

The specimen under observation was mounted on a short-circuiting plunger terminating a length of thin-walled waveguide, thereby providing a system having a low Q-value. This arrangement originated with the original glass dewar system, having a limited space available in the magnet gap. As ultimate sensitivity was not of the utmost importance in the work on ruby this limitation was tolerable. Measurements of the Q-factor using a technique described by Montgomery (1948) indicated an unloaded value of around 400.

Discussions of the theoretical sensitivity of e.p.r. spectrometers have been given by many workers, but certain of them (Feher, 1956, Goldsbrough and Mandel, 1960, and others) deal only with the situation in which the microwave frequency is locked to the cavity resonance, thereby eliminating the effect of dispersion.

Misra (1962) considered the case in which both χ' and χ'' are detected and showed that unless the cavity is on resonance before paramagnetic resonance occurs dispersion will always accompany absorption. Selection of the required component is carried out by using the E-H tuner, a device capable of presenting an impedance of any phase or amplitude. Use of a circuit element possessing this property for the separation of absorption and dispersion has been outlined by Bloembergen et al. (1948) and is illustrated in Figure 3.3, which represents balance and unbalance in phase and amplitude plotted in terms of complex susceptibility. In each case OP represents the signal returning from the cavity and OQ is the signal reflected from the E-H tuner.

In (a), off resonance, OP equals OQ. As the resonance is traversed the susceptibility describes a closed loop, which is a circle if the absorption is that typical of a damped system. The signal emerging from the bridge is represented in amplitude and phase by the vector QP as P follows the change in χ. By deliberately unbalancing the bridge such that OQ is somewhat less than OP while still being in phase, the situation of (b) is obtained. The signal is still represented by QP, but as resonance is traversed the effect of χ' on QP is greatly reduced while the effect of χ'' on altering the magnitude of the vector dominates.

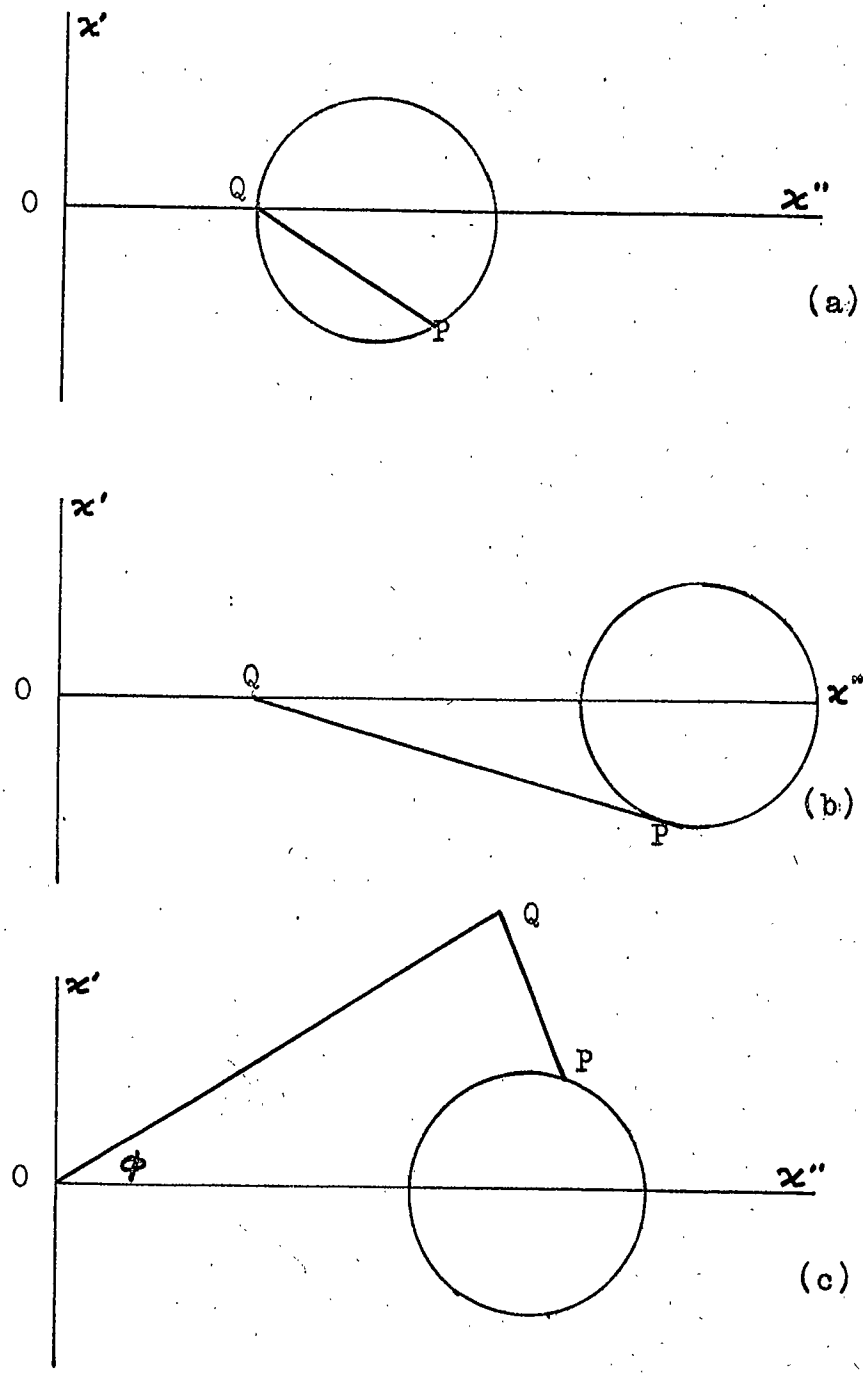

Figure 3.3
Separation of Absorption and
Dispersion by Bridge Balance

This is the condition for the detection of absorption. In (c) a degree of phase unbalance, ϕ, has been introduced. The effect on the vector QP is analogous to that in (b) except that it is now χ' that is responsible for its amplitude changes, whereas the phase changes due to χ'' are relatively small. This is the condition for the observation of dispersion.

3.1.4 The Magnet Assembly

Study of e.p.r. at Q-band necessitates the use of high magnetic fields as a transition having a g-value of 2 occurs at about 12,500 oersteds. The homogeneity of the field must be sufficiently high to prevent spurious broadening of the resonances, and for practical purposes this requires a homogeneity of better than 1 part in 10^5 over a volume of the order of 1 cm^3. The design and construction of high field electromagnets has been discussed by de Klerk (1965).

The magnet used in conjunction with this spectrometer was a Newport Instruments type D, having eight inch diameter pole-pieces with a 4.5 cm gap capable of a maximum field of around 16,000 oersted. Power was supplied by a d.c. generator controlled by a transistorised current stabilising unit. A slow current sweep unit was attached, with a maximum range in either direction of 2 amps.

The magnet was calibrated using a combined proton-lithium resonance magnetometer, and the ability to observe the lithium resonance indicated a field homogeneity of better than 1 part in 5,000 over the probe volume of 4 cm^3. It was found that the field was not linearly dependent on the current in the coils, but tended to saturate with increasing current. To enable linewidths to be measured accurately it was necessary to calibrate the sweep. A nominal sweep of 0.2 amps in the upwards direction in two minutes was used for all linewidth measurements, and the progress of this could be observed on a meter indicating the fraction of the sweep completed. By measuring the field at two points within the sweep, usually the start and a point near the finish, it was possible to calculate the sweep in terms of field units. It was found that the total width of the sweep was dependent on the steady field at the start. This method of calibration was inherently inaccurate as it involved simultaneous measurements of the nuclear resonance and the "sweep completed" meter. It is estimated that the figures obtained are accurate to about 10 %, and this places a limit on the accuracy with which linewidths can be determined.

3.2 ABSORPTION DISPLAY AND MEASUREMENT TECHNIQUES

3.2.1 Video Display

The video display system was simple to use, and provided a convenient means of setting up the spectrometer in readiness for measuring linewidths or relaxation times. A modulation coil was wound around each pole of the magnet and these were driven from the mains supply to give a modulation field of about 30 oersted amplitude. The superhet output was displayed on an oscilloscope giving a visible representation of the resonance signal. This facility was used for the initial setting-up procedure and in particular for the balancing of the bridge to eliminate dispersion. It was found convenient to adjust the two arms of the E-H tuner simultaneously as this gave the most rapid convergence to the balance point. This empirical observation has been discussed by Cullen (1965). Elimination of dispersion was checked visually by sweeping the steady field slowly through the resonance. The absence of any overshoot on the baseline indicated a true absorption signal.

3.2.2 Synchrodyne Detection

The synchrodyne detection system is widely used in e.p.r. spectroscopy since it provides a sensitive, noise-free means of recording resonance lineshapes. A small amplitude modulation is

superimposed on the steady field, which is in fact slowly swept through the resonance. Expansion of the spectrometer output as a Taylor series (Pake, 1962) or a Fourier series (Poole, 1967) shows that this is a signal at the modulation frequency, amplitude modulated with a signal representing the first derivative of the resonance shape. By beating this with a reference signal at the same frequency in a phase-sensitive detector a detected signal proportional to $d\chi/dH$ is obtained. As only signals within a narrow band around the modulation frequency need be accepted, much noise that might otherwise be present can be eliminated. The operation of a synchrodyne system is shown in Figure 3.4

Use of a synchrodyne detection system may result in instrumental distortion of lines unless certain precautions are taken. The effect of modulation amplitude on Lorentzian lineshapes has been studied from a theoretical point of view by Wahlquist (1961), Burger and Gunthart (1962) and Arndt (1965), and a similar treatment by Smith (1964) considered both Lorentzian and Gaussian shapes. The corresponding effects on moments have been considered by Halbach (1960). In general, increased modulation amplitude results in increased broadening and ultimately distortion. Tables given by Smith relate observed and actual linewidths to the modulation amplitude expressed as a fraction of the actual width,

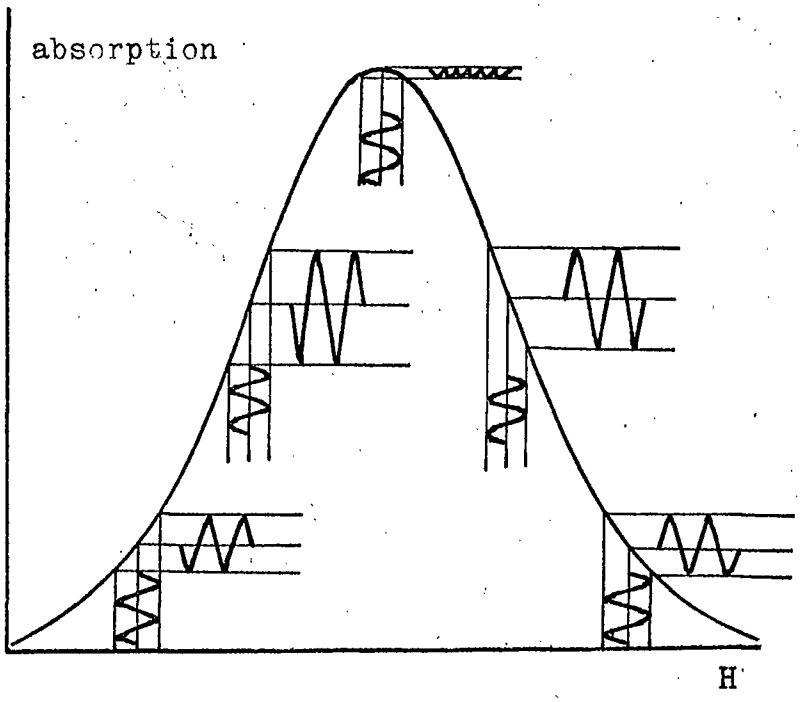

Figure 3.4

High Frequency Modulation

Showing how the amplitude and phase of the spectrometer output (horizontal waveforms) is related to the field modulation (vertical waveforms).

and for both Gaussian and Lorentzian shapes modulation amplitudes of less than one tenth of a linewidth cause negligible distortion.

The effect of modulation frequency is not so noticeable, and the work of Macomber and Waugh (1965) leads to the condition that the modulation frequency should be much less than the width of the line expressed in terms of frequency. Thus the minimum width which it would be practical to observe with a 100 kc/sec system would be 0.1 oersted compared with the widths of 10 or more oersteds observed here.

The system in use here operated at 160 kc/sec. An oscillator provided a fixed level reference signal and a variable level output which was applied via a matching transformer to two small coils attached to the waveguide in the vicinity of the specimen. The superhet output, together with the reference signal, was applied to the phase-sensitive detector. After amplification in a current amplifier, the signal was used to drive a 0 - 5 mA recording meter.

Modulation amplitude broadening was investigated by measuring linewidths in freshly prepared DPPH, a free radical giving a line of accurately known width (Holden et al., 1950) which is widely used as a resonance standard. At maximum modulation amplitude the line, as measured, had a width of 5.5 oersted while

at the minimum amplitude its width was the recognised figure of 1.6 oersted. From the data given by Smith, the maximum modulation amplitude was estimated to be 0.9 oersted, giving a distortion of less than 1 % on a line of width 15 oersted. As an illustration of the effects of modulation broadening, the lines observed in DPPH are shown in Figure 3.5.

3.2.3 Line Measurement Techniques

The usual procedure for measurement of absorption lines was as follows. The spectrometer was set up to observe absorption, using the video display system described in Section 3.2.1. The 50 c/sec sweep was then removed, and with the 160 kc/sec amplitude kept to the minimum possible the steady field was swept through the resonance position at a rate of about 1 oersted/sec. The bandwidth of the 160 kc/sec amplifier was kept to a minimum, usually 100 c/sec, and the gain and meter sensitivity controls were used to prevent the meter from going off scale. Figure 3.6 shows a typical derivative chart obtained in this way. During recording, the start and finish of the sweep were marked, and calculation of ΔH_{ms} then involved just two measurements of length plus reference to the sweep calibration. Calculation of $\Delta H_{\frac{1}{2}}$ was carried out by numerical integration of the derivative trace, a procedure which was not carried out in every case.

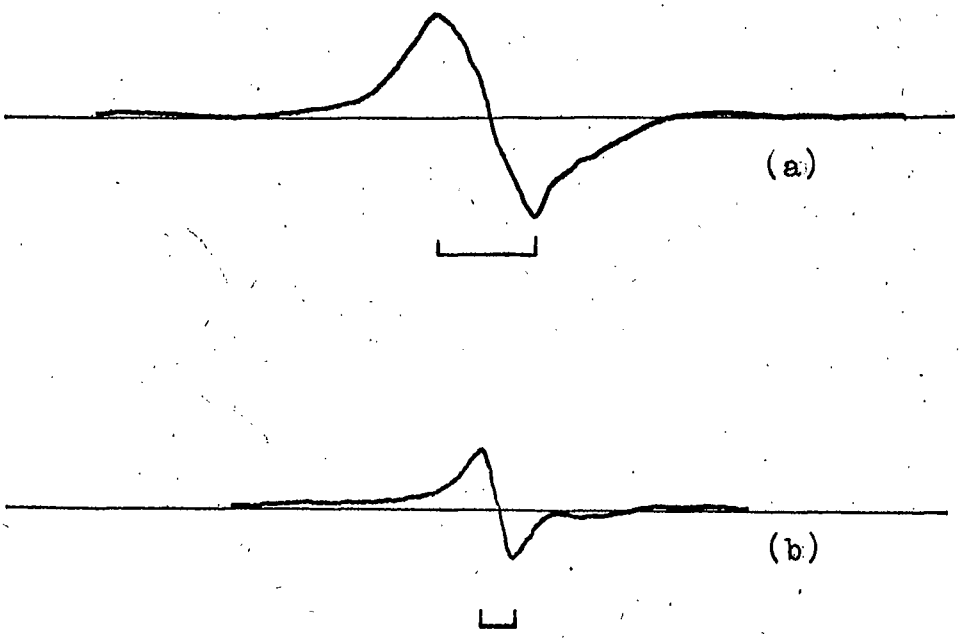

Figure 3.5

Modulation Distortion of E.P.R. Absorptions in DPPH

(a) Modulation amplitude = 0.9 oe, ΔH_{ms} = 5.5 oe

(b) Modulation amplitude < 0.1 oe, ΔH_{ms} = 1.6 oe

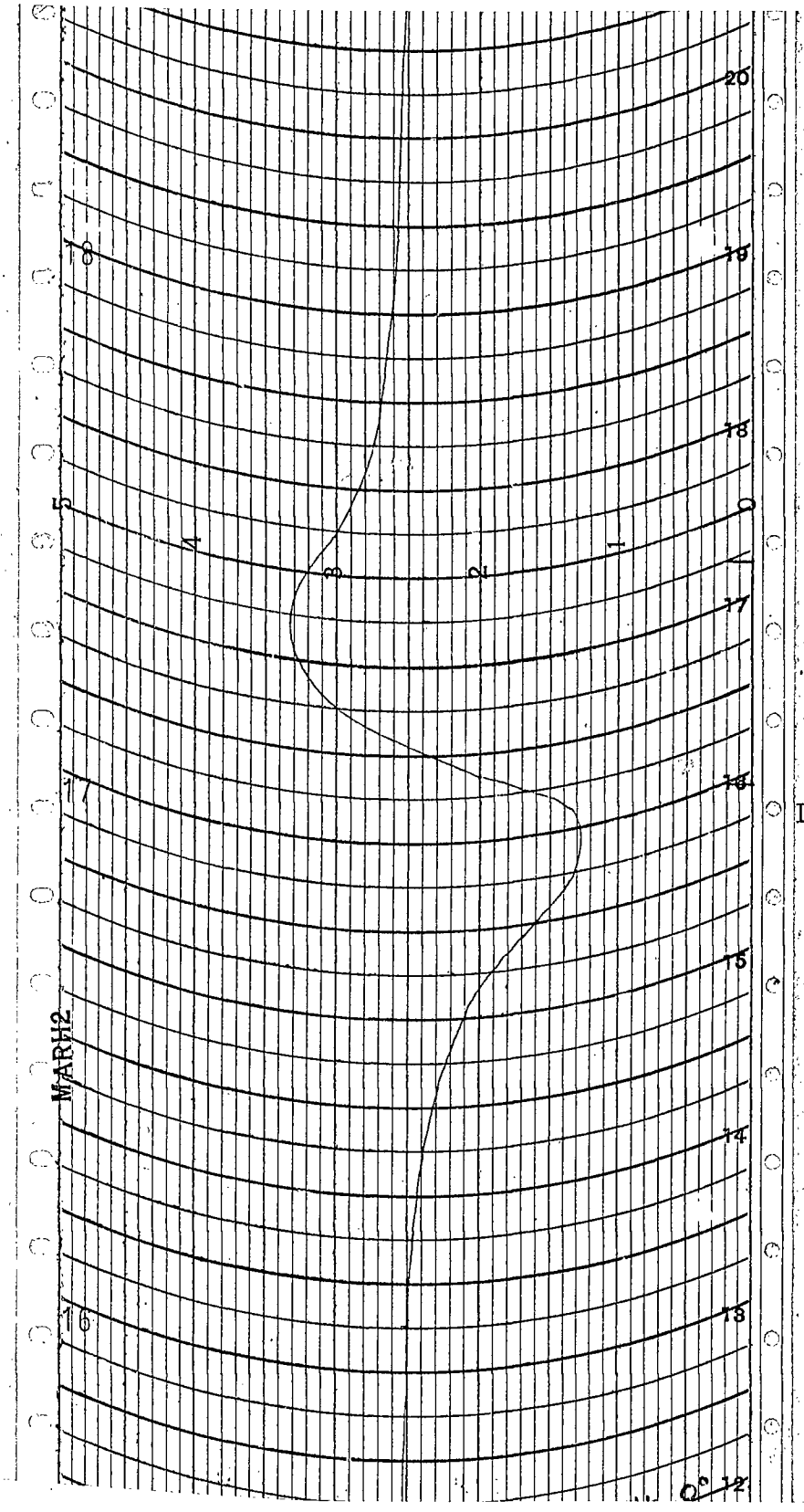

Figure 3.6
Derivative Chart

Ultimately, this calculation was programmed for the computer, allowance being made for the curvature of the y-axis on the charts. Coordinates of the integrated line, $\Delta H_{\frac{1}{2}}$ and the centroid of the line were computed, much of this data being required for the subsequent "Variance" analysis (c.f. Chapter 4). It was estimated that in addition to the error present in ΔH_{ms}, due almost entirely to the sweep calibration, an additional inaccuracy of 2 % was introduced in this calculation of $\Delta H_{\frac{1}{2}}$.

3.2.4 Relaxation Display and Measurement

In the pulse-saturation method of measuring spin-lattice relaxation times (Davis et al., 1958) the behaviour of the spin system is observed following the removal of a saturating pulse of power. At the conclusion of the pulse the populations of the levels are equalised, but relaxation processes conspire to return the system to the thermal equilibrium state. During this process the population difference is monitored by observing the absorption of power from a low level source, an absorption which at low signal levels is proportional to the population difference.

Solution of the rate equations for a two level system results in an exponential relaxation to the thermal equilibrium state, with a single time constant. For a multilevel system the levels other than those defining the transition must be considered,

and in general a system of n levels will exhibit a relaxation characterised by (n - 1) relaxation times (Grant, 1964a). In interpreting the results of relaxation time measurements this factor must be taken into account.

The technique for the display and measurement of relaxation curves was as follows. Once a balanced absorption had been obtained, the 50 c/sec modulation was removed and the field was set at the centre of the absorption. The frequencies of the power and monitor klystrons were brought into coincidence, and pulses, usually 1 μsec wide were applied to the specimen. The oscilloscope display then showed the pulses and the subsequent relaxation to equilibrium as indicated by absorption of monitor power. The superhet receiver proved very insensitive to the effects of the large pulses of power, and the dead time immediately following a pulse was found by Mason to be of the order of 5 μsec. This effect was due to the gross disparity between signal and local oscillator powers during the pulses.

For photographic recording of relaxation curves, the pulse repetition rate was made very slow giving an effective single-shot operation, with the timebase of the Tektronix type 531A oscilloscope being triggered from the pulse. Photography was carried out on Polaroid type 47 film, a typical photograph being

shown in Figure 3.7. The relaxation times were derived from photographs of this type by replotting the coordinates in semi-logarithmic form, and obtaining the gradient of the resulting straight line, or lines if more than one exponential was present. The accuracy of measurements of this nature was estimated by Mason to be about 10 %, mostly due to uncertainties in bridge balance.

3.3 CRYOGENIC TECHNIQUES

All measurements on Nd:$CaWO_4$ and relaxation measurements on ruby necessitated the use of temperatures in the liquid helium range. The existing glass tail dewars (Thorp, 1965) had provided very good, if somewhat hazardous, service, but at the expense of limited space in the magnet gap. To allow for greater versatility of use of the spectrometer, a metal cryostat was designed by Oxford Instruments Ltd., the construction of which is indicated in Figure 3.8. It will be seen that the interspace is pumpable and that in the tail region there are only three walls as compared with four in the glass system. As a result there is room, if required, to insert waveguide of any size up to and including X-band.

The technique of transferring liquid helium into the cryostat was quite straightforward. Pre-cooling with liquid nitrogen took about three hours, the temperature of the specimen being monitored by means of a copper-constantan thermocouple strapped

monitor power
absorption

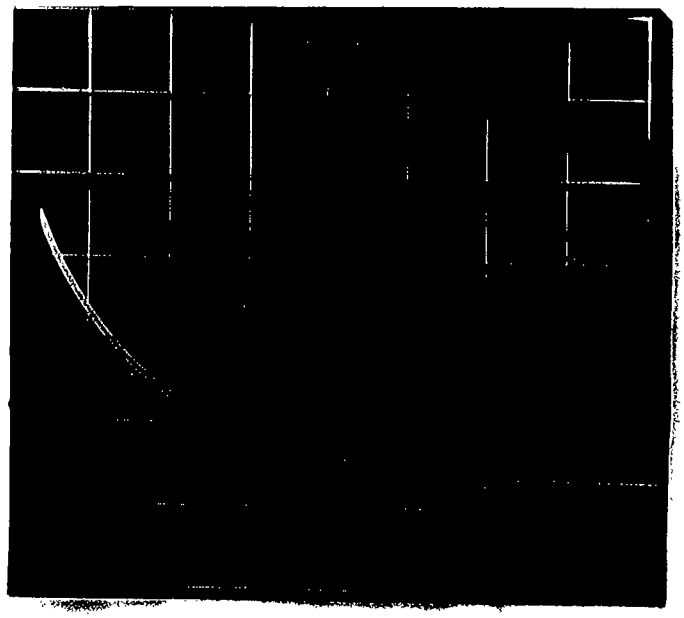

time

Figure 3.7
Relaxation Exponential

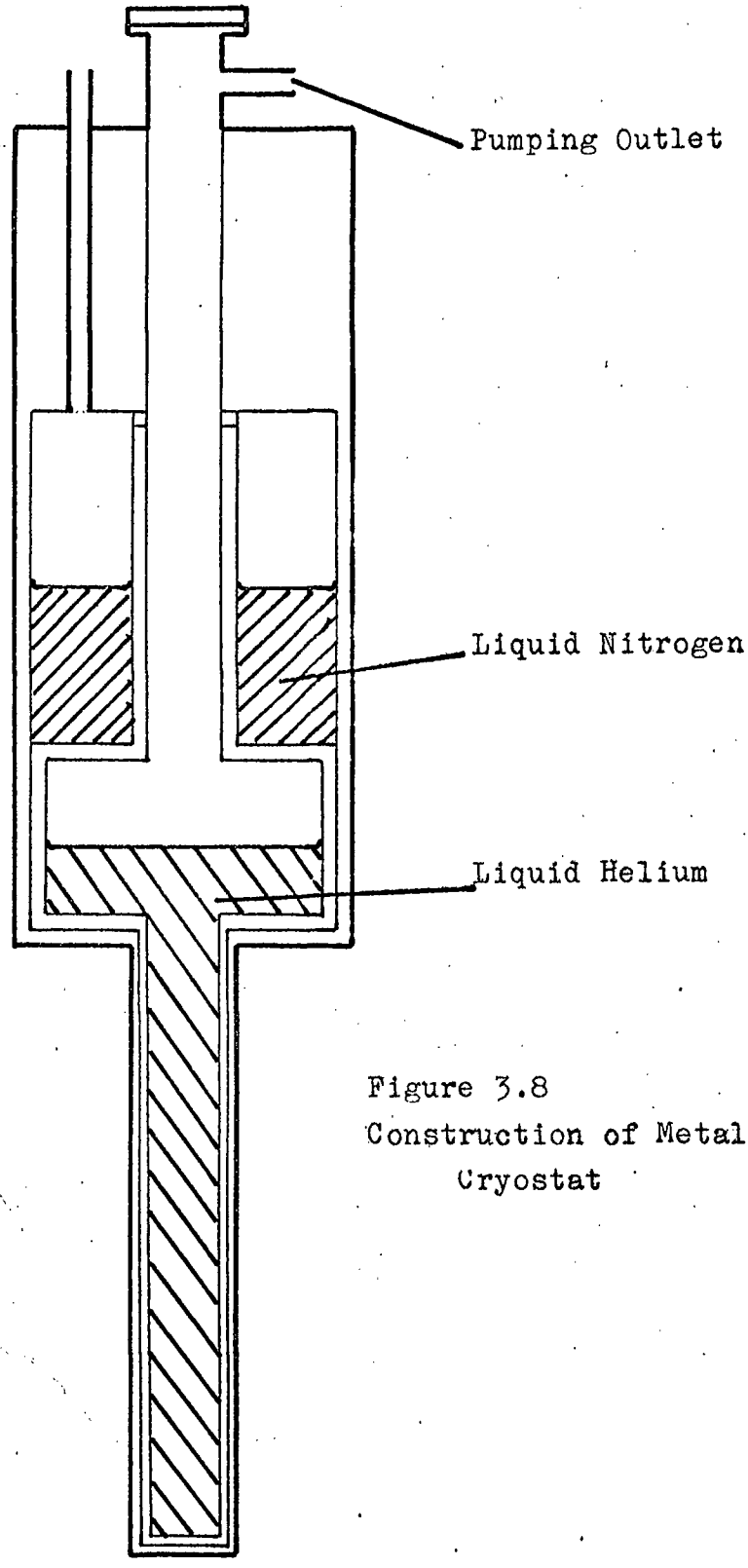

Figure 3.8
Construction of Metal
Cryostat

to the outside of the waveguide. Liquid helium was transferred via a metal syphon, ten minutes sufficing for the transfer of a litre or so without excessive boil off of gas. Once this quantity had been transferred, a temperature of 4.2 ^{o}K could be maintained for several hours. To obtain temperatures below this the inner dewar space was pumped using an Edwards rotary pump. Temperatures below 4.2 ^{o}K were estimated from measurements of the vapour pressure above the liquid using a McLeod Gauge (Clement, 1955).

Chapter 4

E.P.R. LINEWIDTHS IN RUBY - I HOMOGENEOUS BROADENING

4.1 HOMOGENEOUS BROADENING MECHANISMS

The Bloch equations, discussed earlier, are strictly only applicable to a two-level system containing particles whose magnetic moments do not interact strongly, either with each other or with other particles present in the system. In general this is not true of a paramagnetic system, and interactions of the type neglected in the Bloch analysis may play a substantial part in the broadening of the e.p.r. absorptions. In describing interactions of this type, distinction must be drawn between the terms "homogeneous" and "inhomogeneous" as applied to broadening mechanisms by Portis (1953) and modified slightly by Siegman (1964).

An inhomogeneous broadening mechanism is one that spreads the resonant frequencies of different spins over some range, widening the response of the system as a whole without widening the response of any individual spin. On the other hand, a homogeneous broadening mechanism extends the response of every individual spin, and broadens the response of the system as a whole by increasing the coupling between different spins. Consequently, excitation applied to one member of a homogeneously broadened system is shared between all the spins, whereas in the inhomogeneous case particular spins can be excited at their

resonant frequency without transferring energy to neighbours resonant at different frequencies. The present chapter will be devoted entirely to the effects of homogeneous broadening, inhomogeneous effects being dealt with subsequently.

Three factors are chiefly responsible for homogeneous broadening.

a) Spin-Lattice Relaxation

If the lifetime of a quantum state is finite and known, by the Uncertainty Principle there must be an uncertainty in its energy. The lifetime of a spin in an excited quantum state is just the spin-lattice relaxation time, and the lower limit of linewidth is governed by the relation:

$$\Delta f \geq 1/T_1 \qquad (4.1)$$

where Δf is the width of the line in frequency units. In many maser materials the relaxation time is sufficiently long for this mechanism to be relatively negligible.

b) Dipolar Interactions

Each individual spin in a magnetic system is subjected not only to any externally applied magnetic field, but also to the local fields of neighbouring magnetic dipoles. The magnetic field, H, at a distance r from a dipole of moment μ has a value:

$$H \simeq \mu/4\pi r^3 \qquad (4.2)$$

and the importance of this can be gauged from the fact that at a distance of 6 A.U. (a typical inter-site distance) from a dipole of strength one Bohr Magneton the field is about 50 Gauss. The necessity of dilution to reduce spin-spin effects can be readily appreciated, as the resultant field at the site of any spin is the sum of the effects of its neighbours.

c) Exchange Interactions

Paramagnetic spins may in some cases be located relative to one another such that powerful short-range exchange forces become effective. These forces are due to overlap of electron orbitals, either directly or via a third atom, and in crude terms the interaction is one which attempts to align the spins parallel or antiparallel. In highly concentrated materials this leads to ferromagnetism or antiferromagnetism respectively. The interaction may be written in the form $J(S_1.S_2)$, and is said to be isotropic if its value depends solely on the scalar product, and hence on the relative orientations, of S_1 and S_2. In practice, only s-orbitals exhibit isotropic charge densities, and consequently anisotropic exchange might generally be expected. Depending on the relative strength

of the dipolar interactions, exchange may greatly influence the shape of e.p.r. absorptions.

4.2 THEORY OF HOMOGENEOUSLY BROADENED LINES

4.2.1 Calculation of Moments

The first rigorous mathematical description of dipolar broadening was given by Van Vleck (1948) who derived expressions for the second and fourth moments of absorption lines under certain limitations. Starting from a Hamiltonian that included Zeeman, exchange and dipolar energies, it was assumed that magnetisation of the particles was purely spin, that exchange was isotropic and that the system was an isolated Kramers' doublet at a temperature sufficiently high for the levels to be equally populated. The Hamiltonian was expanded in terms of the operators S_+ and S_-, and certain terms corresponding to transitions of the type $\Delta M = 0$, ± 2, ± 3, were discarded. By definition, the mean square frequency, i.e. the second moment, is given by:

$$\langle f^2 \rangle_{av} = \frac{\sum_{nn'} \{ f_{nn'} | \langle n' | S_x | n \rangle |^2 \}}{\sum_{nn'} \{ | \langle n' | S_x | n \rangle |^2 \}} \qquad (4.3)$$

in which $f_{nn'}$ is the frequency corresponding to the transition between the states $|n'\rangle$ and $|n\rangle$, and S_x is equal to $\sum_j S_{xj}$, where S_{xj} is the x-component of the spin angular momentum of the j-th atom. This expression can be written in the form:

$$\langle f^2 \rangle_{av} = \frac{- \mathrm{Tr} | \mathcal{H} S_x - S_x \mathcal{H} |^2}{\hbar^2 \, \mathrm{Tr}(S_x)^2} \qquad (4.4)$$

where Tr represents the trace, or diagonal sum, of the matrix and $\mathcal{H}$ is the retained part of the Hamiltonian, Using this representation, evaluation of the Hamiltonian for each individual atom becomes unnecessary as the diagonal sum of a matrix remains constant regardless of the choice of system of quantisation. The retained part of the Hamiltonian is of the form:

$$\mathcal{H} = H_0 \beta \sum_j S_{xj} + \sum_{k>j} A_{jk} S_j \cdot S_k + \sum_{k>j} B_{jk} S_{zj} \cdot S_{zk} \qquad (4.5)$$

where the second term represents exchange and the third dipolar interaction. $S_j \cdot S_k$ commutes with S_x $(= \sum_j S_{zj})$ and terms containing this disappear from the expression for the second moment, from which Van Vleck concluded that exchange plays no part in determining the second moment. Evaluation of the traces led to a generalised result for the second moment, and a similar, more complex calculation gave the fourth moment, which did include terms representing exchange.

Subsequently, Kittel and Abrahams (1953) extended the theory to cover a magnetically dilute system, and by assuming the absence of exchange showed that at paramagnetic concentrations below 0.01 % the dipolar line would be Lorentzian in shape, having a width proportional to the concentration, whereas in the region above 0.1 % the line would become Gaussian, with a width proportional

to the square root of the concentration. More recently Kaplan (1966) has described a modification which removes the high-field assumption made at the start of the Van Vleck theory.

A method of approach somewhat similar to that taken by Van Vleck was that of Pryce and Stevens (1950) and, although they only derived the second moment, in some respects their result is capable of more general application than that of Van Vleck. Their expression for the second moment, derived under assumptions similar to those made by Van Vleck, showed no dependence on exchange. Glebashev (1956) adopted this approach in his calculation of the second, fourth and sixth moments, as did Dolgopolov and Zhogalev (1966) in their derivation of the temperature dependence of moments. They found that the second moment increased exponentially with temperature until some saturation point was reached.

Extension of the theory to systems posessing crystal-field splitting of the ground state followed, with Ishiguro et al. (1951) considering ions of the spin S=1 and Kambe and Ollom (1956) the central line of a system posessing non-integral spin. Kopvillem (1960) extended this work to embrace a generalised multilevel system exhibiting crystal-field splitting and anisotropy of g-value, and showed that under these conditions exchange enters

the expression for the second moment.

4.2.2 Calculation of Line Shapes

In most cases, calculation of moments of higher order than second proves extremely difficult, and consequently little information regarding the shape or width of the lines is obtainable by this means. Moreover, Grant (1964b) has shown that a knowledge of moments only, even if of a large finite number, yields no information about the complete behaviour of the function within any finite interval as long as an infinite number of higher moments remains unknown. To illustrate this point he shows a Gaussian, several lines of Lorentzian form and a modified delta-function, all posessing the same low order moments.

To attempt to obtain the lineshape directly, Anderson and Weiss (1953) discussed paramagnetic resonance absorption in terms of their model of "random frequency modulation". It was assumed that a spin absorbs a single frequency, which varies over the distribution determined by the dipolar local fields, but that this frequency varies randomly in time at a rate governed by the exchange interaction. Assuming that the random frequency modulation is Gaussian, as resulting from the superposition of many small effects, they obtain the result that when strong exchange interactions are present the line should be Lorentzian with Gaussian

wings. By comparison of their results for moments with those obtained from the Van Vleck theory, two adjustable parameters were fitted, enabling the linewidth to be calculated. The effects of the crystal field were included crudely at a late stage in the calculation. This general approach was developed by Kubo and Tomita (1954) who showed that if there was defined a relaxation function g(t), representing the behaviour of the magnetisation of the system following the removal of a perturbation, then the frequency dependent susceptibility, χ , could be represented by:

$$\chi(f) = \chi' - i\chi'' = \chi_o - i.\frac{f}{V}\int_o^\infty g(t).\exp(-ift)dt \qquad (4.6)$$

where χ_o is the static susceptibility, and V is the volume of the specimen. Thus the absorption lineshape can be constructed from a knowledge of the relaxation function, and in the case of strong exchange Kubo and Tomita confirmed that a Lorentzian line would be expected.

Grant and Strandberg (1964a) abandoned the hitherto conventional approach to lineshape based on single particle considerations, and considered instead the Hamiltonian of a pair of particles having terms representing Zeeman energy, the effects of crystal field, exchange interactions and dipolar interactions. Exchange was assumed to be isotropic, cutting off at a radius r_1,

and the extreme cases of strong and weak exchange were considered. Within a radius r_o ($r_1 > r_o$) discrete sites were considered, but beyond this it was assumed that a continuous distribution of dipoles was a sufficient representation of the system. The possibility of a non-random distribution of spins was allowed for. The discussion assumed that the dipole interaction was small relative to the Zeeman energy, and for e.p.r. transitions this was shown to lead to very little error. The result of a somewhat complex mathematical treatment was a relaxation function, whose Fourier transform gives the lineshape as a function of frequency. In discussing the moments of the line, they showed that these are essentially the Maclaurin coefficients of its Fourier transform, and at vanishing concentrations are approximately linearly dependent on concentration. At low concentrations the lineshape is indistingishable from a Lorentzian and has a width proportional to concentration, whereas at high concentrations it is Gaussian with a width proportional to the square root of concentration.

4.3 E.P.R. LINEWIDTHS IN RUBY

4.3.1 Interpretation by Moments

The problem of the shapes and widths of the e.p.r. absorptions in ruby has attracted attention from many workers. Manenkov and Federov (1960) examined a number of specimens in the

concentration range 10^{-2} - 10^{-5} (Cr-Al) and observed second moments somewhat less than predicted by the Pryce and Stevens theory. In addition they noted that the lines were unaffected by cooling from 300 ^{o}K to 77 ^{o}K, indicating the relative unimportance of spin-lattice interaction as a line broadening mechanism, and that at low concentrations there was a trend towards a constant width of about 12 oersted. Klyshko (1964) observed similar discrepancies between dipolar theory and experiment and concluded that exchange interactions played a major part in determining the width of the ruby e.p.r. absorptions. Manenkov and Federov had suggested exchange as a possible broadening mechanism, but had concluded that owing to the degree of dilution of their specimens this was not the major effect. Al'tshuler and Mineeva (1963) explained the results of Manankov and Federov on the basis of exchange alone, and obtained reasonable agreement with experiment in the concentration region 0.2 % - 0.6 %, although at lower concentrations theory and experiment diverged. They assumed an isotropic exchange interaction of the form:

$$W_{ij} = J(r_{ij})S_i.S_j \qquad (4.7)$$

where:

$$J(r_{ij}) = J(r_o)/r_{ij}^{n} \qquad (4.8)$$

Here, S_i and S_j represent spins at sites i and j, separated by

a distance r_{ij}. The distance r_o is given by:

$$J(r_o) = 2D \qquad (4.9)$$

The calculation was performed with the summation taken only in the region $r > r_o$, as particles closer than r_o form pairs giving spectral lines remote from the main lines (Statz et al., 1961). It was concluded that $J(r_o)$ was about 2.5 cm^{-1}, and that n had a value of 12. Klyshko explained his results by neglecting dipolar interactions over the range $r < r_o$ and exchange at distances greater than r_o. His value of r_o was obtained from experimental values of the second moment.

5.3.2 Results of Grant and Strandberg

Grant and Strandberg (1946b) applied their theory to the e.p.r. lines observed in ruby, and obtained good agreement between theory and experiment. Firstly, they discussed the lineshape resulting from the continuous distribution of dipoles cutting off at an inner radius r_o. At low concentrations (< 0.5 % for the +1/2 to -1/2 transition and < 0.3 % for the $\pm 3/2$ to $\pm 1/2$ transitions) the line was Lorentzian having a concentration dependent width given by:

$$\Delta H_{\frac{1}{2}} = 12.6 \text{ oersted per } 0.1 \text{ \% Cr} \qquad (4.10)$$

At higher concentrations the proportionality fell off and the

dipolar line became Gaussian. To this line was added the effect of interactions between the chromium ions and ions of the host lattice, isolated as a Gaussian of width 12.7 oersted in the limit of vanishing concentration. A further step in the calculation involved the computation of the lattice sum for the discrete sites lying within the radius r_o and the evaluation of the dipole and exchange effects within this radius.

To first order, interactions between the chromium ions themselves are independent of interactions between the ions and the lattice. In these circumstances the overall lineshape is obtained by convolution of the various components, and at low concentrations this results in domination of the lineshape by the Gaussian "residual line" with a near independence of concentration up to about 0.1 %. As concentration increases the Lorentzian dipolar component takes over, but this trend is reversed as the dipolar line becomes itself Gaussian.

The results were calculated for several degrees of microscopic clustering, and in general the effect of near neighbours, while of some significance with regard to moments, is negligible with respect to the actual shape of the central portion of the +1/2 to -1/2 line and causes slight narrowing of the $\pm 3/2$ to $\pm 1/2$ lines at high concentrations.

The residual width of the +1/2 to -1/2 transition at $\theta = 0$ was observed by Manenkov and Federov and ascribed to hyperfine interactions between chromium and aluminium ions. Grant and Strandberg rule out crystal field effects, crystalline misorientations, anisotropy of g-value and microscopic clustering as the cause of this. However it was acknowledged that macroscopic clustering might be responsible for some of the broadening. Spin-lattice relaxation contributes about 1 % of the width, and magnetic dipole interactions between chromium ions and aluminium nuclei result in a Gaussian of 3.7 oersted width, but this still leaves a large amount of broadening unexplained. Grant and Strandberg suggest that this might be explained on the basis of covalent bonding between chromium and aluminium ions, either directly or via the oxygen atoms (Anderson, 1959) and procede to calculate the required degree of mixing of aluminium 3s wave function into chromium 3d as about 0.036. Stettler and Veigele (1964), reporting on the effect of hydrostatic pressure on N.M.R. absorptions, suggest that the maximum degree of covalency in ruby is about 0.15.

4.4 EXPERIMENTAL RESULTS ON RUBY

4.4.1 Description of the Results

To investigate the homogeneous broadening present in ruby, measurements were made on the +1/2 to -1/2 transition at

orientation $\theta = 0^{\circ}$, chosen for reasons connected with the elimination of inhomogeneous effects. At this orientation the transition occurs between the levels of the Zeeman doublet $|\pm 1/2\rangle$, and consequently strain-induced fluctuations in the zero-field splitting have no first order effect on the resonance and produce no broadening. In addition, the rate of change of resonance field with polar angle, $dH/d\theta$, is zero at this orientation, thereby eliminating axial misorientations as a possible source of broadening. At frequencies in the region of 35 Gc/sec this transition occurs at a magnetic field of around 12,600 oersted and is well isolated from any other absorption in the chromium spectrum. The presence of iron in some specimens gives rise to an absorption about five linewidths away, but at separations of this magnitude the cross-relaxation time is relatively long (Mason, 1966) and no distortion of the absorption occurs. The measurements were made at room temperature, the justification for this being the negligible relaxation broadening and the convenience. Figure 4.1 shows the values of ΔH_{ms} observed for the various specimens, plotted as a function of concentration which, for convenience, is shown on a logarithmic scale. On the same axes is plotted the concentration dependence of this parameter as predicted by Grant and Strandberg for this transition at this orientation. This shows

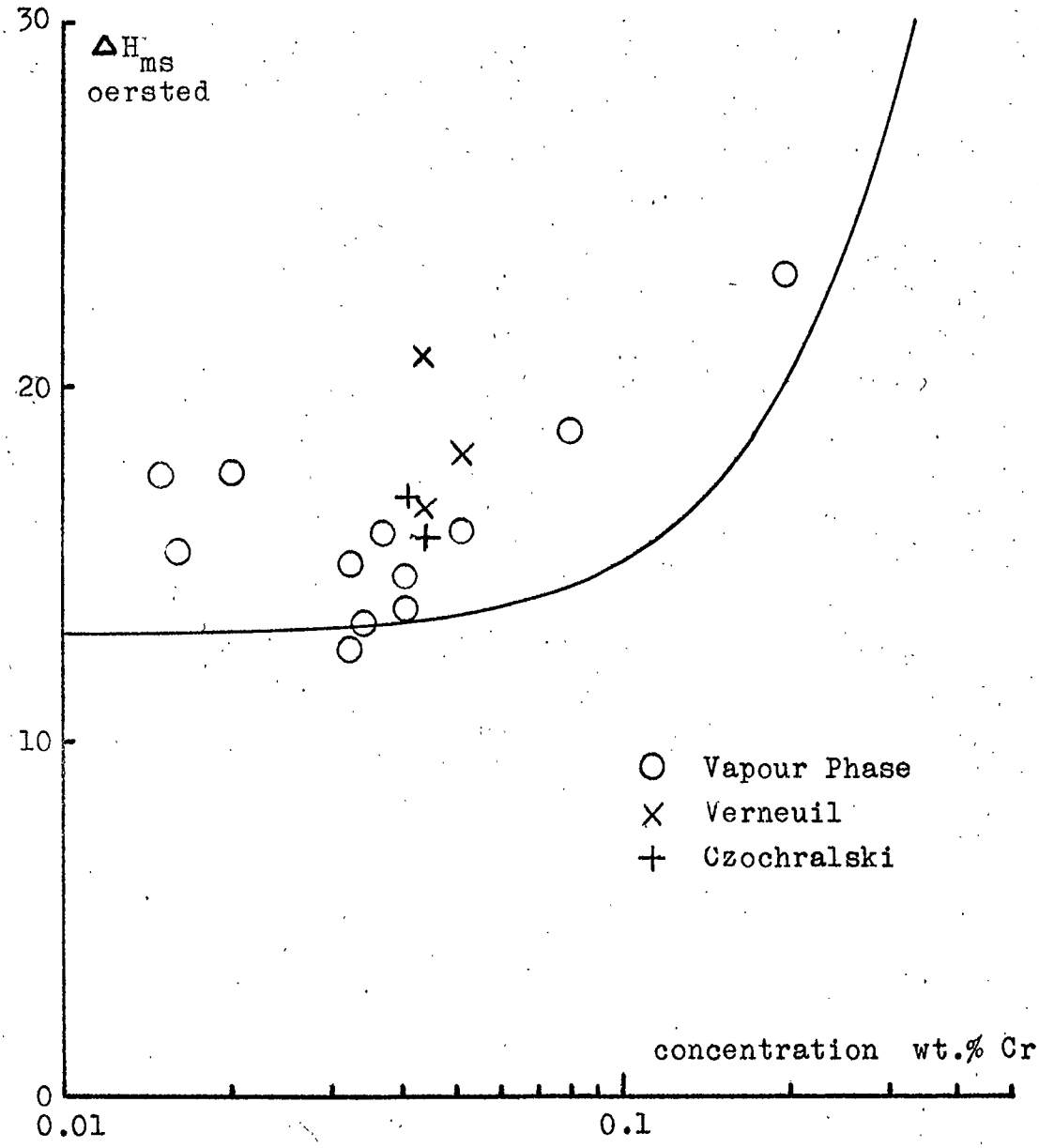

Figure 4.1

Concentration Dependence of Derivative Width
+1/2 to -1/2 transition, $\theta = 0^{o}$

clearly the theoretical concentration independence at low concentrations, and it can be seen that the experimental results tend to reflect this independence, while remaining generally greater than the predicted values. However, in one or two cases this was not so and results very close to theory were obtained. In each case the linewidth shown represents the mean of several measurements, often made on different occasions. The accuracy of the measurements was discussed in Chapter 3, and in general the figures were reproducible to within the estimated degree of accuracy of an individual measurement.

Figures of $\Delta H_{\frac{1}{2}}$ were obtained from the computer analysis of the derivative charts. In addition the ratio R ($R = \Delta H_{\frac{1}{2}} / \Delta H_{ms}$) was calculated. Figure 4.2 shows the dependence of $\Delta H_{\frac{1}{2}}$ on chromium concentration, together with the predicted variation of this quantity. Apart from the single "high-concentration" specimen, there is no trend towards any form of concentration dependence, but the widths are greater than predicted with a somewhat greater scatter than the results of ΔH_{ms}.

The ratio R provides an indication of the shape of the absorptions. For a Gaussian line it has a value of 1.175 whereas for a Lorentzian it equals 1.734. In general the observed lines were nearer Gaussian than Lorentzian, in agreement with the results

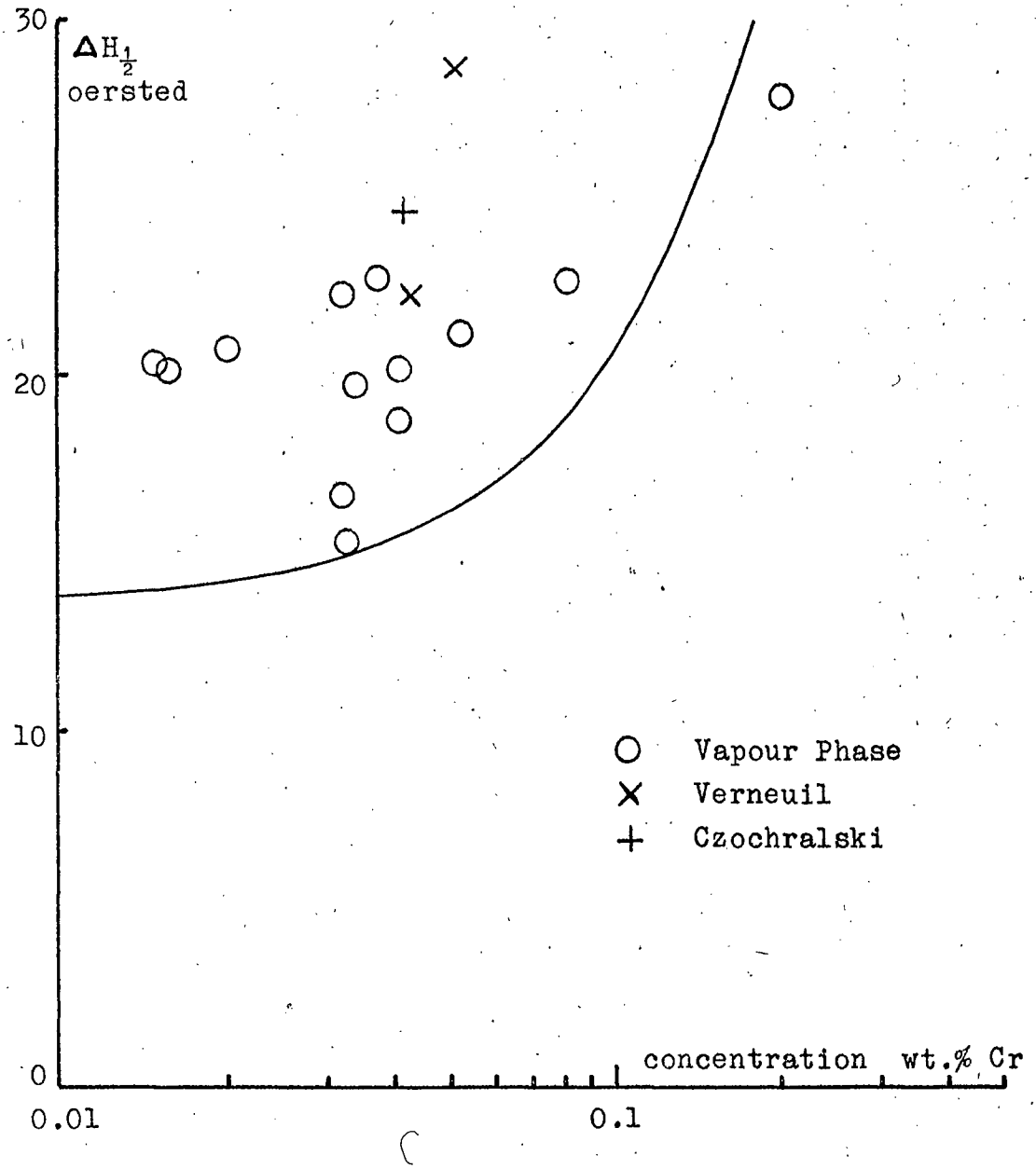

Figure 4.2

Concentration Dependence of Half-Power Width
+1/2 to -1/2 transition, $\theta = 0^{\circ}$

of other workers (Manankov and Federov, Grant and Strandberg). Figure 4.3 shows $\Delta H_{\frac{1}{2}}$ plotted against ΔH_{ms} with the Lorentzian and Gaussian limits included for comparison.

4.4.2 Resolution of Broadening Mechanisms

It was seen in a previous section that the lineshape expected from e.p.r. measurements in ruby is a convolution of a Gaussian of constant width with a Lorentzian whose width is concentration dependent, together with a term representing the near-neighbour lattice sum. This latter term has little effect on the lineshape, although it does affect the moments, and it will be neglected in what follows. In two particular cases of "self-folding" functions, functions that reproduce themselves in shape on convolution with another function of the same type, the width of the final line is directly related to the widths of the components. The cases of interest here are the Gaussian and the Lorentzian, and the linewidth resulting from convolution of any number of functions of one of these types is given by:

$$\Delta H^n = \sum_i \Delta H_i^n \qquad (4.11)$$

where n is 1 for the Lorentzian and 2 for the Gaussian. In the general case of the convolution of two or more arbitrary functions a relation of this nature does not hold and the width of the resultant line is not immediately accessible from a knowledge of

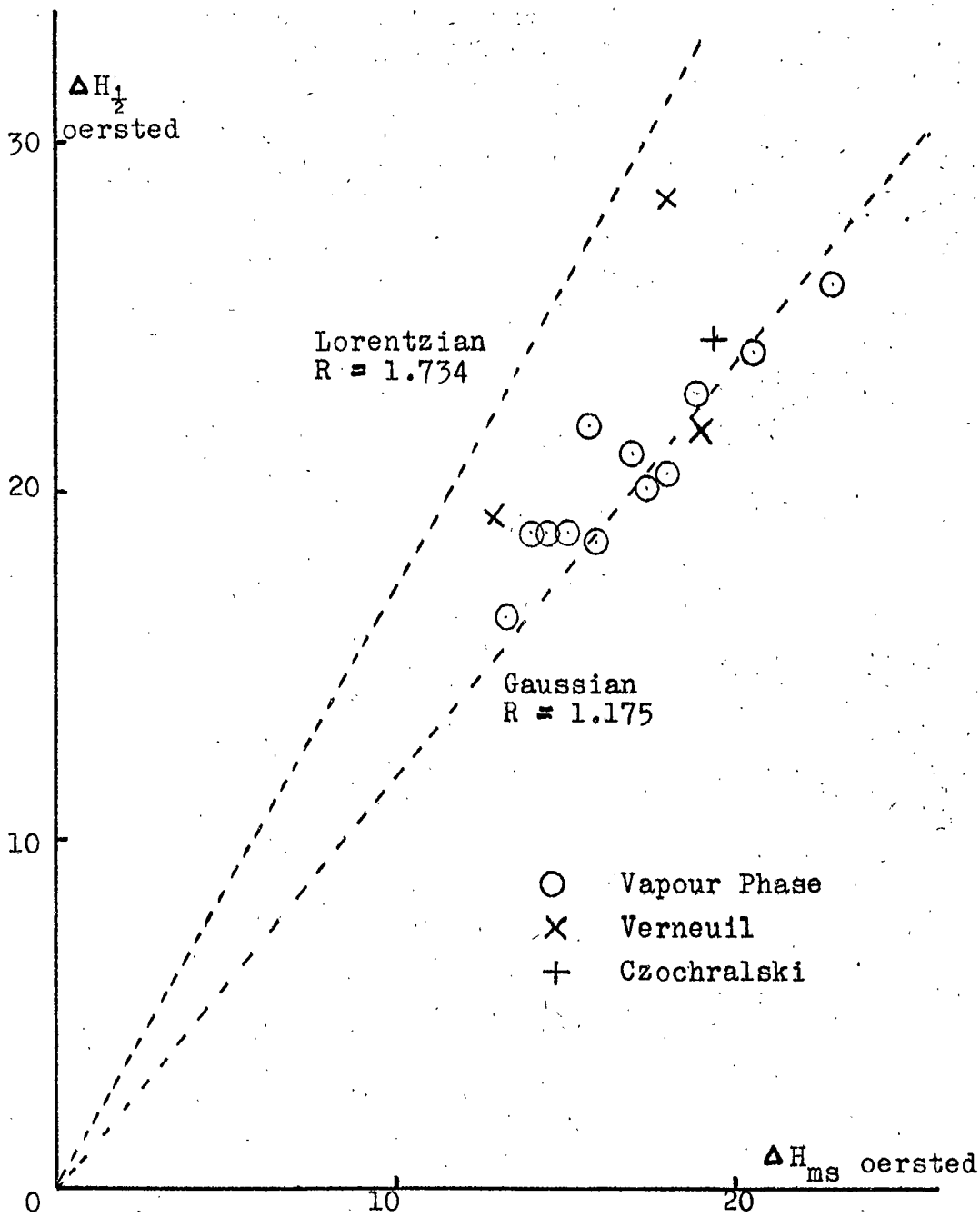

Figure 4.3

Half-Power Width and Derivative Width
+1/2 to -1/2 transition, $\theta = 0^{\circ}$

the widths of the components.

A feature of line profiles which is more amenable to handling in convolution is the second moment. Hughes and MacDonald (1961) have derived expressions for the second moment of a convolution product in terms of the moments of the components, and showed that in the case in which the two components are symmetrical about the origin the second moment of the product reduces to the sum of the second moments of the components, a result deduced previously by Andrew and Finch (1957). This relation holds for asymmetric functions if the origins are located at the centroids. The problem of separating the two or more components then reduces to that of separating the second moments. In the case where all components are of one type the moments are proportional to the widths and Eq. 4.11 holds.

4.4.3 The "Variance" Analysis

Wilson (1962) discussed the use of the second moment in the analysis of x-ray diffraction profiles, and a full treatment of his method, together with a means of correcting for uncertainties in the background level was given by Langford and Wilson (1963). The technique has been adapted to deal with e.p.r. lineshapes. Essentially the method consists of the calculation of the value of the expression:

$$W(R) = \frac{\sum_{-R}^{+R} g(x).x^2}{\sum_{-\infty}^{+\infty} g(x)} \qquad (4.12)$$

where g(x) represents the lineshape function, and R the distances from the origin, located at the centroid, at which the line is truncated for the purpose of evaluation of W(R). Use of this for the analysis of the product of convolution of a Gaussian and Lorentzian depends on certain properties of these functions.

For a Lorentzian as defined in Eq. 1.10 and having a half-power width of 2a, the second moment is infinite. If the line is truncated at distances $\pm$ R from the origin, Wilson shows that the relationship between the second moment, W(R), and R is given by:

$$W(R) = 2aR/\pi - (2a^2/\pi).\ \tan^{-1}(R/a) \qquad (4.13)$$

and in the tails of the line, i.e. for R >5a, the second term has the value of $-a^2$. Hence dW(R)/dR has a value of 2a at large values of R.

Defining a Gaussian as in Eq. 1.11 with a standard deviation of b, it can be shown that:

$$dW(R)/dR = (2R - R^3/b^2).\exp(-x^2/2b^2) \qquad (4.14)$$

which at values of R equal to 5 linewidths has a value of 10^{-3}. Figure 4.4 shows W(R) for Lorentzian and Gaussian functions of equal width, together with their sum, equivalent to W(R) of the convolution product.

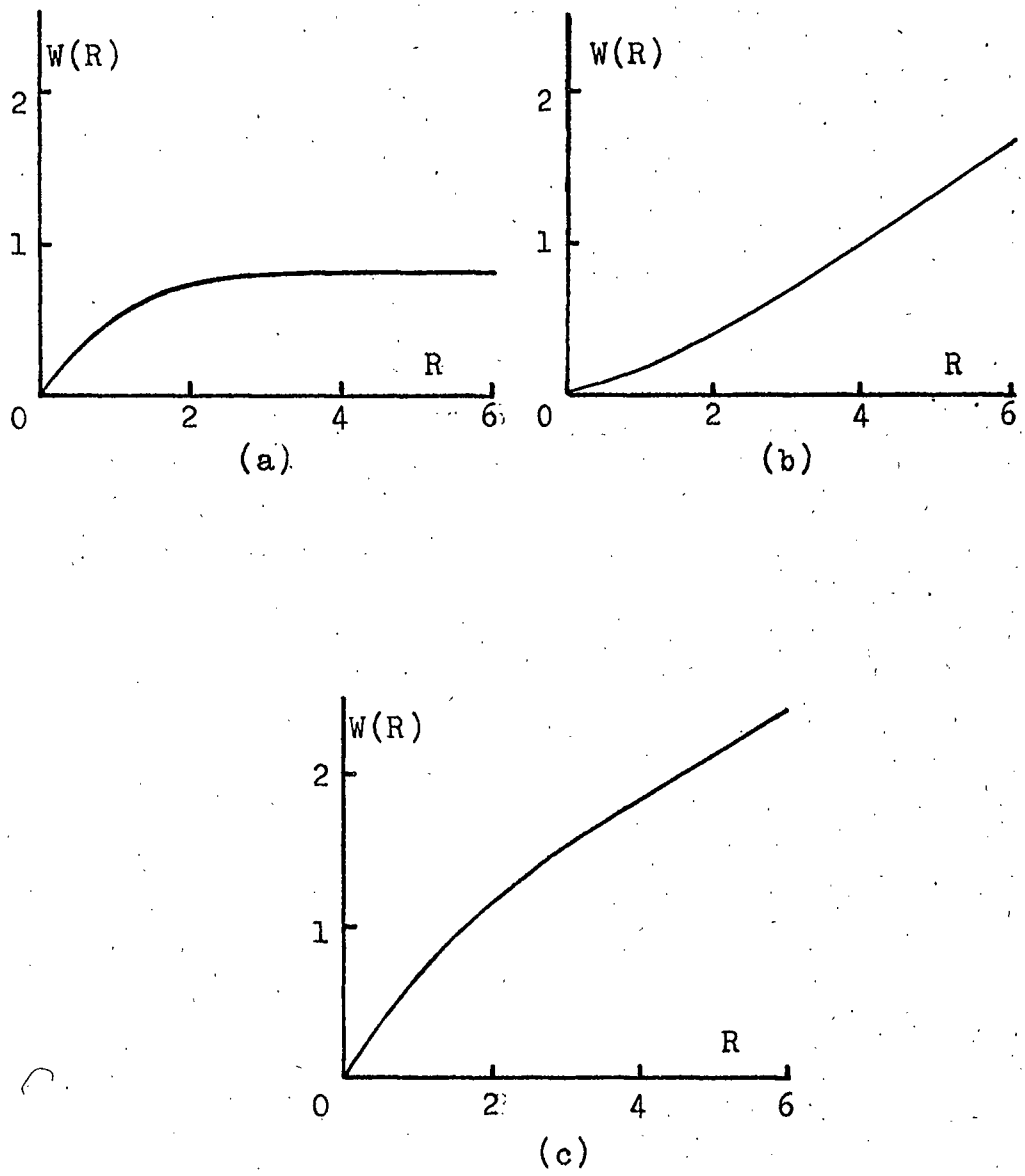

Figure 4.4

Variance-Range Dependences

(a) Gaussian

(b) Lorentzian

(c) Product

(Abscissae in units of ($\Delta H_{\frac{1}{2}}/2$))

Examination of Figure 4.4 shows that in the tails of the composite line it is the Lorentzian component that defines the slope of W(R). The effect of convolution with a Gaussian is merely to lift the tail region of the function W(R) of the Lorentzian by an amount equal to the total second moment of the Gaussian, and any departure from the theoretical intercept of $-a^2$ on the W(R) axis represents this increase of second moment. Correction for uncertainty in the baseline is achieved by adjusting the zero level of the absorption profile until the tail region gives the linear behaviour of W(R). Figure 4.5 illustrates the type of non-linear relationship observed with (a) the baseline too high, equivalent to loss of sensitivity in the tails, and (c) too low. The optimum position in this case is represented by (b).

An analysis of this form was programmed for the Elliott 803 computer. A typical derivative trace from each specimen was digitised and integrated, and the values of W(R) calculated. From the results the values of $\Delta H_{\frac{1}{2}}$ of the Lorentzian and Gaussian components were calculated, and these figures are plotted as functions of concentration in Figure 4.6. The Gaussian widths all lie around the 12 oersted region, while the Lorentzian components have widths almost double this. In each case the results are almost independent of concentration. This analysis forms the subject of

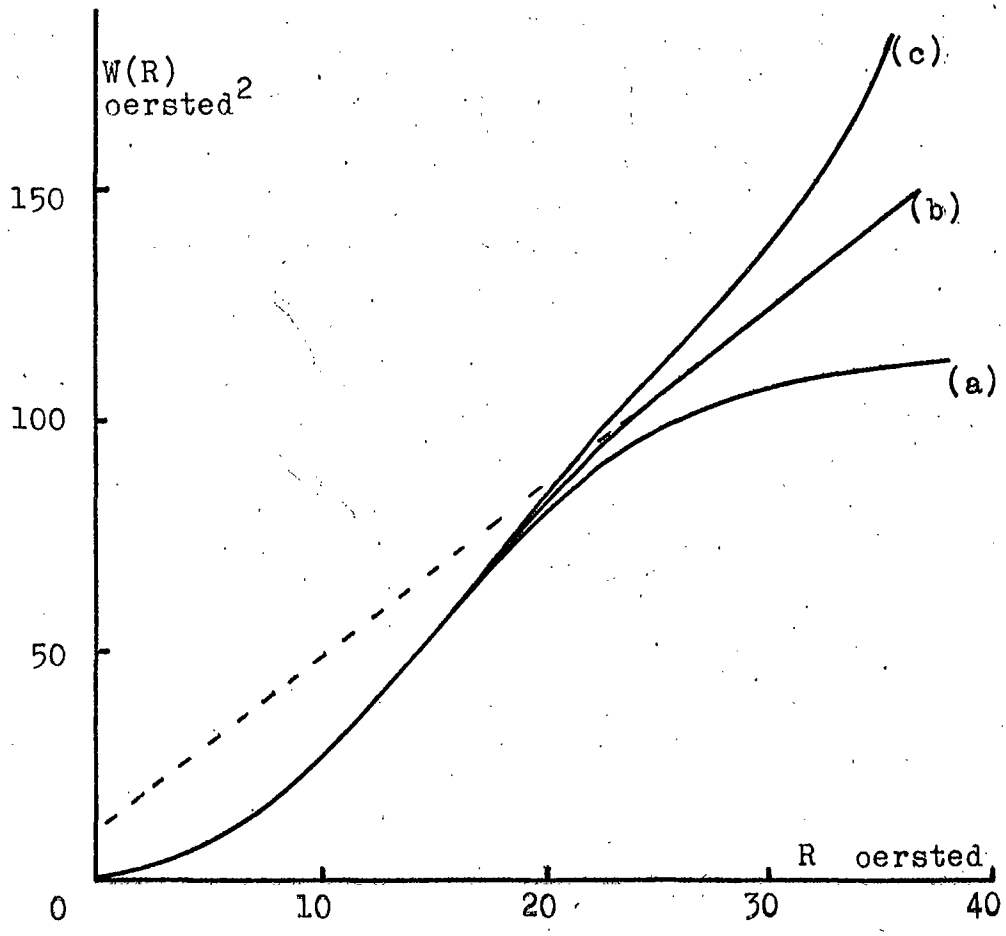

Figure 4.5

Effect of Baseline on Variance-Range Plot

(a) Baseline too high

(b) Baseline optimum

(c) Baseline too low

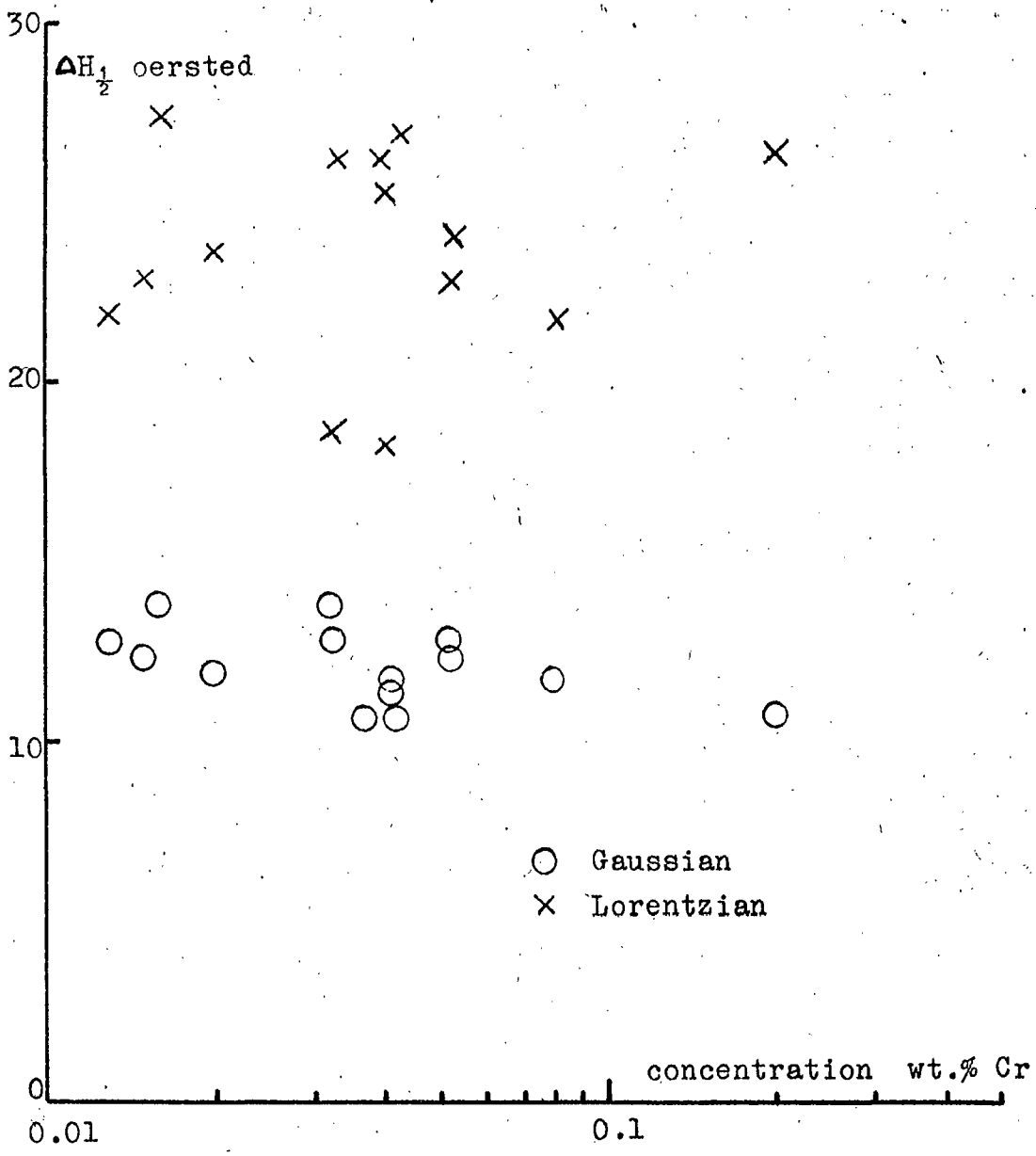

Figure 4.6

Widths of Gaussian and Lorentzian Components of Ruby Linewidth

a Communication published in the Journal of Applied Physics (Kirkby and Thorp, 1967).

4.4.4 Discussion of Homogeneous Broadening in Ruby

The general picture emerging from this work is that in low concentration material, of the type currently being employed as the active medium in masers and lasers, the chromium concentration as determined by chemical or optical techniques has very little effect. The results presented here show divergence from the theory in that the observed widths are somewhat greater than predicted.

The widths of the Gaussian components, as derived by the variance analysis, lie in the region of 12 to 13 oersteds, the figure observed as the width in the limit of vanishing concentration. However, the widths of the Lorentzian components, representing the Cr-Cr self broadening effect, show very little dependence on the chromium concentration as would be expected, but instead indicate an almost constant effective concentration of about 0.15 %.

Grant and Strandberg incorporated what they called microscopic clustering into their theory, with a factor representing the ratio of the probability of a particular site actually being occupied to the probability that it would be occupied assuming a random distribution of chromium ions. At low concentrations,

clustering on this scale does not have any significant effect on linewidth. However they do acknowledge the possibility of macroscopic clustering, with the chromium ions forming isolated pockets of higher than average concentration, and it is believed that this may be responsible for the high effective concentrations observed here. It is interesting to note that the introduction of high concentration regions results in a greater Lorentzian dipolar contribution to the overall line, causing departures from the strict Gaussian shape. Such departures have indeed been observed, as Figure 4.3 shows.

The fine-beam optical absorption experiment indicated that there could possibly be local variations of chromium concentration within a typical ruby specimen, but this method has limitations. Thorp etal. (1964) showed a correlation between dislocation density and chromium concentration, and showed concentration variations of over two orders of magnitude corresponding to variations of dislocation density of about five times. Similar variations of misorientation, and consequently of dislocation density, have been observed here, and have been described earlier.

The three specimens of Verneuil ruby showed higher linewidths than did the Vapour Phase specimens, the mean values of ΔH_{ms} being 18.3 and 15.5 oersteds respectively. In addition,

one specimen was available which had been grown by Vapour Phase addition of chromium to a Verneuil lattice. This showed a width of 13.0 oersted, one of the lowest figures observed. From this evidence it is concluded that a more uniform distribution of chromium results from the vapour doping procedure, and it is tempting to suggest that the discrete particle nature of the feed material in the Verneuil process is reflected in the quality of the distribution of dopant in the end product.

Chapter 5

E.P.R. LINEWIDTHS IN RUBY - II INHOMOGENEOUS BROADENING

The concepts of homogeneous and inhomogeneous broadening of e.p.r. absorptions were outlined in Chapter 4. The factors that combine to produce inhomogeneous broadening will now be outlined, and the concept of the "spin-packet" will be introduced. Siegman (1964) defines the spin-packet as consisting of all those spins within the system which posess the same resonant frequency, or all those spins with which any given spin will share any excitation that it may receive. The overall line in the strongly inhomogeneously broadened case is the envelope of all the spin-packet responses, while the width of each particular spin-packet is governed by the various homogeneous mechanisms present. In the limit of purely homogeneous broadening the entire line is a single spin-packet. The spin-packets may be separated simultaneously in space and frequency, as would occur if the magnetic field were inhomogeneous over the sample volume, or may be intermingled in space as in the case of crystalline inhomogeneities within the specimen. Figure 6.1 represents an inhomogeneously broadened line. The major processes contributing to inhomogeneous broadening are:

(a) Mosaic Structure

Under certain circumstances, notably in materials posessing low-symmetry crystal fields, the resonant

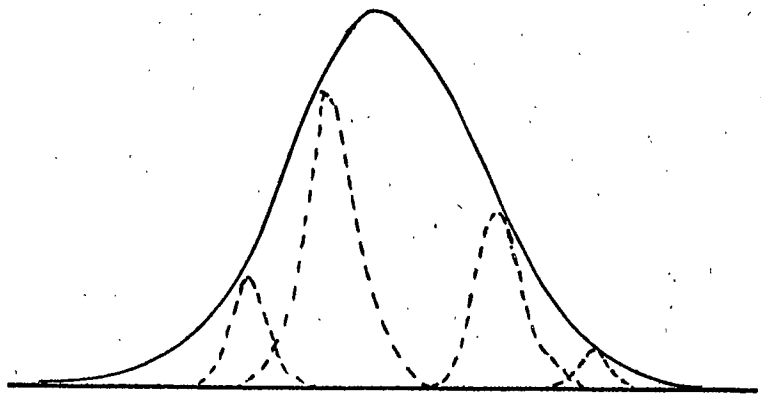

Figure 5.1

An Inhomogeneously Broadened Line and
Some of its Constituent Spin-Packets

magnetic field is strongly anisotropic. If mosaic structure exists in a specimen exhibiting this anisotropy, different regions will come to resonance at different magnetic fields, and the condition for inhomogeneous broadening will be fulfilled.

(b) Electric Field Effects

In certain materials, externally applied electric fields affect the paramagnetic energy levels. This effect is found to be linearly dependent on the magnitude of the field, and may also arise when local excess charges are present. Local variations of electric field at the paramagnetic sites result in local variations in energy level structure, giving rise to inhomogeneous broadening.

(c) Internal Strain

Local strains may distort the crystal field at the paramagnetic sites and, by virtue of the electric field effect just described, may result in inhomogeneous broadening.

5.1 INHOMOGENEOUS BROADENING MECHANISMS

5.1.1 Axial Misorientations

The first detailed consideration of the effects of axial misorientation on e.p.r. linewidths was that of Shaltiel

and Low (1961) who investigated the highly anisotropic behaviour of the linewidths of gadolinium in thorium oxide. The homogeneous line in this material is of the order of 0.1 oersted wide, but at certain orientations linewidths of many times this figure were observed. Shaltiel and Low assumed an isotropic axial distribution of crystallite orientations, with a Gaussian radial distribution, having a standard deviation of $\Delta\theta_o$ and cutting off at some value $\Delta\theta_{max}$. They showed that the observed linewidth would be given by:

$$\Delta H = \Delta\theta_o \cdot \frac{(\partial F/\partial\theta)}{(\partial F/\partial H)} \qquad (5.1)$$

where the resonant frequency, f, is given as a function of magnetic field, H, and polar angle, θ, by:

$$f = F(H,\theta) \qquad (5.2)$$

It was further assumed that resonance was independent of azimuthal angle, ϕ, a valid assumption in many cases.

Wenzel and Kim (1965) took into account the width of the homogeneous line, which is often significant, and considered ruby, in which this is about 15 oersteds. However, their discussion is applicable to any system posessing axial symmetry. The assumptions made as to the nature of the mosaic structure were similar to those of Shaltiel and Low. They showed that if the homogeneous line was represented by the function $g(H - H_o)$ and the crystallite orientations

by $P(H' - H_o)dH$, (having been transformed from a distribution in orientation to one in resonant field) the shape of the line was given by convolution:

$$G(H - H_o) = \int g(H - H').P(H' - H_o)dH' \qquad (5.3)$$

If both $g(H - H')$ and $P(H' - H_o)$ are assumed to be Gaussian, Eq. 5.3 leads to the result:

$$\Delta G = \left[(\Delta g)^2 + (\Delta\theta)^2 (dH/d\theta)^2 \right]^{\frac{1}{2}} \qquad (5.4)$$

where ΔG and Δg represent the widths of $G(H - H_o)$ and $g(H - H')$ respectively, $\Delta\theta$ represents the width of the distribution of misorientations, $dH/d\theta$ is the rate of change of resonant field with polar angle and widths are taken either as half power or derivative peak-to-peak values consistently.

Adam et al. (1963) reported splittings of absorptions at 3 cm wavelength, and attributed this to either the presence of two discrete c-axis directions or local internal strain. Curtis (1964) observed strongly anisotropic linewidths in two specimens of ruby, and showed that there existed a correlation between broadening and axial misorientation as deduced from x-ray measurements. A further analysis of these results was given by Curtis et al. (1965) attached as Appendix 1.

5.1.2 Electric Field Effects

If a paramagnetic ion is located within a crystal electric field posessing a symmetry lower than cubic the ground state may be split. This appears as the splitting parameters D and E of the spin-Hamiltonian. Bloembergen (1961) pointed out that if a paramagnetic ion is situated at a lattice site not posessing inversion symmetry with respect to the crystal field, application of an electric field would result in a change of crystal field splitting directly proportional to the magnitude of the applied field. This effect is due to interaction between the applied field and the odd part of the crystal field (i.e. that part undergoing change of sign on inversion at the paramagnetic site) and can be represented by an addition to the Hamiltonian of a term $\mathcal{H}'$ having the form:

$$\mathcal{H}' = \sum_i \sum_{j \geq k} \tfrac{1}{2} R_{ijk} E_i (S_j S_k + S_k S_j) + \sum_{ijk} T_{ijk} E_i H_j S_k \quad (5.5)$$

The first term represents the effect of the applied field E_i on the zero-field splitting, and the second is responsible for changes in g-value and is usually negligible. Sites related by inversion have equal and opposite values of R_{ijk} and under the action of an applied field a resonance will split into two components which may or may not be resolved. A theoretical description has been given

by Artman and Murphy (1963, 1964) and discussions of results of electric field experiments by Royce and Bloembergen (1963) and Krebs (1967).

Application of a uniform electric field to the whole specimen merely results in a shift of the resonance position, with the additional possibility of splitting if the symmetry conditions are fulfilled. If different sites experience different electric fields the absorptions will be observed to be inhomogeneously broadened as different regions will experience different shifts of resonance frequency. Mims and Gillen (1966) considered this effect in uncompensated Ce:$CaWO_4$, assuming that within the specimen there existed a set of randomly distributed charge defects resulting in localised electric fields. Each paramagnetic ion experiences the resultant field due to all the charge defects in its vicinity, and the observed line is the sum of the effects at all the paramagnetic sites. By statistical summation they obtained agreement between theoretical and experimental results, which showed considerable anisotropy of linewidth in the azimuthal plane. The line broadened by this effect was shown to be intermediate between Gaussian and Lorentzian in shape, and to have a width proportional to the two-thirds power of the defect concentration.

Instead of studying angular dependence of linewidth,

Manenkov et al. (1963) investigated the three transitions observed in ruby at $\theta=0^{\circ}$. Figure 1.5 shows that at this orientation crystal field splitting plays no part in determining the position of the +1/2 to -1/2 transition, but that it does enter into the energies of the other major transitions. These workers studied a specimen having a concentration of 0.05 % and showed that the $\pm 1/2$ to $\pm 3/2$ transitions exhibited substantial broadening relative to the +1/2 to -1/2 transition. The difference was ascribed to local inhomogeneities of crystal field, having magnitudes of around 10^{-3}, but the causes of these were unspecified.

5.1.3 Strain at Paramagnetic Sites

Local distortion of the host lattice in the vicinity of a paramagnetic site may seriously alter the crystal field at that site, resulting in changes in the parameters D and E. This effect is related to that described in the previous section. The deviation of D from the figure expected in a perfect sample may be described by a term "$\mathcal{H}$" in the Hamiltonian having the form:

$$\mathcal{H}'' = \sum_{ij} D_{ij} S_i S_j \qquad (5.6)$$

where the summation is carried out over cartesian axes. D_{ij} is a symmetric traceless tensor related linearly (Sturge, 1965) to the strain e_{lm} by:

$$D_{ij} = \sum_{lm} G_{ijlm} e_{lm} \qquad (5.7)$$

where l and m are also summed over x, y and z and G is the magnetoelastic tensor. Early experiments on this topic involved the application of simple hydrostatic pressure (Clark et al., 1964) but later work, notably that of Feher (1964) on MgO and Hemphill et al. (1966) on ruby, involved the application of uniaxial stress in definite directions. The latter group evaluated the various terms of the magnetoelastic tensor, and were able to confirm the predictions of Van Vleck (1940) and Mattuck and Strandberg (1960) regarding the predominance of a term quadratic in spin in the spin-lattice interaction.

A distribution of stresses is needed for inhomogeneous broadening since a uniform stress merely shifts the resonance uniformly. Koloskova (1962) discussed the effects of dislocations on the shapes of resonance lines, assuming that the lattice distortions arose solely from this cause. She considered firstly the stress fields existing around dislocations of various types and, by averaging over lattice points with the assumption of a uniform distribution of dislocations, derived an expression for the second moment of the lines. A cubic lattice was assumed, considerably simplifying the form of the tensor G, the terms of which were calculated from theoretical considerations. The theory predicted a linewidth proportional to the square root of the

dislocation density. No account was taken, however, of the homogeneous broadening.

Wenzel and Kim estimated the broadening caused by a variation of the values of D_{ij} between different sites in ruby. They treated the term $\mathcal{H}''$ as a first order perturbation on the spin-Hamiltonian and showed that the resonant magnetic field was given by:

$$H' = H + \sum_{ij} D_{ij}(\langle a|S_iS_j|a\rangle - \langle b|S_iS_j|b\rangle).dH/d(E_a - E_b) \qquad (5.8)$$

where $|a\rangle$ and $|b\rangle$ are the levels between which the transition occurs and H is the resonant field in the unpeturbed state. The distribution of H' in the vicinity of H is governed by the distribution of D_{ij}, which Wenzel and Kim assumed to be Gaussian. They showed that the strain broadening of the line would be represented by:

$$\Delta H_s = \left[\sum_{ij} \sigma_{ij}^2 (\langle a|S_iS_j|a\rangle - \langle b|S_iS_j|b\rangle)^2 \right]^{\frac{1}{2}} \qquad (5.9)$$

where the terms σ_{ij} represent the widths of the D_{ij} distributions, now expressed in magnetic field units.

Stoneham (1966) approached the problem of strain from a statistical point of view, using a method outlined by Chandresekhar (1942). He derived an expression for the distribution of strains resulting from an arbitrary distribution of dislocations and showed that although the various strain components could not, in general, be assumed to be independent, in the particular case

in which a substantial part of the linewidth arises from spin-spin interactions an assumption of this nature could be made. This situation applies in dilute ruby.

5.2 EXPERIMENTAL LINEWIDTH RESULTS

The inhomogeneous broadening of e.p.r. absorptions in ruby was investigated by examining the widths of the three $\Delta M=1$ transitions. Figure 5.2 shows the experimentally observed variation of resonant field with polar angle for these transitions at 35 Gc/sec. Since the maximum available field was 16,000 oersted, the +3/2 to +1/2 transition was not observable at polar angles below 30°. Functional forms for the angular dependences have been given by Bleaney (1951) and Low (1960). Ignoring the slight anisotropy of g-factor these reduce to:

$$+1/2 \text{ to } -1/2: \quad hf = g\beta H + (\text{second order terms in } D^2) \qquad (5.10)$$

$$\pm 3/2 \text{ to } \pm 1/2: \quad hf = g\beta H \pm D(3\cos^2\theta - 1) + (\text{second order terms in } D^2) \qquad (5.11)$$

At high frequencies the effect of the terms in D^2 is considerably reduced, although in the complete absence of any term in D in the energy of the +1/2 to -1/2 transition this effect cannot be completely neglected, as Figure 5.2 shows.

The experimental results were analysed on the basis of the hybrid strain and mosaic model of Wenzel and Kim. The system

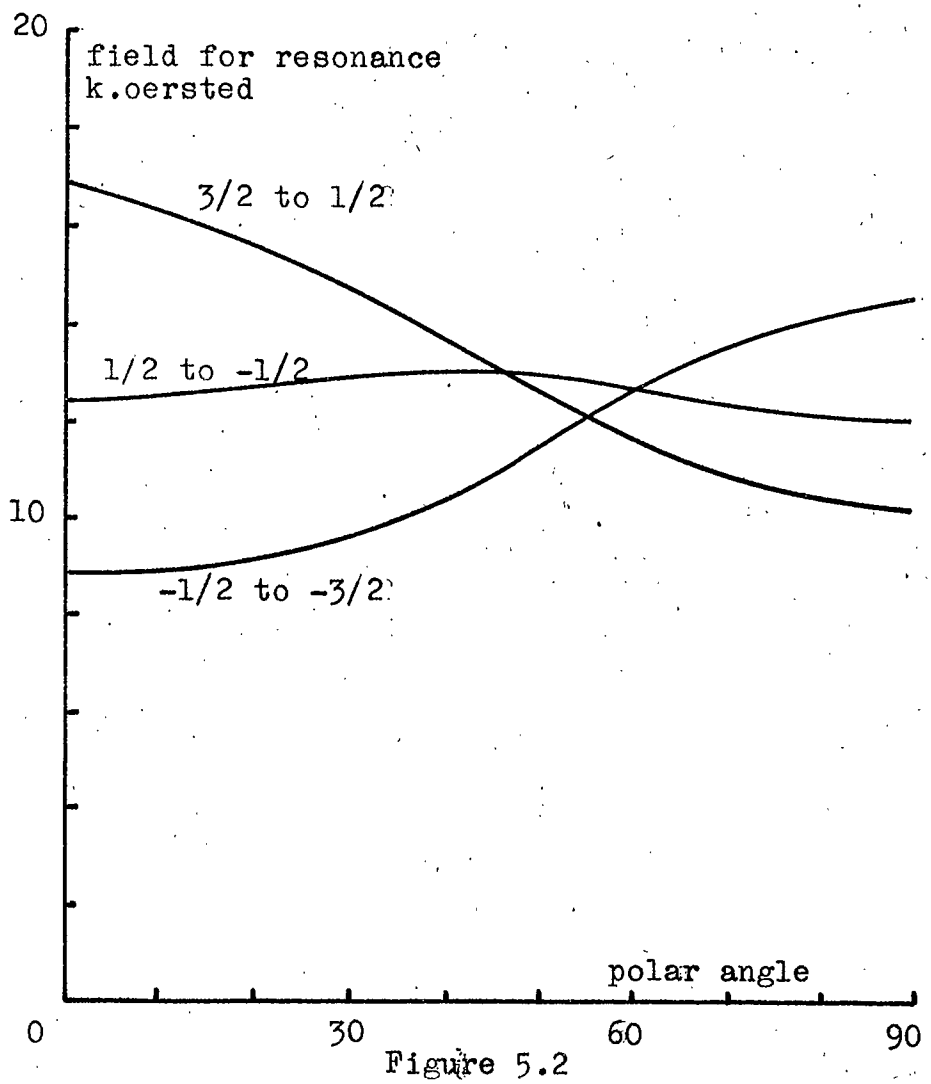

Figure 5.2

Isofrequency Plot for Ruby at 35 Gc/sec

is postulated to consist of a set of crystallites, each of which is assumed to be subject to random local strains. To a first approximation these effects are assumed to have Gaussian distributions and to be statistically independent. The linewidth is then given by:

$$\Delta G = \left[(\Delta g)^2 + (\Delta \theta)^2 (dH/d\theta)^2 + \sum_{ij} \sigma_{ij}^2 (\langle a|S_i S_j|a\rangle - \langle b|S_i S_j|b\rangle)^2 \right]^{\frac{1}{2}} \tag{5.12}$$

where the notation is consistent with that used earlier. In using Eq. 5.12 it has been assumed that all the substitutional chromium ions are in the trivalent state and are located at aluminium sites. In consequence, electric field effects have been ignored. The various terms in Eq. 5.12 contain angular dependent parameters, with the possible exception of Δg, which has been discussed previously and will be assumed in what follows to be constant. Values of $dH/d\theta$ were obtained directly from Figure 5.2, and for the $\pm 3/2$ to $\pm 1/2$ transitions there was good agreement between these figures and those obtained by direct differentiation of Eq. 5.11.

Wenzel and Kim pointed out that in a system posessing axial symmetry, the only matrix elements contributing to Eq. 5.12 are those in S_x^2, S_z^2 and $(S_x S_z + S_z S_x)$. The values of these were computed using the Pauli spin matrices for S=3/2 (Schiff, 1955)

and taking into account the mixing of states at angles other than $\theta=0^{\circ}$. The results of this calculation are given in Appendix 2, together with the values of $dH/d\theta$. In order to perform this calculation it was first necessary, in the absence of any published figures, to calculate the eigenvectors for ruby at Q-band. These results are given in Appendix 3.

Figures 5.3 to 5.6 inclusive show typical angular dependences of the widths of the $\Delta M = 1$ absorptions observed in the four classes of material that could be identified among the specimens examined. Some information concerning these has been presented already in Table 2.1 (page 37).

The greatest degree of anisotropy of the +1/2 to -1/2 transition was exhibited by the Vapour Phase 0° material, and the behaviour shown here was typical of all specimens of this type. The width of this transition in 90° material of both Vapour Phase and Verneuil types showed a relative independence of polar angle, and again the behaviour shown here is typical. The +1/2 to -1/2 line in Czochralski ruby L2 was relatively narrow, with a pronounced ~~minimum~~ maximum around 50°. This behaviour was not exhibited by the other Czochralski ruby, L1, which showed rather broader lines and an angular dependence typical of the 90° material. However, this latter ruby was known to be rather highly strained

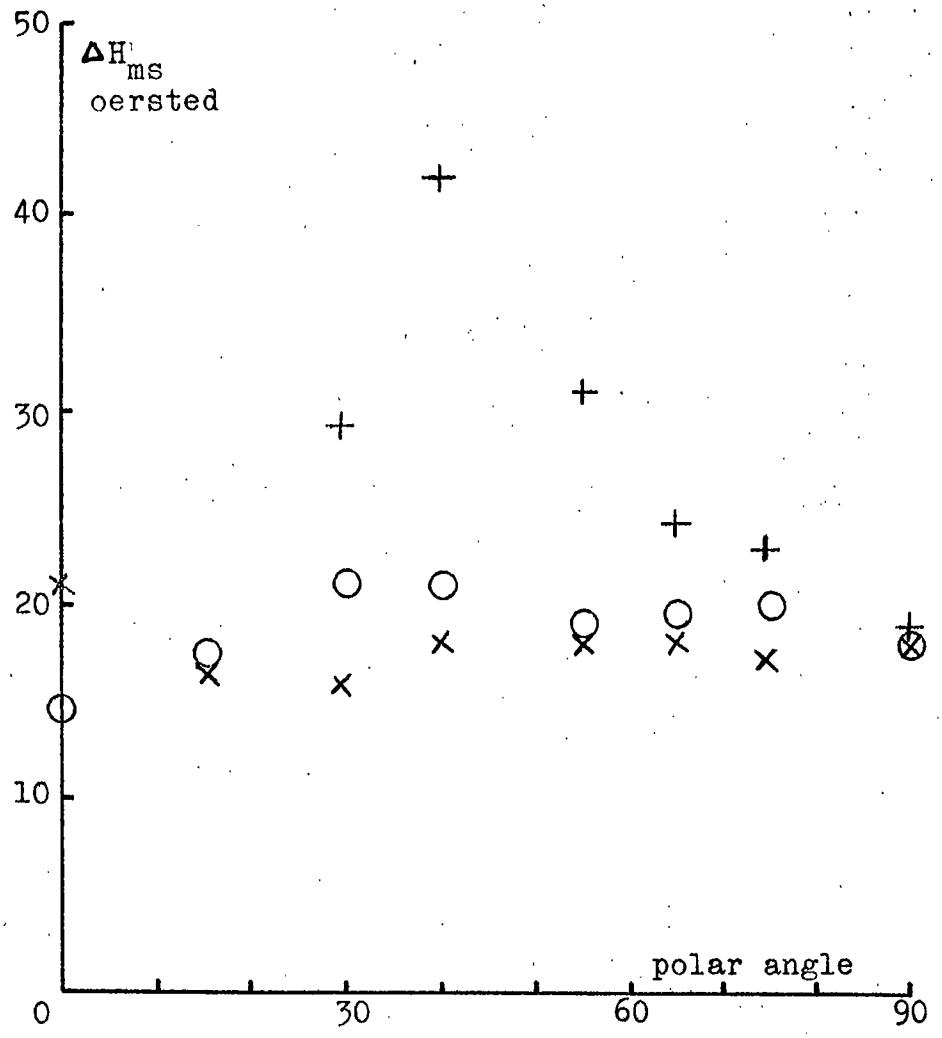

Figure 5.3

Angular Dependence of Linewidth
0^{o} Vapour Phase Ruby, 0.041 %

+ +3/2 to +1/2
○ +1/2 to -1/2
× -1/2 to -3/2

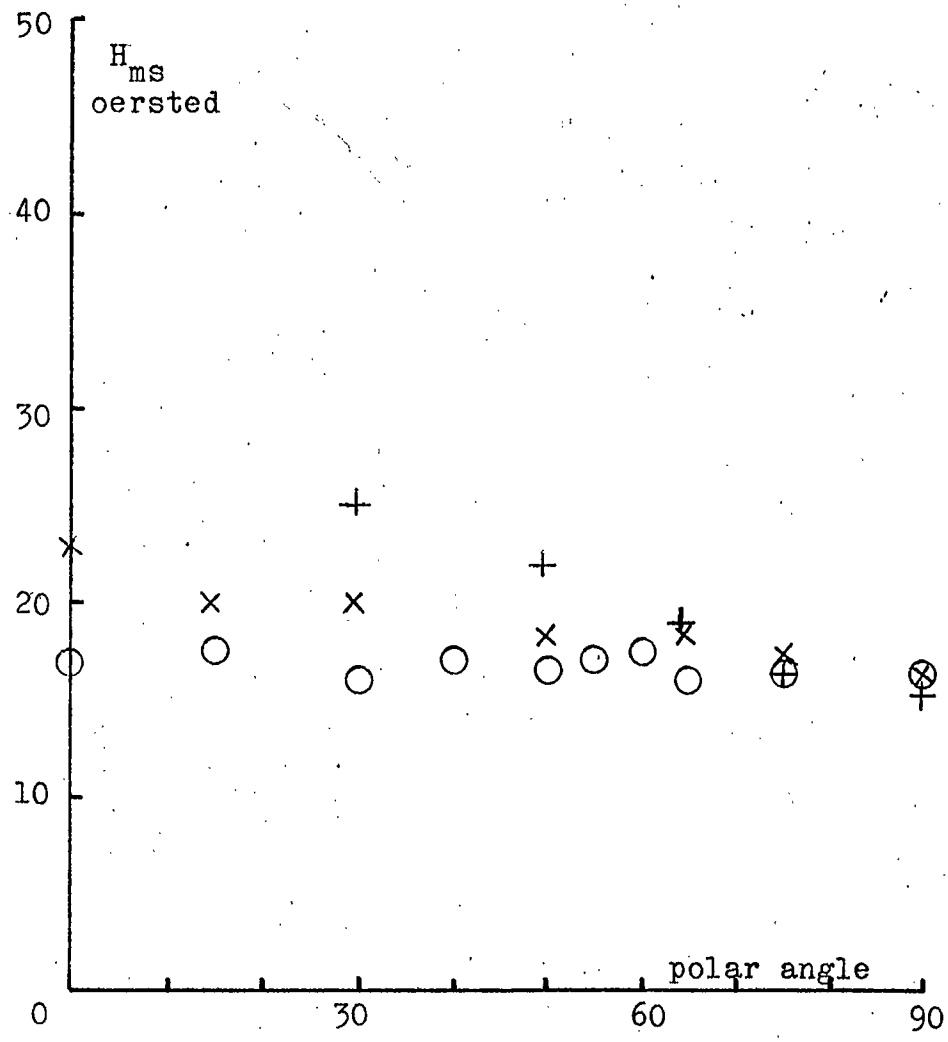

Figure 5.4
Angular Dependence of Linewidth
90° Vapour Phase Ruby, 0.015 %

+ 3/2 to 1/2
○ 1/2 to -1/2
× -1/2 to -3/2

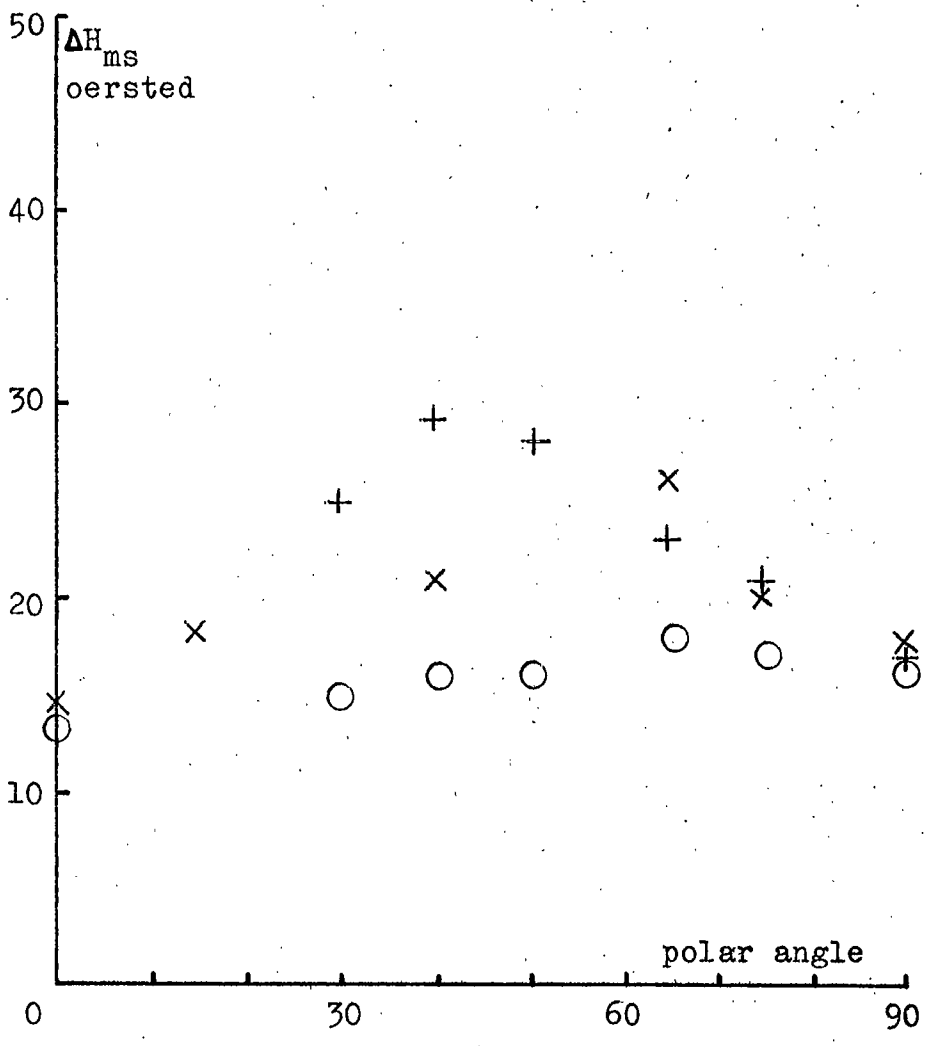

Figure 5.5

Angular Dependence of Linewidth
90° Verneuil Ruby, 0.015 %

+ +3/2 to +1/2
○ +1/2 to -1/2
× -1/2 to -3/2

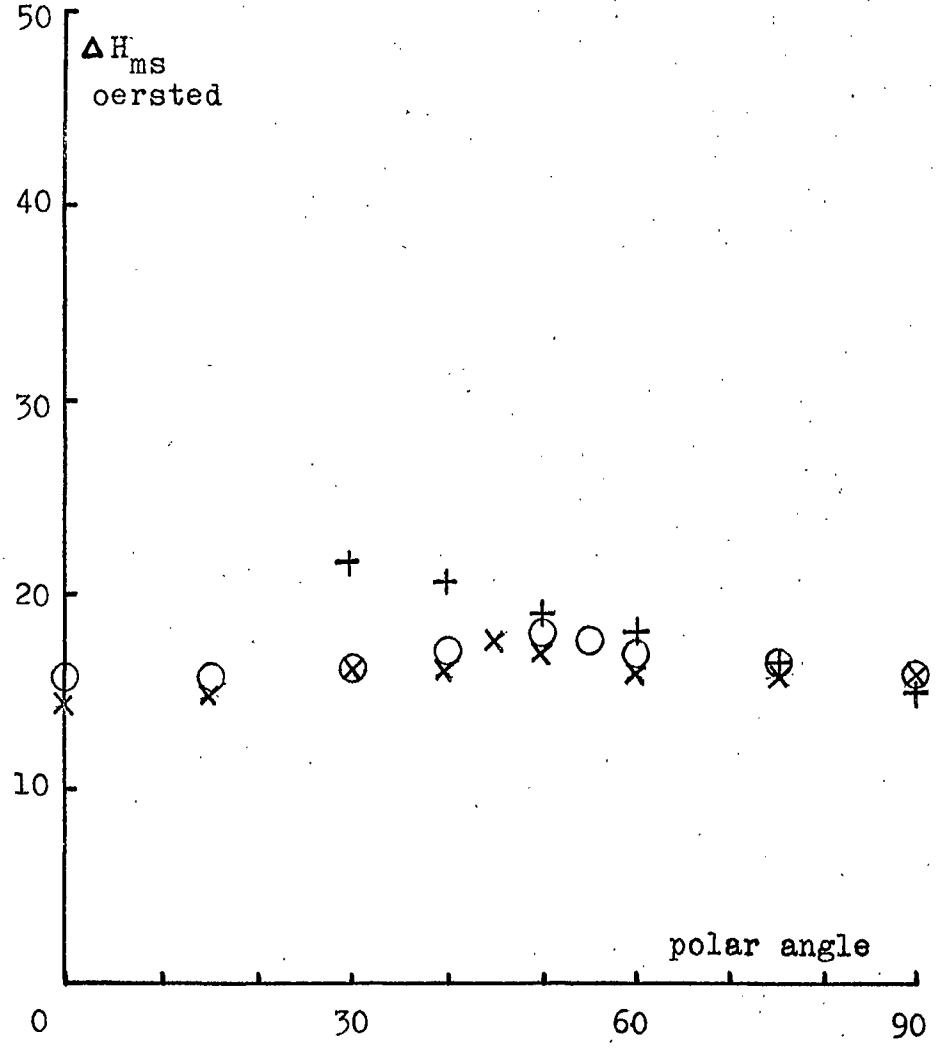

Figure 5.6

Angular Dependence of Linewidth
60° Czochralski Ruby, 0.045 %

\+ +3/2 to +1/2
○ +1/2 to -1/2
× -1/2 to -3/2

as it shattered on cooling from the etching temperature of 320° C (D.R. Mason, private communication).

The other two $\Delta M = 1$ transitions exhibit varying degrees of anisotropy. In most cases the +3/2 to +1/2 showed considerable broadening at polar angles around 45°, but several cases in which the width of the -1/2 to -3/2 transition approached that of the +1/2 to -1/2 were observed, one being shown in Figure 5.3.

The shapes of some of the absorptions were investigated, and showed a tendency towards a Gaussian form. For example, 31 measurements of the +1/2 to -1/2 transition gave a mean value of R ($=\Delta H_{\frac{1}{2}}/\Delta H_{ms}$) of 1.19, 8 measurements of the +3/2 to +1/2 gave R = 1.22 and 16 measurements of the -1/2 to -3/2 resulted in R = 1.25. The values for the Gaussian and Lorentzian limits are 1.18 and 1.73 respectively. There was no obvious trend towards any dependence of shape on polar angle, although among the results from any particular specimen there were noticeable variations of R with orientation.

5.3 ANALYSIS OF LINEWIDTH RESULTS

Equation 5.12 contains four parameters whose values depend on polar angle and transition, namely $dH/d\theta$, and the three terms of the form: $(\langle a|S_i S_j|a\rangle - \langle b|S_i S_j|b\rangle)^2$, all of which are tabulated

in Appendix 2. Analysis of the experimental data was carried out by treating together all the results obtained from a particular transition in a given specimen, and performing a least squares analysis to obtain values of ΔH_{ms}, $\Delta\Theta$, and the three terms in σ. To simplify the notation, Eq. 5.12 can be written as:

$$H = v + a.w + b.x + c.y + d.z \qquad (5.13)$$

where: $a = dH/d$

$$b = (\langle a|S_x^2|a\rangle - \langle b|S_x^2|b\rangle)^2$$

$$c = (\langle a|S_x^2|a\rangle - \langle b|S_z^2|b\rangle)^2$$

$$d = (\langle a|S_xS_z + S_zS_z|a\rangle - \langle b|S_xS_z + S_zS_x|b\rangle)^2$$

are the tabulated quantities and:

$H = (\Delta G)^2$, $v = (\Delta g)^2$, $w = (\Delta\theta)^2$, $x = \sigma_{xx}^2$, $y = \sigma_{zz}^2$, $z = \sigma_{xz}^2$.

At the best fit of the parameters v, w, x, y and z to the observation H

$$\sum_1^n (v + a_s.w + b_s.x + c_s.y + d_s.z - H_s)^2$$

is a minimum, the standard least squares condition. Differentiating this expression with respect to v, w, x, y and z in turn results in five equations in five unknowns:

$$\begin{aligned}
&(1)v + (a)w + (b)x + (c)y + (d)z = (H)\\
&(a)v + (a^2)w + (ab)x + (ac)y + (ad)z = (aH)\\
&(b)v + (ba)w + (b^2)x + (bc)y + (bd)z = (bH)\\
&(c)v + (ca)w + (cb)x + (c^2)y + (cd)z = (cH)\\
&(d)v + (da)w + (db)x + (dc)y + (d^2)z = (dH)
\end{aligned} \qquad (5.14)$$

where (ab) indicates $\sum_{1}^{n} a_s b_s$, where n is the number of individual items of data in the set under consideration.

Calculation of the numerical coefficients relevent to each set of data, and the solution of the resultant simultaneous equations was programmed for the computer. The solution gave the best fit to the observed linewidths of the homogeneously broadened linewidth Δg, the width of the distribution of crystallite misorientations $\Delta\theta$, and the three strain parameters, σ_{xx}, σ_{zz} and σ_{xz}, with $\Delta\theta$ given as an angle and the other quantities in magnetic field units. Owing to the symmetry of the tensor G_{ijlm} with respect to interchange of i and j or l and m, the term σ_{xz} represents the widths of both D_{xz} and D_{zx} and no further separation of these quantities is possible.

The results of this analysis are given in Table 5.1, where the specimens are grouped by growth. As a check on the method, and the reliability of the figures quoted in Table 5.1, the figures obtained were used to recalculate the linewidths that would be expected. A comparison was then made between these figures and the experimental results. In general there was quite good agreement as far as the +1/2 to -1/2 transition was concerned, although the agreement was only qualitative for the other transitions. However, during the solution of Eqs. 5.14 for these particular

Ruby	Δg	$\Delta\theta$	σ_{xx}	σ_{zz}	σ_{xz}
467	24.0	23'	5.61	8.92	8.10
G2B	19.1	26'	9.44	6.52	6.39
G2A	18.2	39'	7.45	6.19	5.92
464	12.9	15'	5.61	6.27	6.53
312B	13.6	11'	6.69	6.65	3.19
312C	17.8	20'	6.64	7.41	2.79
344	12.9	17'	5.90	6.25	6.92
337C	13.0	15'	6.16	6.36	3.05
319	19.5	27'	4.71	7.50	6.71
354	16.8	30'	7.49	8.39	6.54
252	16.7	13'	3.68	5.40	5.99
374	15.7	14'	3.74	5.87	5.30
367	12.9	27'	6.29	6.34	3.07
458	13.4	15'	6.69	6.77	5.09
L1	13.2	12'	6.73	6.73	5.08

Table 5.1

Results of Least Squares Analysis of Linewidth Results

($\Delta\theta$ in minutes of arc, all other quantities in oersteds)

transitions, numbers greater than the computer capacity of 10^{70} were generated necessitating approximations. In consequence, only the results from the +1/2 to -1/2 transition are presented here. Figure 5.7 shows predicted and experimental results for the +1/2 to -1/2 transition in ruby 319, a Vapour Phase specimen with a concentration of 0.08 %.

5.4 DISCUSSION OF RUBY RESULTS

Table 5.2 compares calculated values of homogeneous linewidth, derived from the analysis procedure, with experimental results for the +1/2 to -1/2 transition at $\theta = 0^{\circ}$ (c.f. Chapter 4). The agreement is not perfect, and the calculated values are greater than the experimental values for just over half of the specimens. As already mentioned, the accuracy of a single linewidth measurement was estimated to be about 10 %, due mainly to inaccuracy in calibrating the magnetic field sweep. However, this figure should be improved by averaging the several measurements generally made at each orientation. The data used for analysis, and consequently the results also, were expressed in terms of peak-to-peak derivative widths, and these discrepancies may just be reflecting the difficulty of determining a valid parameter to represent linewidth in the case which is neither Lorentzian nor Gaussian.

One simplification which was made in carrying out the

DURHAM UNIVERSITY SCIENCE 17 JAN 1968 SECTION LIBRARY

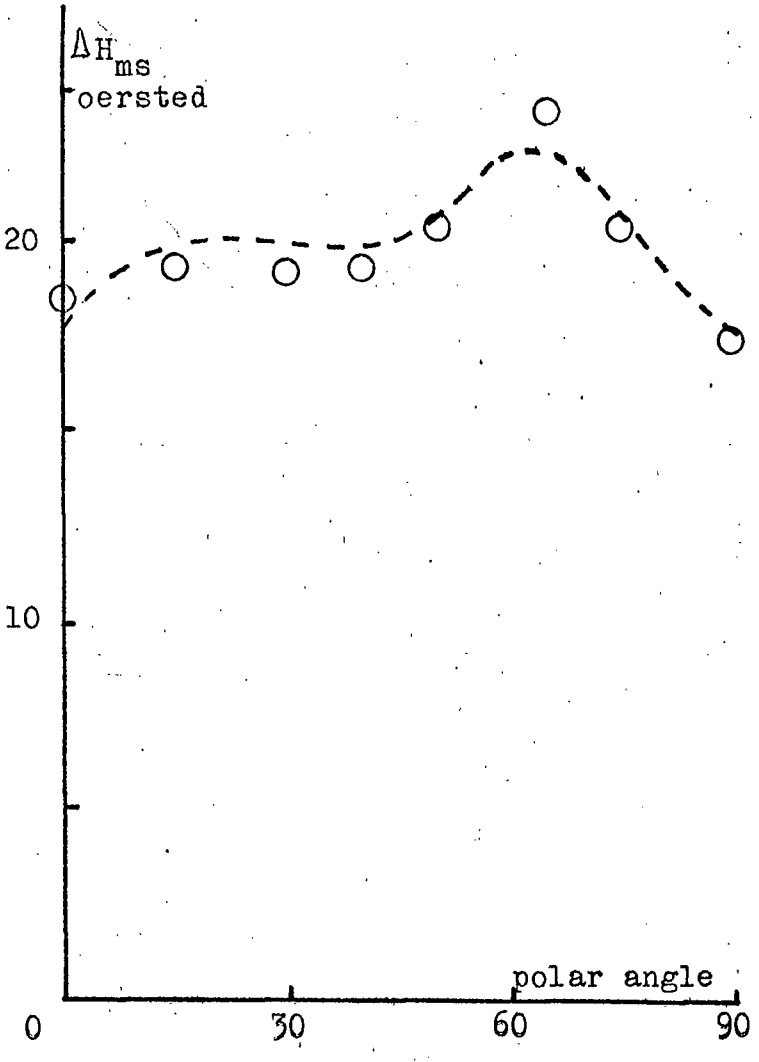

Figure 5.7

Experimental and Predicted Linewidth Figures
0^{o} Vapour Phase Ruby, 0.08 %

(Experiment: open circles
Prediction: dashed line)

Ruby	Δg(calc.)	Δg(expt.)	e_{xx}	e_{zz}	e_{xz}
467	24.0	15.2	0.015	0.082	0.011
G2B	19.1	17.5	0.044	0.002	0.009
G2A	18.2	14.8	0.026	0.029	0.009
464	12.9	12.4	0.008	0.107	0.010
312B	13.7	13.4	0.089	0.007	0.005
312C	17.8	14.5	0.106	0.007	0.004
344	12.9	15.8	0.013	0.078	0.010
337C	13.0	15.9	0.080	0.001	0.005
319	19.5	18.5	0.010	0.097	0.009
354	16.8	22.9	0.038	0.060	0.009
252	16.7	17.4	0.030	0.098	0.009
374	15.7	13.0	0.008	0.086	0.007
367	12.9	16.5	0.081	0.086	0.007
458	13.4	18.0	0.048	0.032	0.009
L1	16.8	15.0	0.013	0.057	0.009

Table 5.2

Linewidth and Strain Results

(Linewidths in oersteds)

calculation was the assumption that the homogeneous width was independent of polar angle. Grant and Strandberg (1964b) have indicated that this is not so, and in deriving the Cr-Al dipolar width they arrived at an expression for the second moment containing the trignometric term:

$$16.42 - 19.60\cos^2\theta + 18.70\cos^4\theta - 10.34\sin^3\theta \cos\theta \cos 3\phi$$

With $\phi = 0^\circ$, this expression has been evaluated, giving the result that if the dipolar width at 0° is taken to be 3.7 oersted (the value calculated by Grant and Strandberg) then at 50° this is reduced to 1.7 oersted. In the absence of any information concerning the angular dependence of the remainder of the homogeneous broadening it is difficult to predict the total angular dependence, but assuming that the only anisotropic component is the dipolar interaction then the maximum possible anisotropy of the line is about 1 oersted. The effect of ϕ on the linewidth would be negligible and any azimuthal variation would be difficult to observe.

The 0° material exhibits somewhat larger values of $\Delta\theta$, although as Table 5.1 shows, this is only a generalised trend. The lowest figures are shown by the Czochralski specimens, a result also obtained from the X-ray measurements. Figure 5.8 shows the standard deviations of the misorientation measurements plotted against the values of $\Delta\theta$ derived from the linewidth analysis.

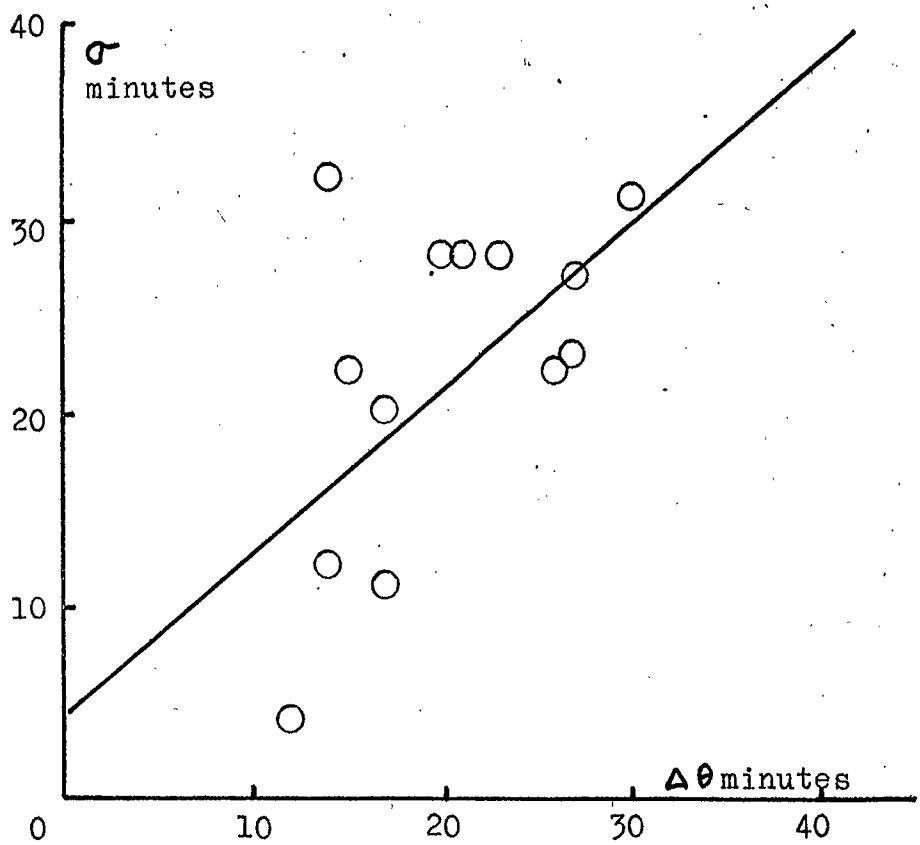

Figure 5.8

Relationship Between Misorientation Figures Derived from X-Ray and E.P.R. Measurements

(σ: standard deviation of X-ray measurements
$\Delta\theta$: obtained from analysis of E.P.R. results)

The straight line best fitting the points was obtained from the two lines of regression (Topping, 1955, p.104). The fit of the points to the line is by no means perfect, but it does indicate a trend towards a linear relationship.

On the basis of measurements on two of the specimens studied here, Curtis et al. (Appendix 1) concluded that the parameter most responsible for broadening resulting from crystalline misorientations was the mean value of mosaic misorientation, and in his earlier work Curtis (1964) specifically excluded the standard deviation of the misorientation measurements as a relevent parameter. However, owing to the inability of the X-ray method to distinguish signs of misorientations, the mean misorientation has a finite value, rather than the figure of zero that it would have if the distribution were symmetrical about the origin. Furthermore, if the orientation distribution conforms to one of the standard mathematical forms, the mean is directly related to the standard deviation.

The three terms σ_{xx}, σ_{zz} and σ_{xz} represent the widths of the distributions of zero-field splitting resulting from strain, as indicated in Eq. 5.7. A typical value of σ, 5 oersted, corresponds to a spread in 2D of 5×10^{-4} cm^{-1}, which with 2D taken as 0.38 cm^{-1} gives:

$$\Delta(2D)/2D \simeq 10^{-3}$$

Manenkov et al. observed values of this ratio in ruby of between 1×10^{-3} and 6×10^{-3}.

The terms of the G-tensor have been evaluated by Hamphill et al. and their values have been used in what follows. Expanding Eq. 5.7 gives:

$$\begin{aligned}
\sigma_{xx} &= 4.57e_{xx} - 1.94e_{yy} - 3.20e_{zz} - 0.43e_{yz} - 1.50e_{xz} \\
\sigma_{zz} &= -2.63e_{xx} - 2.63e_{yy} + 6.40e_{zz} \\
\sigma_{xz} &= -1.50e_{xx} + 1.50e_{yy} + 1.97e_{xz} - 0.63e_{xz}
\end{aligned} \tag{5.15}$$

where the numerical constants and the values of σ are expressed in wavenumbers. Eq. 5.15 comprises three simultaneous equations in six unknowns. However, by calling in the axial symmetry of the ruby lattice it is possible, at least as an approximation, to put $e_{xx} = e_{yy}$, $e_{xz} = e_{yz}$, and assuming the absence of shear strains in the X-Y plane $e_{xy} = 0$. Transforming from strain to σ as the independent variable gives:

$$\begin{aligned}
10^3.e_{xx} &= -18.5\ \sigma_{xx} - 12.2\ \sigma_{zz} + 23.8\ \sigma_{xz} \\
10^3.e_{zz} &= 19.3\ \sigma_{xx} - 9.6\ \sigma_{zz} - 20.0\ \sigma_{xz} \\
10^3.e_{xz} &= 1.45\ \sigma_{xz}
\end{aligned} \tag{5.16}$$

where the terms in σ are now in magnetic field units. Values of e were calculated using Eqs. 5.16 and are listed in Table 5.2.

The terms e_{xx} and e_{zz} represent normal or compressive strains, acting in the directions of the x-axis and z-axis respectively, while e_{xz} represents shear stress acting in a plane containing the z-axis. This latter results from the assumption of axial symmetry, and the inseparability of σ_{xz} and σ_{zx} owing to the symmetry of the G-tensor with respect to interchange of suffices.

It must be borne in mind that the values of e given in Table 5.2 represent the widths (between points of maximum slope) of the distribution of strain. If it is assumed that these distributions are centred on conditions of zero strain then the figures give an indication of the absolute magnitudes of the strains present at the paramagnetic sites. If this is not the case then, apart from very accurate measurements of the line position, there is no way of assessing absolute magnitudes.

A slight dependence of the values of e on growth orientation was observed, and is illustrated in Table 5.3 where the mean values for each orientation are given. No dependence of strain on chromium concentration was observed. The values of e_{xz}, representing shear stress exhibit somewhat less spread than the two normal strains. As discussed in Chapter 2, relief of shear strain during annealing results from motion of dislocations, a phenomenon which requires a certain critical stress to be exceeded

Orientation	e_{xx}	e_{zz}	e_{xz}
0^{o}	0.043	0.047	0.008
60^{o}	0.029	0.045	0.009
90^{o}	0.042	0.053	0.008

Table 5.3

Strain and Growth Orientation

Specimen	σ_{tot}	$\Delta\theta$	e_{xx}	e_{zz}	e_{xz}
312B(1)	28'	11'	0.089	0.007	0.005
312B(2)	30'	17'	0.125	0.033	0.007
312B(3)	90'	19'	0.012	0.118	0.012

Table 5.4

Heat Treatment of Ruby 312B

for its occurence. Although no information regarding ruby or corundum appears to be available, critical shear stress in metals is generally temperature dependent (Barratt, 1952, p.350). Variations in e_{xz} may thus be indicating small variations in the amounts of strain left unrelieved during the annealing process, and these could be due to differences of annealing temperature.

The values of e_{xx} and e_{zz} exhibit somewhat greater diversity, with the figures for the 60^{o} orientation, that of e_{xx} in particular, being somewhat lower than those for the other orientations. These figures represent compressive strains, possibly resulting from the juxtaposition of irregularly shaped crystallites posessing differing orientations. Calculations based on the theory given by Likhachev (1961) were mentioned earlier, and the results suggested that the expected strains would be less than 10^{-2} in magnitude. It must be remembered that the figures derived here represent the strain in the immediate vicinity of the paramagnetic sites and need not necessarily be typical of the bulk material. It should also be remembered that the numerical results of Tables 5.2 and 5.3 are the result of the certain approximations, and the deductions made from them may be, at best, valid only qualitatively. However, with this in mind, the results confirm the conclusions of Chapter 2 regarding the relative superiority of the Czochralski

material. Among the other types of ruby, there appears to be little difference, either between Vapour Phase and Verneuil or between 0° and 90° growth orientation, in the degrees of strain and crystallite misorientation. Figures 5.3 to 5.6 indicate certain characteristics of linewidth angular dependence which appear to be typical of different classes of material, and these were mentioned earlier. However, these features do not remain very apparent once the data has been analysed, but in view of the number of specimens on which measurements have been made it is concluded that these similarities are not fortuitous.

5.5 ARTIFICIAL DEGRADATION OF CRYSTAL QUALITY

In collaboration with D.R. Mason one specimen of Vapour Phase ruby was subjected to various treatments in an attempt to alter the physical properties. Irradiation with 40 keV X-rays from a tungsten target had been found to result in the formation of Cr^{4+} ions giving a distinctive additional line to the spectrum (Hoskins and Soffer, 1964, Mason and Thorp, 1966) but there was no noticeable effect on the spectrum of the Cr^{3+} ions. The specimen, ruby 312B, was a Vapour Phase sample having a concentration of 0.041 %, and three stages in its treatment can be distinguished:

312B(1) Specimen as cut from annealed boule.

312B(2) After heating for about two minutes at about 1900 $^{\circ}$C.

312B(3) After further heating in an oxy-gas flame until surface was molten.

After each treatment the specimen was allowed to cool in the atmosphere and then examined by X-rays and e.p.r. A summary of the results is given in Table 5.4. Qualitatively it was observed that whereas in states (1) and (2) the behaviour of the +1/2 to -1/2 transition was typical of the 0° growth material, in state (3) the behaviour was that of the 90° material. This is attributed to the fact that the relative orientations of dimensions and crystal axes of the specimen was typical of the 90° boules and thus there was a certain similarity in cooling conditions.

From Table 5.4 it is apparent that increasing severity of heat treatment results in increased misorientation and strain. The sole exception to this is e_{xx} which shows a sharp decrease in state (3). This may indicate a transition to a more uniformly strained condition, having a narrower distribution of strains about some non-zero value.

Chapter 6

E.P.R. LINEWIDTHS IN NEODYMIUM SCHEELITE

In recent years, the system of materials comprising compounds posessing the Scheelite structure doped with rare earth ions has aroused considerable interest. The neodymium ion has been extensively studied as it exhibits a strong emission in the infra-red, terminating about 2,000 cm^{-1} above the ground state, enabling $Nd:CaWO_4$ (Johnson and Thomas, 1963) and $Nd:CaMoO_4$ (Duncan, 1965) to exhibit continuous laser action at room temperature. There is by now a substantial accumulation of e.p.r. results from these materials, but to date there appears to have been no study of linewidths and relaxation times in a range of specimens of the same type but differing concentrations. In this chapter and part of Chapter 7 are presented the results and preliminary interpretation of the e.p.r. of neodymium in calcium tungstate (Scheelite).

6.1 CRYSTAL STRUCTURE

The melting point of calcium tungstate is 1535 ^{o}C (Nassau and Broyer, 1962), rendering it suitable for growth by the Czochralski technique. This process was used for growth of the material studied here. The lattice exhibits tetragonal symmetry, 4/m, and the unit cell, shown in Figure 6.1, contains two complete molecules (Hempstead and Bowers, 1960). Each calcium ion is surrounded by

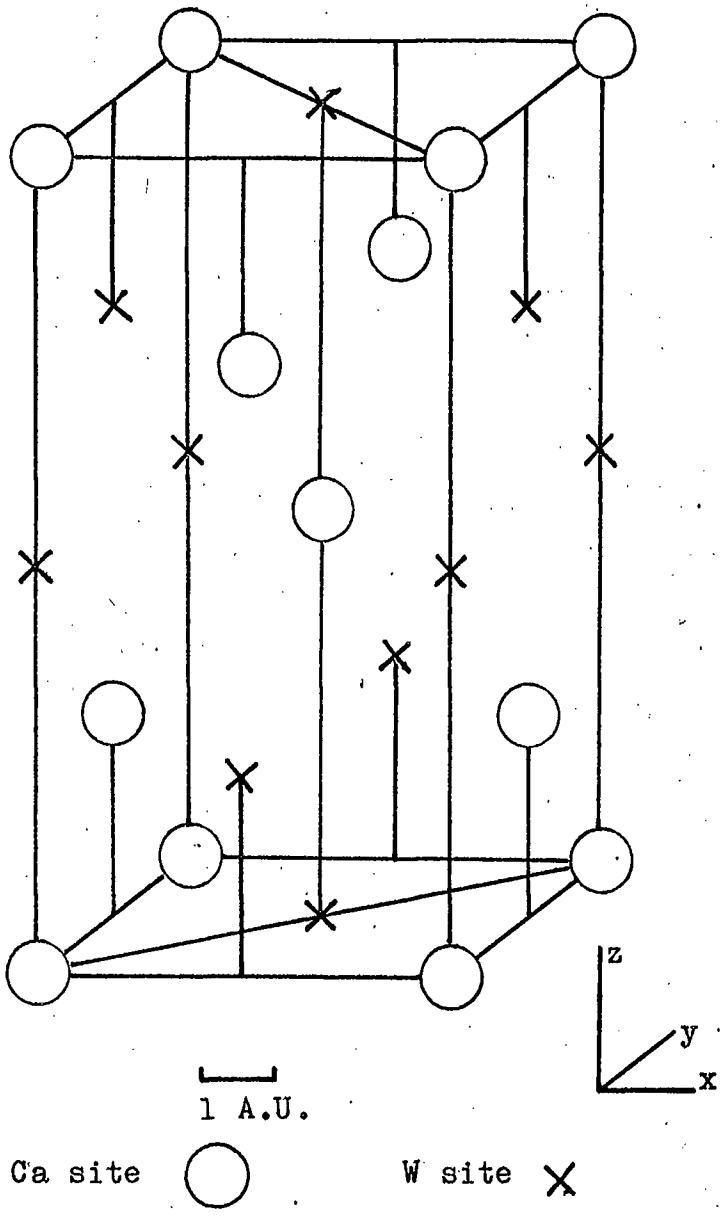

Figure 6.1

Unit Cell of Calcium Tungstate

(For simplicity the oxygen sites have been omitted)

eight oxygen ions, and the major interatomic distances are (Zalkin and Templeton, 1964):

Ca - O : 2.46 A.U. W - O : 1.78 A.U.

while the unit cell has dimensions a = 5.243 A.U., c = 11.376 A.U. The calcium sites occur in pairs, with the symmetry of one type derived from that of the other by reflection, resulting in magnetic equivalence.

Levingstein et al. (1963) investigated various etchants, and by using a mixture of hydrofluoric and chromic acids showed a correspondence between etch pits and dislocations on the {100} surfaces. Evidence was presented concerning the existence of two different types of dislocations, but no dislocation density figures were reported. From X-ray studies, Nassau and Broyer reported measurements of axial misorientations having magnitudes of about ten minutes of arc over distances of about 5 cm. These were estimated to be an order of magnitude less than the misorientations observed by them in Verneuil ruby and the differnece is an indication of the improvement in crystal quality resulting from growth at lower temperature.

The thermal expansion coefficient of calcium tungstate is highly anisotropic, the values reported by Nassau and Broyer at 1,000 ^{o}C being:

$\parallel$ c-axis $27.2 \times 10^{-6}\ {}^{o}C^{-1}$, $\perp$ c-axis $16.8 \times 10^{-6}\ {}^{o}C^{-1}$

As a result of this, and the greater thermal gradient along the growth axis of the boule, 90° growth material would be expected to be less strained than material grown in the 0° orientation.

Substitution of trivalent rare earth ions into either the divalent calcium or hexavalent tungsten sites presents problems in charge compensation, as any substitution should obviously preserve the charge neutrality of the lattice as a whole. In addition, the relative radii of the ions must be considered. Rare earth ions typically have radii in the region 0.85 to 1.4 A.U. and are thus more suited to substitution at the calcium site (radius 0.99 A.U.) than at the tungsten site (radius 0.62 A.U.)

Charge compensation is readily achieved during growth by the formation of calcium vacancies in such a manner that one vacancy neutralises two trivalent ions. This results in a chemical constitution of the form:

$$(Ca_{1-3x}Nd_{2x})WO_4.$$

As an alternative, compensation may be carried out by the deliberate introduction of cations into the melt, often in greater quantity than that of the rare earth ion. Monovalent ions, typically sodium or yttrium, are commonly used resulting in:

$$(Ca_{1-2x}Nd_xNa_x)WO_4$$

although Duncan obtained compensation for Nd^{3+} at the calcium site

by the substitution of Nb^{5+} at the molybdenum site in $CaMoO_4$. Chromium appears to substitute at the tungsten site in the hexavalent state giving:

$$Ca(W_{1-x}Cr_xO_4)$$

a result not altogether unexpected considering that the chromium ion has a radius of 0.63 A.U., only 0.01 A.U. greater than that of the tungsten ion that it replaces.

The possibility of rare earth substitution at the tungsten sites was at first not ruled out, and was indeed believed to explain some of the paramagnetic phenomena observed. However, Ranon and Volterra (1964) discounted this possibility on the grounds that the charge and size of the typical rare earth ion were incompatible with substitution at the small hexavalent tungsten site.

6.2 PARAMAGNETIC RESONANCE IN CALCIUM TUNGSTATE

As indicated in Chapter 1, paramagnetic resonance of neodymium in calcium tungstate occurs between the levels of the lowest doublet of the ground manifold $^4I_{9/2}$. The nature of the spin-lattice interactions is such that at temperatures above 15 ^oK the resonance is appreciably broadened, as a result of which most of the reported work has been carried out at 4.2 ^oK or below. The broadening of the line has been used (Kask et al., 1963) as a measure of spin-lattice

relaxation time.

In addition to the primary spectrum exhibiting tetragonal symmetry, the Hamiltonian of which was given in Chapter 1, two weaker spectra, each consisting of four lines and exhibiting orthorhombic symmetry, have been observed (Kedzie and Kestigian, 1963). The axes of the orthorhombic magnetic system do not correspond with those of the crystal, but have to be individually specified. The polar coordinates of the three axes of the g-tensor have been given by Volterra et al. (1966) as:

$$g_1 = 3.086,\ \theta_1 = 49.5^\circ,\ \phi_1 = 42.0^\circ$$

$$g_2 = 2.373,\ \theta_2 = 73.5^\circ,\ \phi_2 = 146.5^\circ$$

$$g_3 = 1.523,\ \theta_3 = 45.0^\circ,\ \phi_3 = 253.5^\circ$$

Ranon and Volterra noted that the orthorhombic spectra showed rather less departures from the tetragonal form than would have been expected from neodymium at the tungsten site, and proposed that these spectra were the result of charge compensation. In particular, a small orthorhomobic distortion was shown to be consistent with a nearest neighbour calcium vacancy. A similar suggestion concerning Ce:$CaWO_4$ was made by Klein and Mims (1962) and the absence of the orthorhombic spectra in chemically compensated material was noted by Garrett and Merritt (1964) in Nd:$CaWO_4$ and

by Nemanch and Veihmann (1967) for Yb:$CaWO_4$.

The isofrequency plot (35 Gc/sec) for the central line of the tetragonal spectrum is shown in Figure 6.2. The form of this is due entirely to the anisotropy of the g-factor. At the orientation of 90°, the lines of the hyperfine spectrum were resolvable, and all the expected lines were observed. At angles away from this the central line became broadened, often to such an extent that accurate measurements of its shape were impossible, and the hyperfine lines became indeterminate. Despite the vacancy compensation reported to be the compensating mechanism in the specimens examined (Webster, private communication) there was no evidence of orthorhombic spectra. If such spectra were present, they were below the limit of detection of the spectrometer.

6.3 HOMOGENEOUS BROADENING

Following the plan adopted for ruby, the homogeneous broadening of the e.p.r. absorptions in Nd:$CaWO_4$ will first be discussed. The mechanisms responsible for this have not yet been fully explained, but Kurkin and Shekun (1967) suggest that the major component of broadening is dipolar in origin, and they base their analysis of linewidth in Nd:$CaMoO_4$ on this. Discussion of homogeneous broadening will be based on linewidth measurements made at $\theta = 90^{\circ}$. Unlike the situation at the corresponding orientation

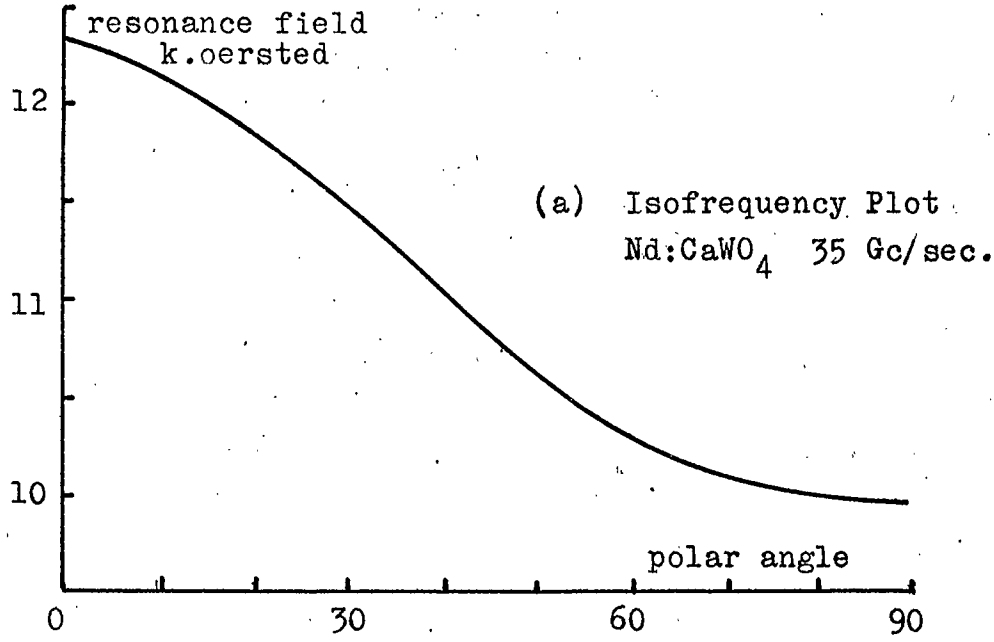

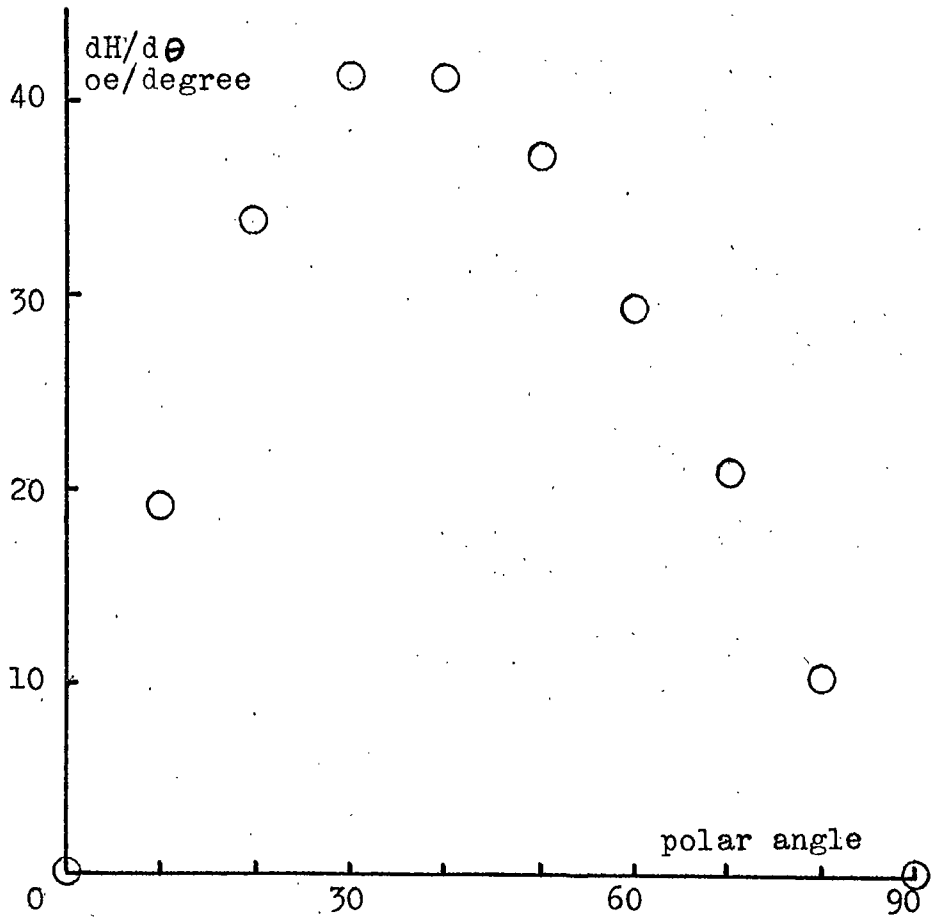

(b) $Nd:CaWO_4$ Angular Variation of $dH/d\theta$

Figure 6.2

in ruby, the inhomogeneous mechanisms have very little effect at this orientation. The choice of 90° rather than 0° was not voluntary; at 0° the fall-off in sensitivity was too great to allow of reliable measurements being consistently made.

Over the concentration range available (0.01 % to 1.0 %) there was an appreciable variation of linewidth, as shown in Figure 6.3. At low concentrations there was a trend towards a constant width, a phenomenon observed in ruby. A similar trend can be observed in the results for two specimens of $Nd:CaMoO_4$ reported by Kurkin and Shekun.

The appearance of a concentration independent width at low concentrations makes it hard to resist drawing an analogy with ruby and postulating a linewidth resulting from the action of both concentration-dependent and concentration-independent processes. To test this hypothesis, the results were fitted to an expression of the form:

$$(\Delta H_{ms})^2 = (\Delta H_o)^2 + (A.C)^2 \qquad (6.1)$$

where ΔH_o is the concentration-independent width, C is the concentration and A is a constant of proportionality determining the width of the concentration-dependent component. A linear dependence on concentration was chosen as, in the range available, the dipolar line would have a width linearly proportional to

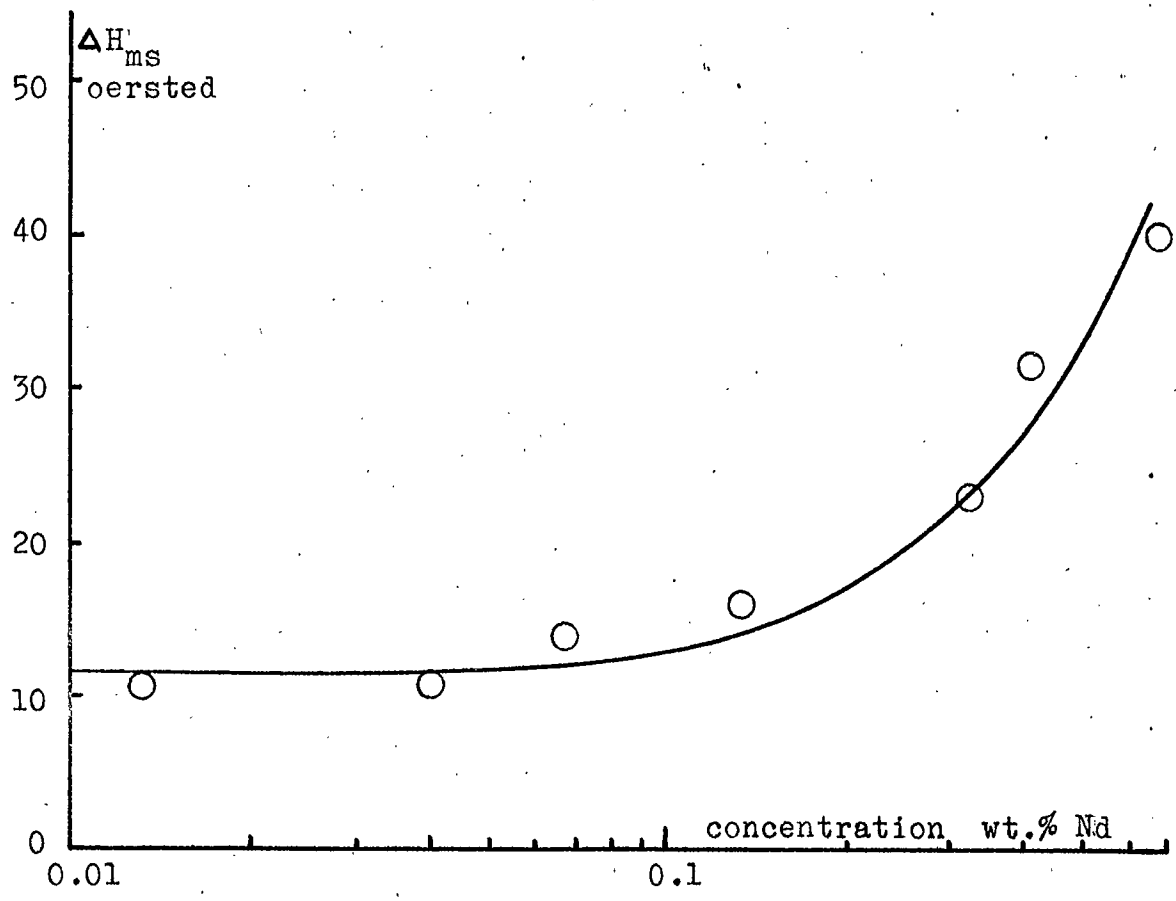

Figure 6.3

Nd:$CaWO_4$, Concentration Dependence of Derivative Width

$\theta = 90^\circ$ 4.2 °K

concentration (Kittel and Abraham, 1953). The best fit by a least squares method gave:

$$\Delta H_o = 11.6 \text{ oersted}, \quad A = 41.2 \text{ oersted/\% conc.}$$

and the dependence given by these figures is shown as the full line in Figure 6.3. The paramagnetic 4f electrons of the neodymium ion are well shielded by the closed 5s and 5p shells, making the possibility of exchange rather unlikely. The theories of dipolar broadening predict Lorentzian lineshapes so the combination of widths in Eq. 6.1 is inaccurate. A full analysis of the lineshapes has not been carried out, but Posener (1959) shows that the loss of accuracy in assuming Eq. 6.1 in these circumstances is not very great.

The residual linewidth, ΔH_o, will now be explained on the basis of the ideas put forward by Grant and Strandberg (1964b), and outlined in Chapter 4. It would seem unlikely that covalent bonding between the paramagnetic ions and ions of the lattice occurs, by virtue of the shielded nature of the 4f electrons. Isotopes of both calcium and tungsten, posessing nuclear spins of 7/2 and 1/2 respectively, do exist although only ^{183}W is present in any substantial proportion. The possibility of magnetic dipole interactions between the paramagnetic ions and these nucleii is thus offered, and an order of magnitude calculation based on the

theory given by Grant and Strandberg was carried out as followes. The second moment of the dipolar line resulting from the interaction contains the term:

$$C_{jk} = (gg'/hr_{jk}^3)(3\cos^2\theta_{jk} - 1) \qquad (6.2)$$

where the j-th atom is the one under consideration and the atoms indexed by k are those of the other species. Expanding this term in spherical harmonics and incorporating the orientation of the system leads to:

$$(3\cos^2\theta_{jk}-1)^2 = (4/5) + (32/21)\sum_m Y_{2m}^*(\theta_H,\phi_H).Y_{2m}(\theta_k,\phi_k) + (32/35)\sum_m Y_{4m}^*(\theta_H,\phi_H).Y_{4m}(\theta_k,\phi_k) \qquad (6.3)$$

where θ_H and ϕ_H specify the magnetic field orientation relative to the crystal axes. For the case of ruby, symmetry dictates that m can only have values of integral multiples of 3. In the tetragonal case, m has values of integral multiples of 4, and only terms Y_{20}, Y_{40} and Y_{44} appear. (For ruby, the corresponding terms are Y_{20}, and Y_{40} and Y_{43}). Expansion of Eq. 6.3 is relatively easy using the standard forms of the spherical harmonics. However, in the restricted conditions of the present measurements, $\theta = 90^\circ$, $\phi = 0^\circ$, the terms in Y_{43} (for ruby) and Y_{44} (for calcium tungstate) both vanish. Thus to a first approximation, the figure calculated by Grant and Strandberg for $\sum C_{jk}^2$ for ruby can be used for calcium

tungstate. A further approximation arises when it comes to consideration of the positions of the ions in the lattice. However if the similarity of the lattice dimensions of ruby and calcium tungstate is taken as an indication of similarity of ionic positions, thus justifying the use of the ruby lattice-sum, a calculation of linewidth can be performed. Treating the dipolar interaction between neodymium and tungsten (^{183}W) and using the appropriate nuclear g-factor for tungsten (Andrew, 1958) gives a linewidth of about 7 oersted. This is in order of magnitude agreement with the width of 10.4 oersted measured in the lowest concentration sample. A more exact calculation of the lattice-sum for this material would be desirable.

6.4 INHOMOGENEOUS BROADENING

Measurements of linewidth were made, where possible, at 10° intervals of polar angle between 0° and 90°. The width of the central line of the spectrum was highly anisotropic, typical results being shown in Figure 6.4, and in some specimens the broadening at intermediate angles was so great that it proved impossible to obtain meaningful results. The linewidth at 0° were consistently greater than those at 90°, but the degree of excess varied between samples. Kurkin and Shekun observed a similar anisotropy in $Nd:CaMoO_4$, but in this case the width at 90° was

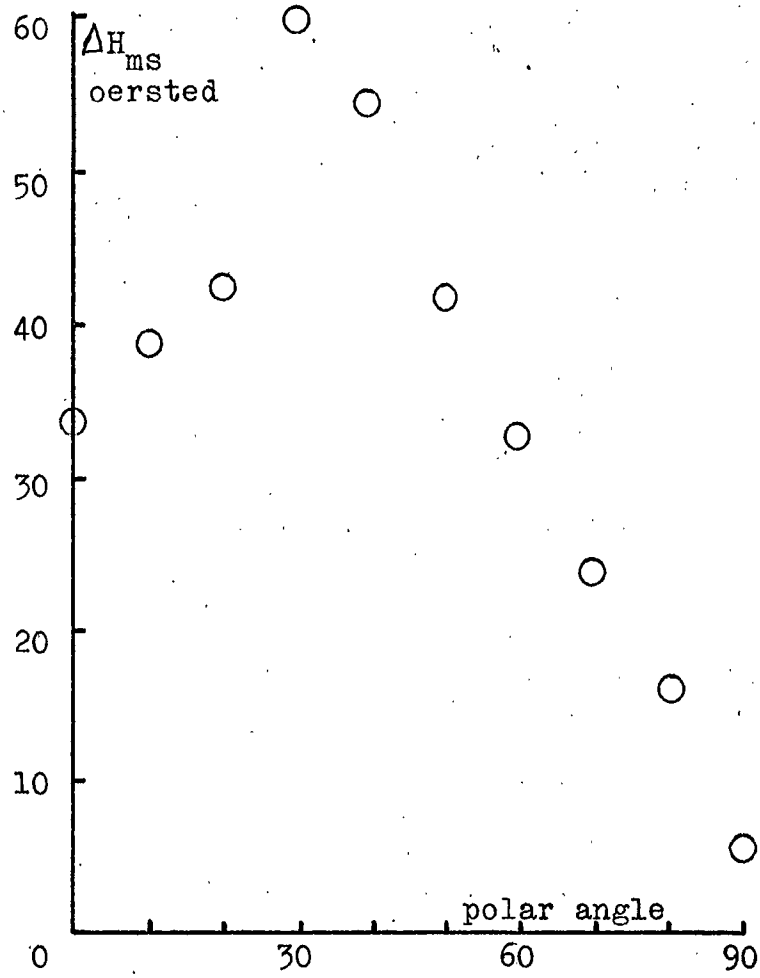

Figure 6.4
Angular Dependence of Linewidth
Nd:$CaWO_4$, 0.06 %, 4.2 ^{o}K

greater.

As in the case of ruby, axial misorientations, strain and electric field effects will be considered as inhomogeneous mechanisms broadening the already homogeneously broadened line. From the results of their analysis of the angular dependence in Nd:$CaMoO_4$, Kurkin and Shekunconcluded that the dipolar width (which they did not attempt to explain further) was quite anisotropic having minima of 10 oersted at 0^o and 90^o and a maximum of 30 oersted around 40^o. Broadening in excess of these values was often considerable, and was attributed to local fluctuations of g-factor and axial misorientations. Expansion of Eq. 6.3 suggests that the dipolar interactions, both Nd-Nd and Nd-W, will exhibit anisotropic behaviour, but a detailed consideration of this must await exact evaluation of Eq. 6.3.

The effect of uniaxial stress on the e.p.r. spectrum of Nd:$CaWO_4$ was investigated by Zaitov and Shekun (1966). They presented results for the G-tensor, some four orders of magnitude less than the values obtained for ruby by Hemphill et al. (1966). The conclusions drawn from this is that the direct coupling of the spins to the lattice is very slight, a result not inconsistent with the screened position of the 4f ions. In view of this evidence, internal strain will be neglected as a possible source of broadening.

The effects of internal electric fields on e.p.r. of [illegible] rare earths in calcium tungstate have been described by Mims and Gillen (1966) who observed strongly anisotropic linewidths exhibiting direct correlations with the electric field shift in resonance position. A calcium defect was estimated to produce an electric field of 50 kV/cm at a range of 77 A.U., giving, in the case of erbium, shifts of around 30 oersted. Mims (1965) measured the components of the electric field effect tensor, giving the figures for neodymium as at least an order of magnitude less than those for erbium. Electric field broadenings of a few oersteds might reasonably be expected.

If electric field broadening effects are present they will be manifested as an anisotropy of the linewidth observed on rotation in any plane of the system. By choosing to make measurements in the plane perpendicular to the c-axis it is possible to eliminate axial misorientations and anisotropy of homogeneous width as possible causes of anisotropy. Table 6.1 shows the results of measuring ΔH_{ms} as a function of ϕ, azimuthal angle in the X-Y plane. Very little dependence on the angle could be observed, and from this it was deduced that electric fields are not contributing appreciably to the broadening of absorptions in the specimens examined here.

ϕ	15	30	45	60	75	90
ΔH_{ms}	8.9	9.1	9.9	9.5	9.4	9.7

Table 6.1

Variation of ΔH_{ms} in the X-Y Plane

As yet, the specimens have not received the same investigation as the ruby samples discussed earlier, and only qualitative data is available concerning crystal texture. In general, the quality of the material is better than that of the average ruby, a result attributed to the lower growth temperature, and in no case was splitting of X-ray diffraction spots observed. From this it is concluded that if mosaic structure is present, and from the method of growth this is quite likely, the individual crystallites are somewhat larger than the region illuminated by the X-ray beam. Insufficient measurements of the long-range c-axis misorientation have been made to enable any useful conclusions to be drawn.

Analysis of the linewidth figures was complicated by the unknown angular dependence of the width of the homogeneous line. As a starting point it was assumed that values at angles intermediate between 0° and 90° could be obtained by linear interpolation between the observed linewidths for these angles,

at which the inhomogeneous broadening would appear to be negligible. Using a relationship:

$$(\Delta H_{ms})^2 = \Delta H(\theta)^2 + (\Delta\theta . dH/d\theta)^2 \qquad (6.4)$$

together with the values of $dH/d\theta$ obtained from the isofrequency plot and given in Figure 6.1 and the interpolated values of $\Delta H(\theta)$, the homogeneous width, the values of $\Delta\theta$ were calculated. Using the mean value of $\Delta\theta$ thus obtained, it was possible to arrive at new values of $\Delta H(\theta)$. In Figure 6.4 the results obtained by a process of this kind are indicated. The true significance of the values of $\Delta H(\theta)$ is confused by the fact that an error of 1 oersted in the width of the broadest line results in a change of double that figure in the corresponding value of $\Delta H(\theta)$.

These results suggest that although the assumption of linear dependence provides a starting point for a calculation, it does not result in a consistent fit of theory to experiment. The lattice sum calculation should provide a more reliable functional dependence of the homogeneous linewidth.

6.5 CONCLUSIONS

This chapter describes the results of what may be described as a preliminary investigation of the causes of line broadening in Nd:$CaWO_4$. Much work remains to be carried out, in particular a

systematic X-ray investigation, and the calculation of dipolar broadening referred to several times already.

Chapter 7

SPIN-LATTICE RELAXATION MEASUREMENTS

7.1 RELAXATION PROCESSES

It is not proposed to describe in detail the various theories put forward to explain spin-lattice relaxation, but merely to outline the processes qualitatively and to indicate the results. The early theory of Waller (1932) considered modulation of the internal dipolar interactions by lattice phonons as the relaxation mechanism, but agreement with the experiments of Gorter (1936) was poor. Following the lead of Heitler and Teller (1936) Van Vleck (1940) treated modulation of the crystal field as the relaxation process, and a modified version of this treatment was given by Mattuck and Strandberg (1960). Orbach (1961) presented an alternative treatment of the orbit-lattice Hamiltonian and went on to establish the existence of a further relaxation process operative under certain conditions. Donoho (1964) expressed the spin-lattice Hamiltonian as an operator quadratic in spin and linear in strain, identical with $\mathcal{H}''$ of Eq. 5.6, and made explicit calculations for ruby.

In the relaxation process the relaxing spin gives up a quantum of energy equal to the difference between its initial and final energy states. In considering this theoretically, three different mechanisms must be considered.

In the Direct Process a spin relaxation from $|b\rangle$ to $|a\rangle$ occurs simultaneously with the creation of a phonon of energy E. Using an appropriate interaction Hamiltonian the Direct process can be shown to have a temperature dependence of the form:

$$1/T_{1D} = AT \qquad (7.1)$$

where the constant A includes a term in H^4 in the case of an isolated Kramers' doublet, giving a strong field dependence.

The Raman Process involves the simultaneous absorption of a phonon of energy E_1 and the emission of another of energy E_2 resulting in a transition, subject to the condition $E_2 = E_1 + E$. For a Kramers' system the relaxation can be shown to obey:

$$1/T_{1R} = BT^9 \qquad (7.2)$$

If the Debye energy, (i.e. the energy of the most energetic phonon that the lattice can support), $k\theta_D$, is greater than the crystal field splitting, Δ, to the first level above the ground level a resonant two phonon process, the Orbach Process (Orbach, 1961), occurs. At low temperature this obeys the law:

$$1/T_{1R} = C.\exp(-\Delta/kT) \qquad (7.3)$$

For a system in which all these processes are occuring simultaneously the individual relaxation times add inversely giving:

$$1/T_1 = AT + BT^9 + C.\exp(-\Delta/kT) \qquad (7.4)$$

a result which holds for an isolated Kramers doublet. For a multilevel system the Raman process shows a T^{-7} (Klemens, 1962) or under certain conditions a T^{-5} (Orbach and Blume, 1962) dependence.

The calculations of Donoho were based on an interaction Hamiltonian of the form:

$$\mathcal{H}'' = \sum_{ij} \sum_{lm} G_{ijlm}\, e_{lm}\, S_i S_j \qquad (7.5)$$

where e_{lm} is the local strain. By computing the strain associated with the passage of a phonon, Donoho evaluated relaxation times, with the assumption that the strain at a paramagnetic site was the result of the superposition of the normal modes of the crystal. In fact substitution of an ion at a lattice site is likely to cause an alteration in the local strain and thus influence the relaxation behaviour. Klemens considered the case in which the characteristic frequency of the defect was greater than the Debye cut-off frequency and showed that under these circumstances the Raman process had an exponential dependence. If the Debye frequency is greater than the defect frequency phonons propagate through the lattice and the strain is not localised (Castle et al., 1963). The effect of this is to alter the magnetic field dependence of the Direct process and the temperature dependence of the Raman process.

7.2 EXPERIMENTAL RESULTS : I RUBY

7.2.1 Texture Dependence

In his study of relaxation mechanisms in ruby, Mason (1966) observed large variations in relaxation time, far exceeding the possible errors of measurement, in nominally identical specimens. These were attributed to lattice disorders, possibly strain at paramagnetic sites, resulting from crystalline misorientations. Plotting Mason's relaxation time measurements against the c-axis misorientation figures of Table 2.1 gave an approximately linear relationship (Mason and Thorp, 1967) with relaxation time decreasing as misorientation increased. In Chapter 2, the standard deviation of the misorientation measurements was suggested as suitably representing the degree of misorientation in a specimen, and the relationship between relaxation time and this parameter is shown in Figure 7.1. In addition to Mason's results for the +1/2 to -1/2 transition at 90°, the extremely long relaxation time obtained by the present author from the Czochralski ruby L2 is included, showing remarkable agreement. With data regarding internal strain available from Chapter 5, a further comparison was made, as shown in Figure 7.2 where relaxation time is plotted against e_{xx}. A somewhat similar behaviour was obtained from e_{zz}.

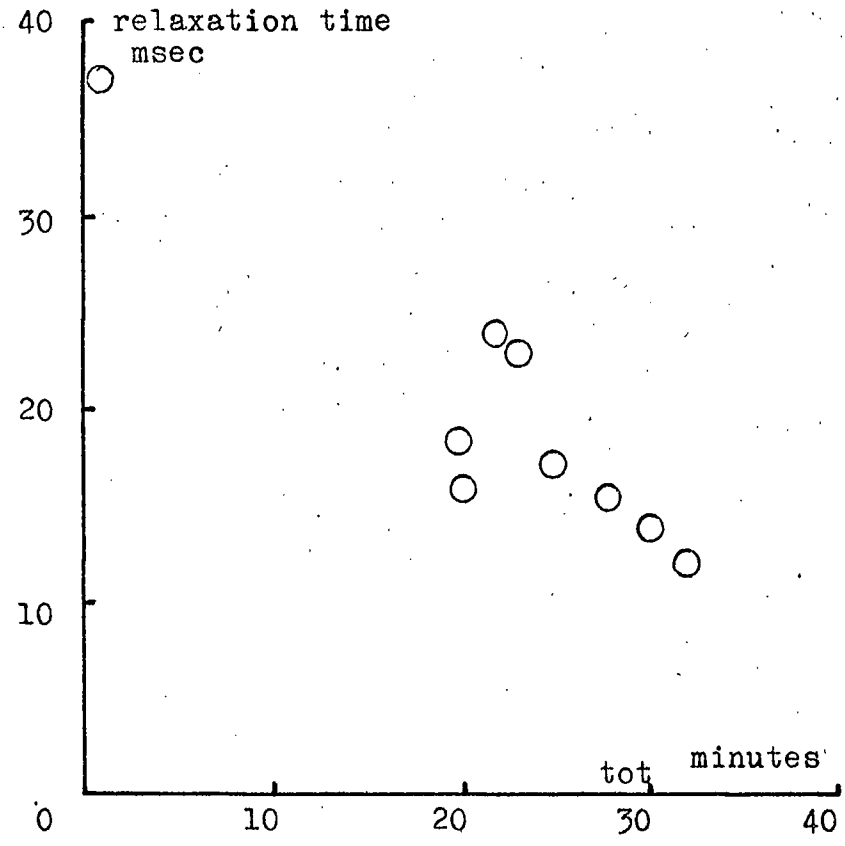

Figure 7.1

Dependence of Relaxation Time on
Standard Deviation of Misorientation
Ruby, $\theta = 90^{\circ}$, 4.2 $^{\circ}$K

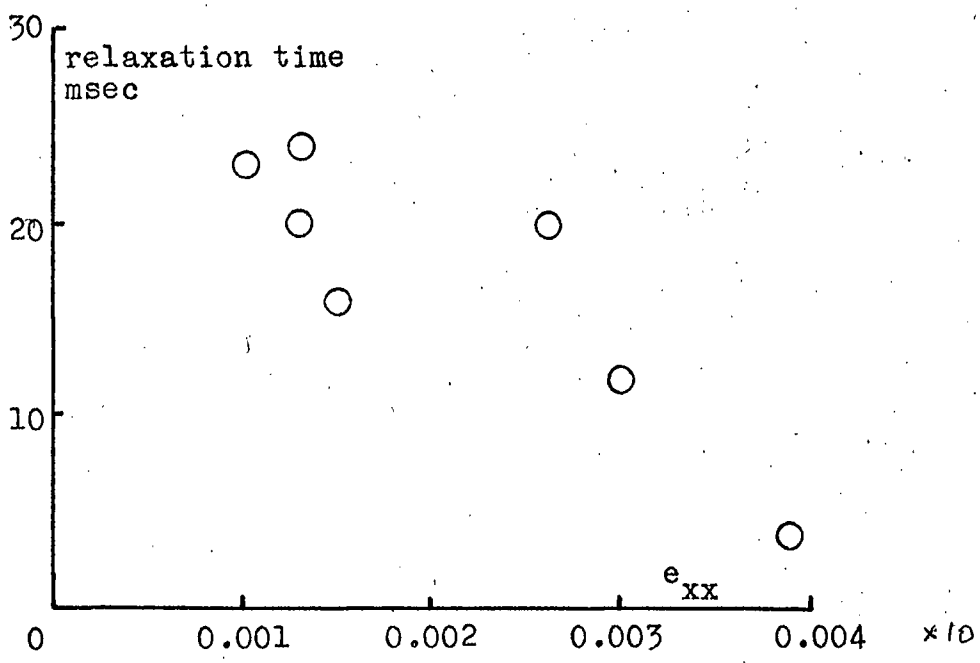

Figure 7.2

Dependence of Relaxation Time on Strain
Ruby, $\theta = 90^{\circ}$, 4.2 $^{\circ}$K

At 4.2 ^{o}K the Direct process is the predominant relaxation mechanism in ruby, with the temperature at which Direct and Raman processes become equivalent being around 40 ^{o}K. The temperature dependence observed in the ruby L2 was found to be the simple T^{-1} behaviour expected in the Direct region and similar dependences in this region were observed by Mason. This appears to confirm the predictions of Castle et al. regarding the effect of defects on relaxation in the direct region, but as no measurements were made on L2 at temperatures above 4.2 ^{o}K no check on the behaviour in the Raman region could be made.

7.2.2 Angular Dependence in Czochralski Ruby

Figures 7.3 to 7.5 show the angular dependence of relaxation time observed for the three $\Delta M = 1$ transitions in the Czochralski ruby L2. In each case only single exponentials could be distinguished, in agreement with the calculations of relaxation amplitude of Donoho (Private communication to D.R. Mason). Together with the experimental results are shown the predictions of Donoho for 35 Gc/sec, scaled down by a factor of one third. Mason obtained agreement for Vapour Phase results by scaling down by one sixth. The agreement was quite good for the +1/2 to -1/2 transition, moderately good for the -1/2 to -3/2 and poor for the +3/2 to +1/2, the relaxation times of which were similar to those observed in

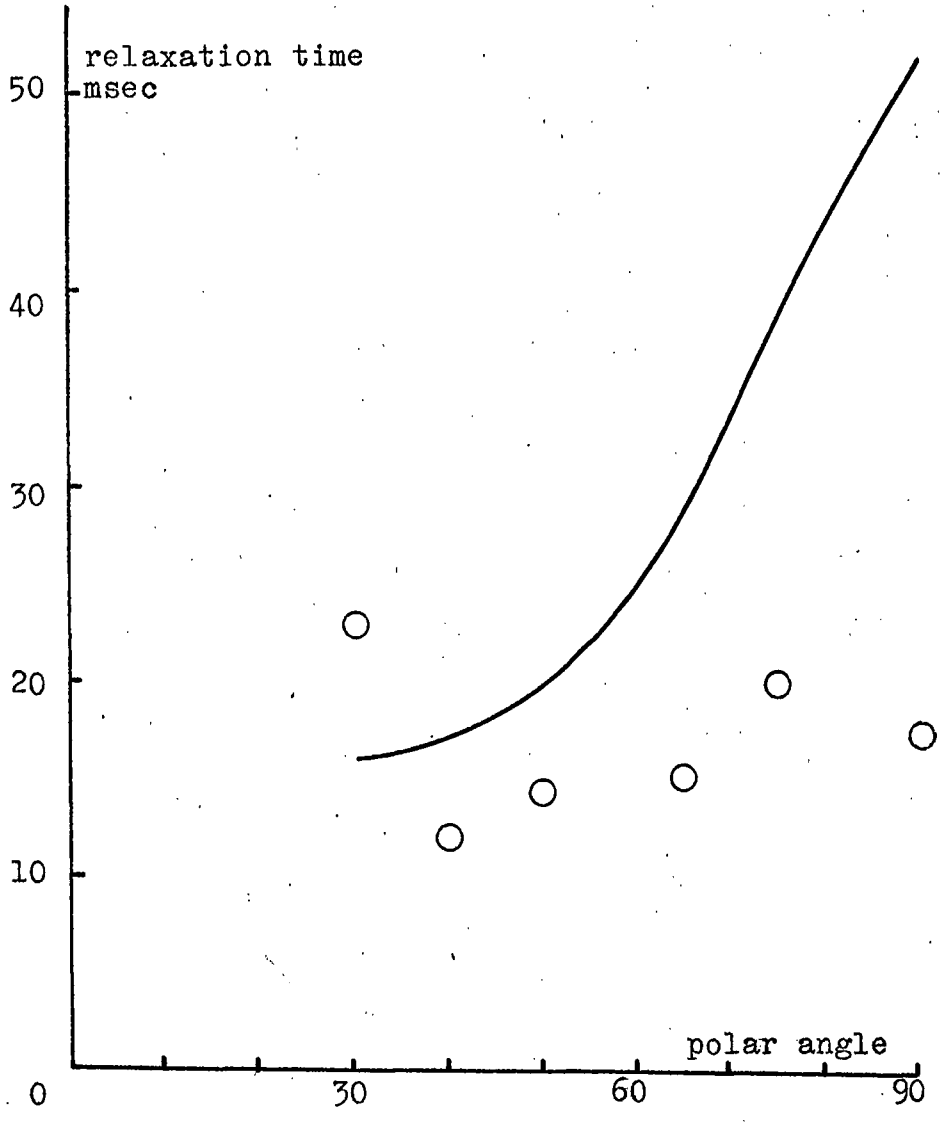

Figure 7.3

Angular Dependence of Relaxation Time
Czochralski Ruby, 0.045 %, 4.2 ^{o}K
+3/2 to +1/2

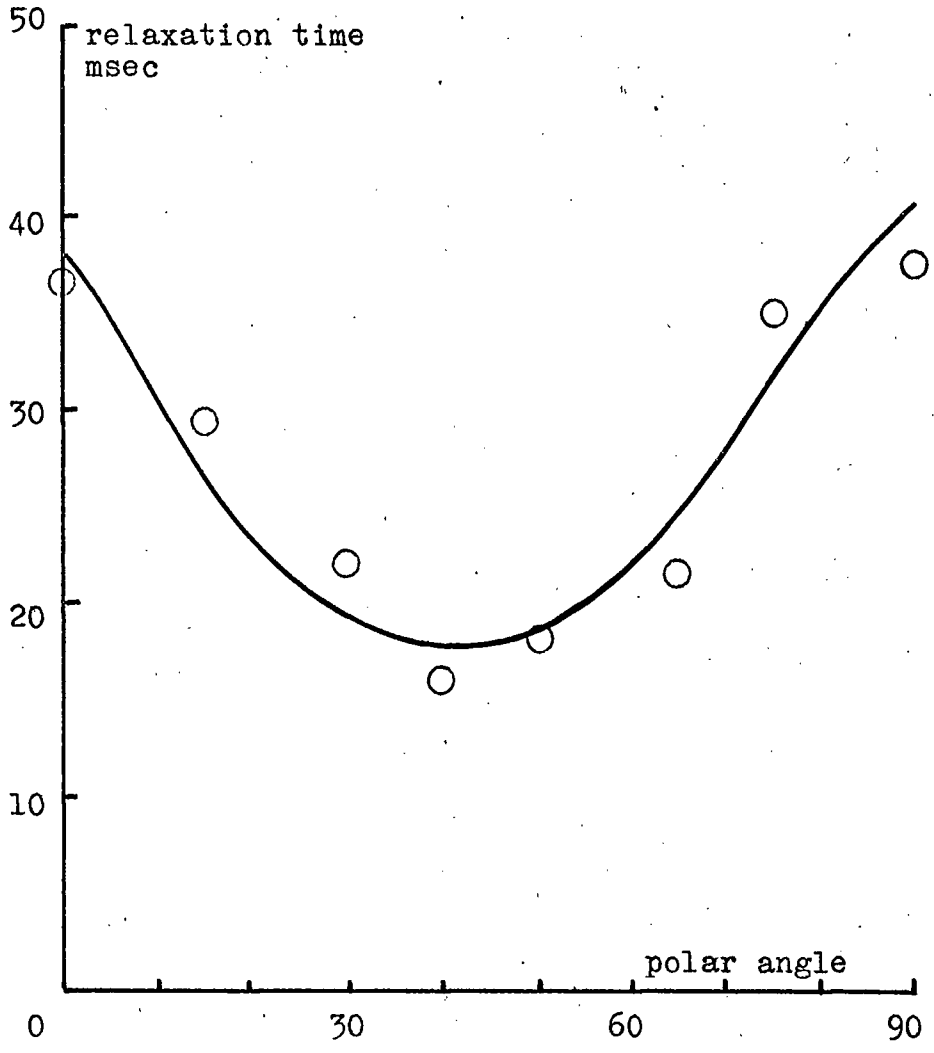

Figure 7.4

Angular Dependence of Relaxation Time
Czochralzki Ruby, 0.045 %, 4.2 ^{o}K
+1/2 to -1/2

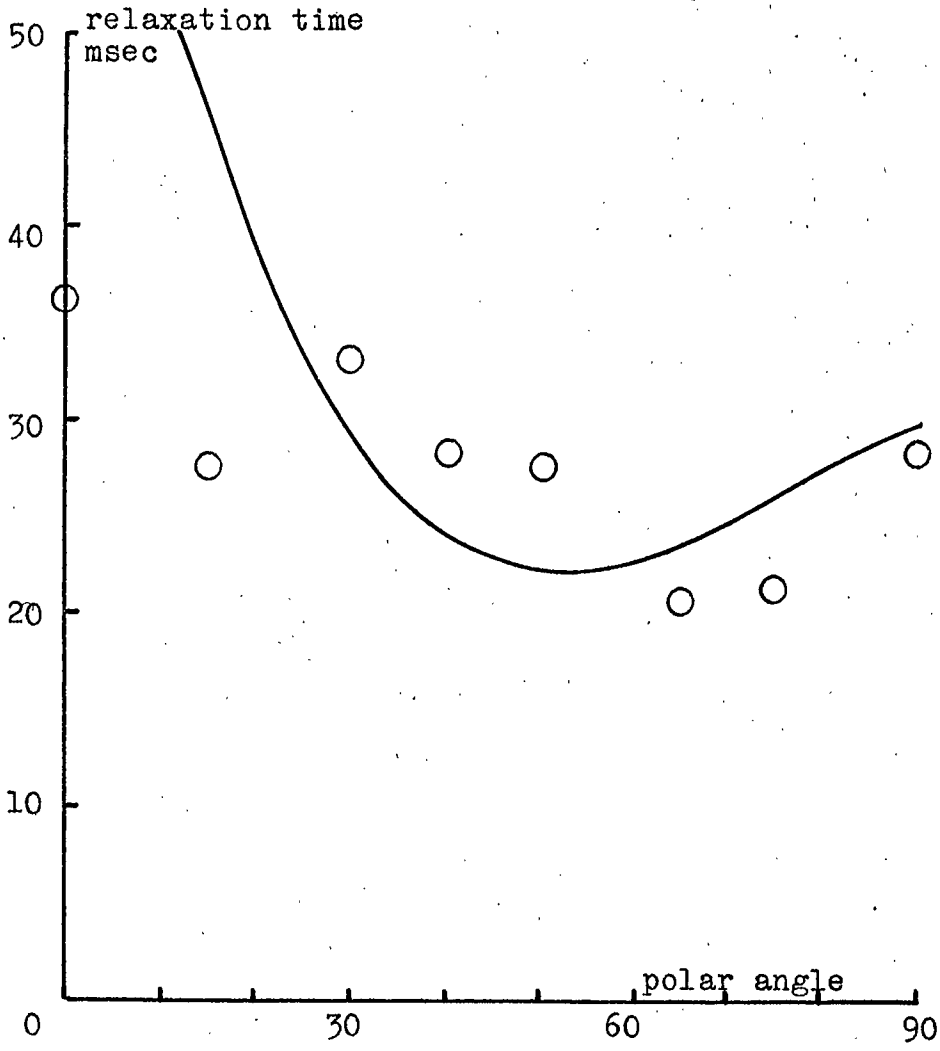

Figure 7.5

Angular Dependence of Relaxation Time
Czochralski Ruby, 0.045 %, 4.2 °K
-1/2 to -3/2

flame fusion material. The divergences between modified theory and experiment were similar to those observed by Mason and explained by him on the basis of harmonic cross relaxation. For example, the +3/2 to +1/2 has a 3:2 cross-relaxation at 90° and another of 5:3 near 70°, and similar processes may be invoked to explain the divergences of the -1/2 to -3/2 at low polar angles.

The most important feature of these results is the incidence of relatively long relaxation times. The original Czochralski ruby, L1, gave a relaxation time of the +1/2 to -1/2 at 90° of 17.5 msec, a value close to those observed in flame-fusion material. Brown (1967) reports a figure of 35.0 msec for L2 using the Pulse-Response technique (Brown and Thorp, 1967), (compare 37.5 msec by pulse saturation method) and has observed a similar relatively long relaxation time at 71 Gc/sec, with 12.5 msec as opposed to the average for Vapour Phase material of about 4 msec. This increase in relaxation time in L2 is attributed directly to the improvement in crystal quality and lends further support to the suggestion that the Czochralski ruby L1 was relatively poor in this respect.

7.3 EXPERIMENTAL RESULTS : II Nd:$CaWO_4$

7.3.1 Temperature Dependence

Measurements of spin-lattice relaxation times as a

function of temperature in the liquid helium range were made on a $Nd:CaWO_4$ specimen having a concentration of 0.1 %. The observed temperature dependence is shown in Figure 7.6 for temperatures in the range 1.8 to 4.2 ^{o}K at an orientation of 90^{o}. Below 2.5 ^{o}K the direct process appears to dominate the relaxation, but above this figure the temperature dependence becomes ~~curved~~ non-linear. Using the values of velocity of sound measured by Gerlich (1964) the Debye temperature was estimated to be 765 ^{o}K, corresponding to a cut-off frequency of 1.8×10^{13} c/sec. As this is greater than the overall splitting of the ground manifold, (Johnson and Thomas, 1963) the existence of an Orbach mechanism may be expected. However, Johnson and Thomas report the splitting, Δ, to the first level above the ground level to be about 115 cm^{-1}, and consequently the Orbach relaxation can be neglected relative to the other processes. Using a least squares procedure, and assuming that the ground doublet is effectively isolated, the experimental results were found to obey the relation:

$$1/T_1 = 16T + 3.8 \times 10^{-4} T^9 \qquad (7.6)$$

where the relaxation time, T_1, is given in milliseconds and T is the absolute temperature. The fit of this relationship to the experimental points is shown in Figure 7.6. For a more concentrated

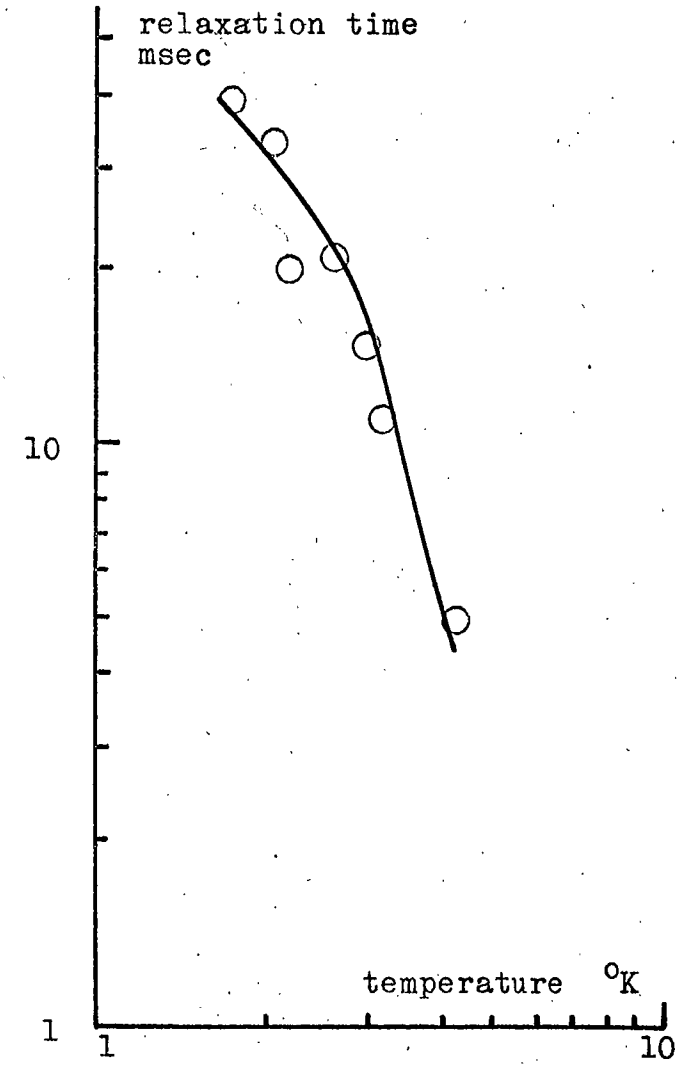

Figure 7.6

Temperature Dependence of Relaxation Time
$Nd:CaWO_4$, 0.06 %, $\theta = 90^{\circ}$, 4.2 °K

specimen, (0.5 %), Antipin et al. (1967) obtained (at 35 Gc/sec and $\theta = 90^{\circ}$):

$$1/T_1 = 26T + 4.5 \times 10^{-5}T^9 + 8.7 \times 10^{10}\exp(-136/T) \qquad (7.7)$$

indicating a splitting, Δ, of 136 $^{\circ}$K or 95 cm^{-1}. For Nd:$PbMoO_4$ they observed the Raman term to be $1.7 \times 10^{-5}T^9$ whereas calculations based on the work of Scott and Jeffries (1962) gave $2.2 \times 10^{-4}T^9$.

7.3.2 Angular Dependence

Figure 7.7a shows the angular dependence of relaxation time, measured in a specimen having a concentration of 0.06 %. This form of behaviour was typical of all the specimens examined. In almost every case there was a local minimum in the region of $\theta = 30^{\circ}$, and an otherwise steady increase from 0° to 90°. A tentative explanation has been made by considering separately the Direct and Raman processes. Larson and Jeffries (1962a) evaluated the constants A and B of Eq. 7.4 as:

$$A = K_1 \sum_{nm}\left[\sum_i (2\beta\Lambda/\Delta_i)(\langle a|\underline{H}.\underline{J}|i\rangle\langle i|v_n^m|b\rangle + \langle a|v_n^m|b\rangle\langle i|\underline{H}.\underline{J}|b\rangle)\right]^2 \qquad (7.8)$$

$$B = K_2 \sum_i 1/\Delta_i^4\left[\sum_{nm}\langle a|v_n^m|i\rangle^2 \times \sum_{nm}\langle i|v_n^m|b\rangle^2\right] \qquad (7.9)$$

where in each case $|a\rangle$ and $|b\rangle$ define the transition under consideration and $|i\rangle$ represents a higher level at Δ_i. The term A thus becomes field dependent and, if g is anisotropic, angular

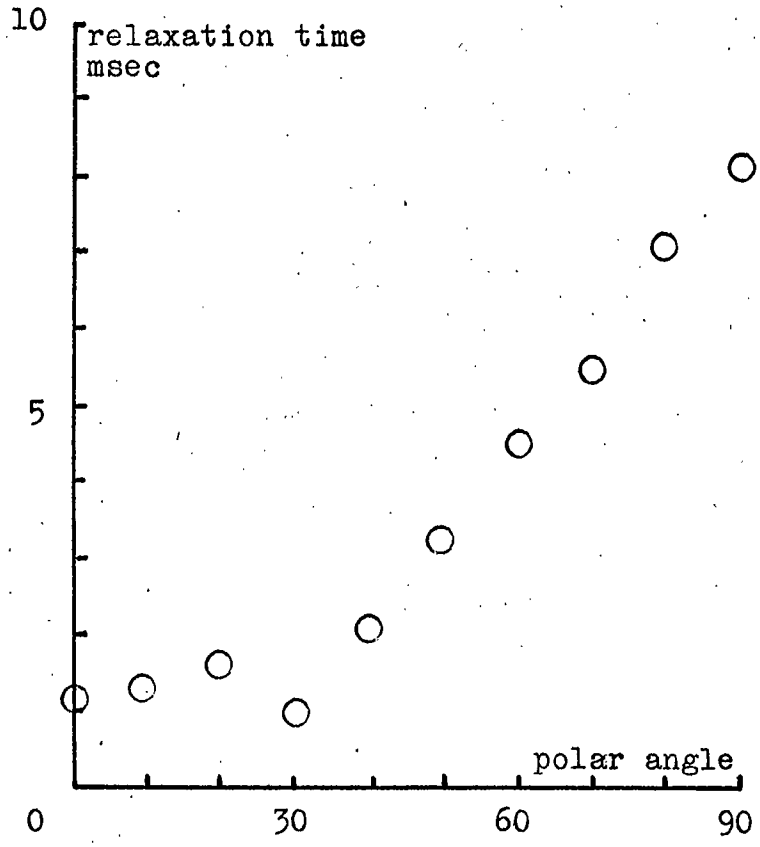

(a) Angular Dependence of Relaxation Time

$Nd:CaWO_4$, 0.06 %, 4.2 ^{o}K

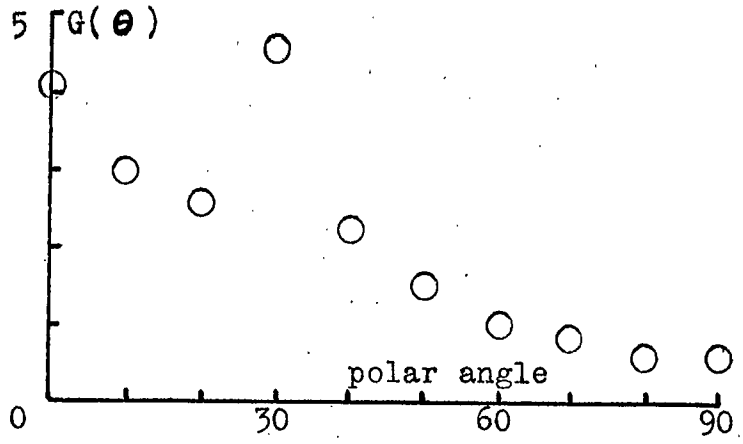

(b) The Angular Dependence Function G(θ)

Figure 7.7

dependent whereas B remains constant unless the Zeeman splitting approaches the crystal field splitting in magnitude. At constant frequency, a behaviour of the form:

$$1/T_{1D}(\theta) \propto G(\theta)/g^2(\theta) \qquad (7.10)$$

is expected, where $G(\theta)$ is a dimensionless factor containing all of the angular dependence.

Using the ratio T_{1D}/T_{1R} derived from the results of the previous section for 4.2 ^{o}K and $\theta = 90^{o}$, values of T_{1D} were calculated, from which $G(\theta)$ was derived. This is shown in Figure 7.7b. The behaviour of relaxation time as a function of polar angle in $CaWO_4$ does not appear to have been examined elsewhere, but the results of Larson and Jeffries for neodymium in various rare earth double salts exhibits a similar behaviour.

The origin of the local minimum around 30^{o} may be cross relaxation to an impurity ion. Larson and Jeffries (1966b) report that Cerium is a common impurity associated with neodymium, and with the Orbach process dominant even in the helium region this would provide an efficient cross relaxation mechanism.

7.3.3 Concentration Dependence

Figure 7.8 illustrates the concentration dependence of relaxation time, measured at 4.2 ^{o}K and $\theta = 90^{o}$. The crystal field theory of spin-lattice relaxation leads to concentration independence,

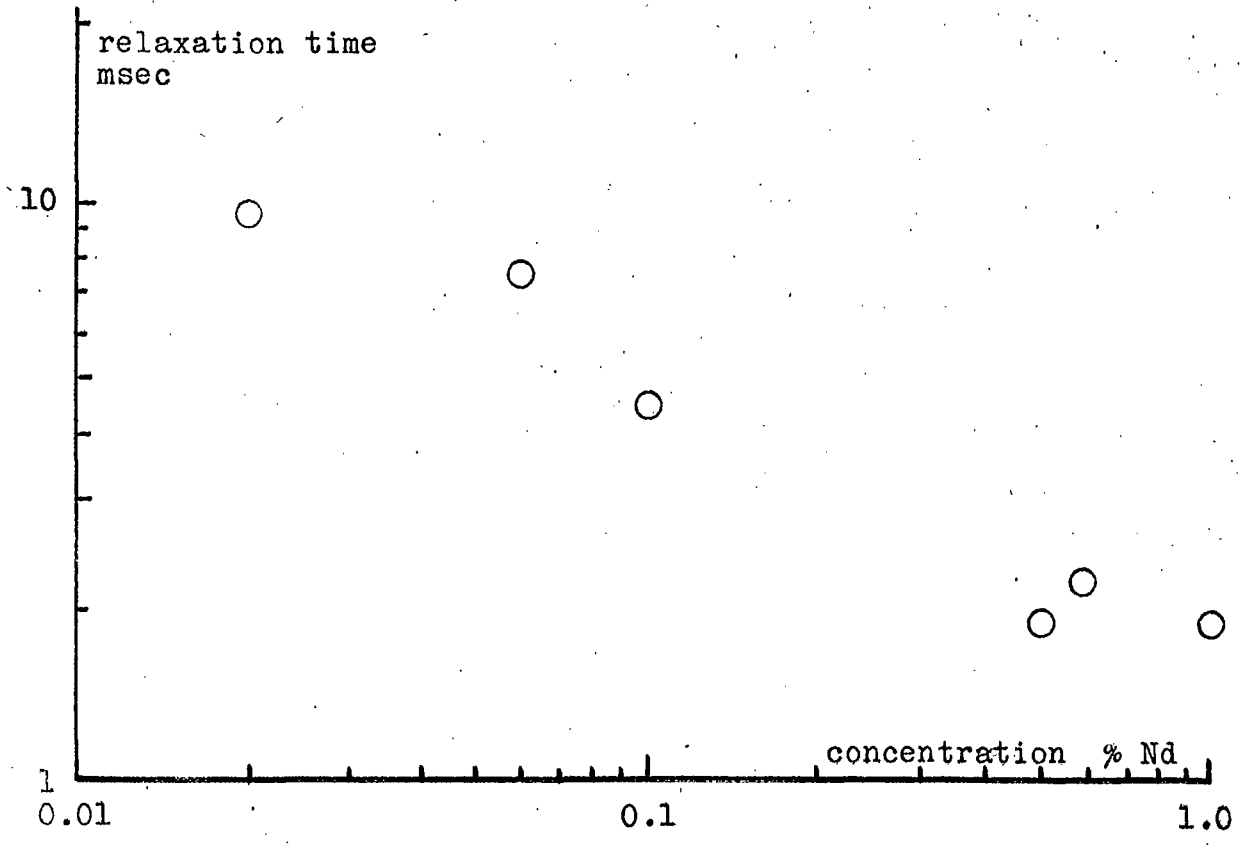

Figure 7.8

Concentration Dependence of Relaxation Time
$Nd:CaWO_4$, $\theta = 90^{\circ}$, 4.2 $^{\circ}K$

but Kochelaev (1960) has shown that a concentration dependence can be accounted for by considering the substitutional ions as point defects. The resultant phonon scattering is greatest in the low energy range and consequently the direct region is more affected than the Raman. For the Direct region, Kochelaev found:

$$T_{1D} \propto c^{-4/3} \qquad (7.11)$$

Bloembergen and Wang (1954) have shown that clusters of ions, by being strongly exchange coupled, may relax extremely rapidly. A mechanism of this nature would provide a concentration dependence.

The power of the concentration dependence observed here is somewhat less than unity, and is an almost linear function of polar angle, ranging from 0.13 at $\theta = 0^{\circ}$ to 0.55 at 90°. The picture is obviously confused by the mixture of Direct and Raman relaxation occuring at 4.2 $^{\circ}$K, and the angular dependence of the Direct process may account for the dependence of the power of concentration dependence.

APPENDIX 1

Reprint of Paper Published in

British Journal of Applied Physics

1965, 16, 1681-5

BRIT. J. APPL. PHYS., 1965, VOL. 16

The influence of crystalline texture on electron spin resonance linewidths in synthetic ruby

D. A. CURTIS,† C. J. KIRKBY and J. S. THORP

Department of Applied Physics, University of Durham

MS. received 30*th July* 1965

Abstract. The widths of the $-\frac{1}{2}$ to $-\frac{3}{2}$ and $-\frac{1}{2}$ to $+\frac{3}{2}$ transitions in synthetic vapour phase ruby have been measured as a function of polar angle θ for specimens showing different degrees of mosaic imperfection. Anisotropic line broadening was observed with maxima near $\theta = 45°$. The magnitude of the broadening was proportional to the mean mosaic misorientation giving an increase in total linewidth of up to two times for misorientations of less than 1°.

1. Introduction

Synthetic laser and maser materials, while being in substantially single-crystal form, often show textural imperfections and mosaic structure to an extent dependent on their growth history. In all of these materials the presence of mosaic structure may lead to anisotropic broadening of electron spin resonance transitions. In maser amplifiers both the signal bandwidth and the pumping efficiency are influenced by linewidths, and the object of the present work was to establish the magnitude of the anisotropic broadening in ruby. This paper gives results for some selected crystals which were chosen on the basis of an extensive x-ray survey as representing high and low degrees of mosaic imperfection occurring in crystals grown by the same method (Thorp, Curtis and Mason 1964, Curtis and Thorp 1965).

2. Experimental work

Synthetic rubies grown by flame fusion from the vapour phase were used (Jack and Stephenson, unpublished) because of their chemical purity (Thorp *et al.* 1961). The textures of the specimens were examined using the Laue back reflection x-ray technique. By obtaining comparative data at different positions on a specimen and by making detailed observations of the subdivision of the diffraction spots, estimates of both the c axis misorientation and the mean mosaic misorientation were made. The resonance measurements consisted of measuring the widths of the transitions as a function of the polar angle θ between the direction of the crystallographic c axis and the d.c. magnetic field. These were made with a 35 Gc/s spectrometer, using a reflection technique, microwave bridge and phase-sensitive detector. Several precautions were taken to ensure that true line shapes were recorded. The magnetic field, measured by proton resonance, was homogeneous over the specimen to 1 part in 5000. The detector crystals were operated in the square law region and the monitor signal power level was reduced to about 100 μW to avoid saturation effects. The amplitude of the high frequency modulation field was sufficiently small compared with the linewidth to enable modulation distortion to be ignored (Smith 1964) and the d.c. magnetic field was swept slowly through the resonance value to avoid distortion due to the bandwidth of the recorder. Finally the filling factor η and temperature T were chosen so that the admixture of χ' (the real part of the susceptibility) into χ'' (the imaginary part) was reduced to negligible proportions.

A detailed analysis (Curtis 1964 Ph.D. Thesis, University of Durham) revealed that several conditions had to be satisfied to ensure that the admixture of χ' into χ'' was negligible. Of these the most important as regards spectrometer design was that $Q_L \ll Q_M$ where Q_L

† Now at Kamerlingh Onnes Laboratorium, Leiden, Holland.

is the loaded Q-factor of the cavity away from magnetic resonance and Q_M is the magnetic Q-factor, which depends on both η and T. The specimen dimensions were chosen as 10 mm × 7 mm × 3·5 mm so as to have crystals reasonably representative of those used in masers and a value of $\eta \simeq 0{\cdot}01$ was achieved by using a cavity formed from a 100 cm length of waveguide terminated at one end by an iris and at the other by a short-circuit. The measurements were made at 77°K. The recorded derivatives of the absorption lines obtained from the phase sensitive detector and recorder gave directly the linewidth ΔH_{ms} between the points of maximum slope. The widths at half-height $\Delta H_{1/2}$ were obtained by numerical integration of the derivative recordings. The overall accuracy was ± 10%.

3. Results

Some details of the textures of the two specimens selected for detailed study are given in table 1.

Table 1. Texture of ruby specimens

	Specimen A	Specimen B
Mosaic misorientation	0° 30′	0° 5′
Total variation in c axis direction over specimen	0° 40′	0° 45′
Dislocation density	$2{\cdot}6 \times 10^5$ cm^{-2}	$2{\cdot}5 \times 10^5$ cm^{-2}
Chromium concentration	0·026	0·052

Crystals with nearly identical values of overall c axis wander were used as we wished to study only the effects of mosaic misorientation. The values of misorientation given represent the mean of eight separate x-ray exposures taken at different points of the (0001) and (000$\bar{1}$) faces of each specimen. The dislocation densities quoted represent the average values over the specimens and were obtained from etch pit counts assuming a one-to-one correspondence between etch pits and dislocations (Thorp, Curtis and Mason 1964). The one-to-one correspondence was supported by estimates of the dislocation density derived from the x-ray photographs. Scheuplein and Gibbs' (1960) experiments on lattice strain also support the assumption. The chromium concentrations, given as atomic percentages, were obtained by optical spectrographic analysis.

The values of $\Delta H_{1/2}$ for the $-\frac{3}{2}$ to $-\frac{1}{2}$ transition were measured as a function of polar angle for both specimens. Other transitions measured were the $+\frac{1}{2}$ to $+\frac{3}{2}$ for specimen B over the range $\theta = 30°$ to $\theta = 90°$, the $-\frac{1}{2}$ to $+\frac{1}{2}$ transitions for both specimens at $\theta = 0°$ and $\theta = 55°$ and the $-\frac{1}{2}$ to $+\frac{3}{2}$ transitions for both A and B between $\theta = 15°$ and $\theta = 90°$. The results, some of which are given in figure 1 showed that pronounced anisotropic broadening was obtained with the less perfect crystal, specimen A. In an ancillary

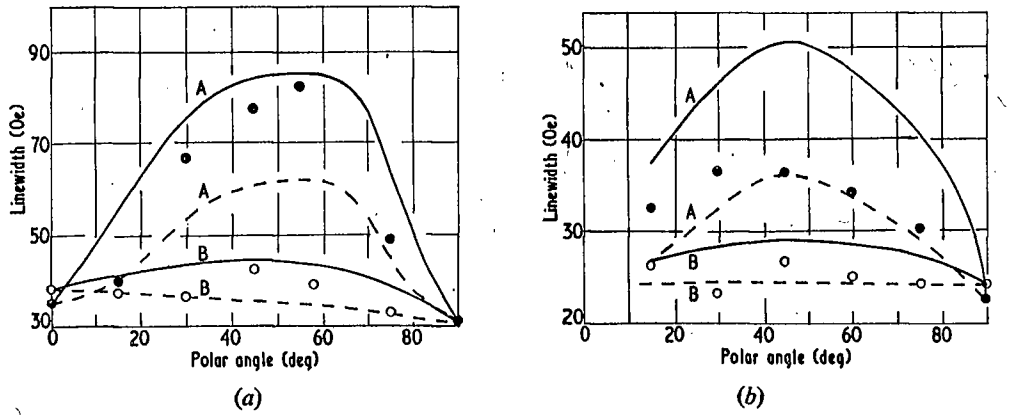

Figure 1. Variation of linewidth with polar angle. Full line, Lorentzian; broken line, Gaussian prediction; closed circle, specimen A; open circle, specimen B. (*a*) Curve for $-\frac{1}{2}$ to $-\frac{3}{2}$ transition. (*b*) Curve for $-\frac{1}{2}$ to $+\frac{3}{2}$ transition.

experiment the field values for resonance were noted as a function of polar angle for each transition and from these results the corresponding values of $dH/d\theta$ were derived; these are given in table 2.

Table 2

Polar angle (deg.)	$dH/d\theta \times 10^{-3}$ (Oe rad^{-1})		
	$-\frac{3}{2}$ to $-\frac{1}{2}$	$+\frac{1}{2}$ to $+\frac{3}{2}$	$-\frac{1}{2}$ to $+\frac{3}{2}$
0	0	0	0
15	2·4		−1·8
30	5·0	−5·9	−2·8
45	6·1	−6·2	−3·4
55	6·3	−4·8	
60	6·3	−4·4	−3·0
75	3·8	−2·1	−2·2
90	0	0	0

The value of $dH/d\theta$ for the $-\frac{1}{2}$ to $+\frac{1}{2}$ transition is generally an order of magnitude smaller than for either of the other first-order transitions, e.g. about $-$ 0·87 Oe rad^{-1} at $\theta = 55°$.

4. Discussion

The magnitude of the broadening ΔH due to angular misorientations in the lattice can be estimated from the expression

$$\Delta H = \frac{dH}{d\theta}\Delta\theta. \tag{1}$$

Here $dH/d\theta$ is the rate of change with polar angle of the resonance value of magnetic field for the transition under investigation and the parameter $\Delta\theta$ represents the distribution of c axis directions produced by imperfections in the crystal. Shaltiel and Low (1961) showed that for a cubic crystal the correct value for $\Delta\theta$ was a parameter α_0 characterizing a Gaussian distribution of crystallites about a rotation axis. This distribution was assumed to cut off at a value corresponding to the maximum misorientation present in the crystal. It was also assumed that the rotation axes were isotropically distributed and that the transition proba-

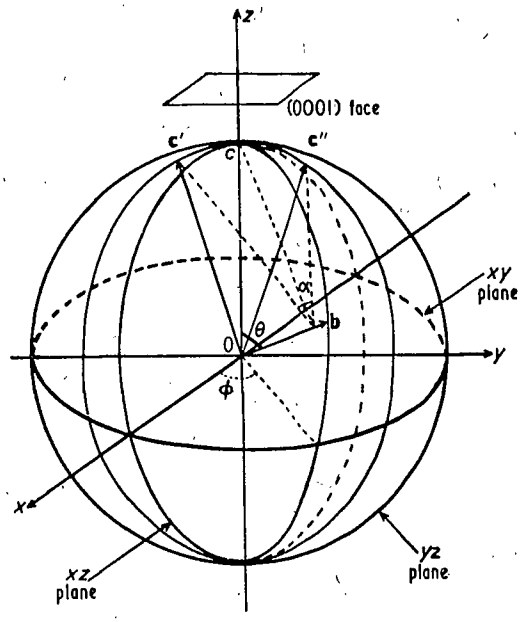

Figure 2. Distribution of orientations in ruby.

bility did not vary with polar angle sufficiently rapidly to affect the linewidth. Agreement with experiment was obtained for gadolinium in thorium oxide, a cubic material.

The situation in ruby, which is trigonal, is shown in figure 2. Here the mean c axis direction is taken as the z axis of the spherical coordinates. The basal slip dislocations form a set of rotation axes and one of these is represented by **b**. The possible directions of **b** are limited to regions within $70° \leqslant \theta \leqslant 80°$ and to $(\phi \pm 5°)$, $\{120° + (\phi \pm 5°)\}$ and $\{240° + (\phi \pm 5°)\}$ (Scheuplein and Gibbs 1960). The mosaic blocks may be rotated about **b** by any angle up to a maximum α, so that the c axis can take up any direction in the region limited by $\mathbf{c}'$ and $\mathbf{c}''$. The distribution of c axes when viewed along the z axis is shown in figure 3. The prismatic slip dislocations are distributed in a cone about the mean c axis

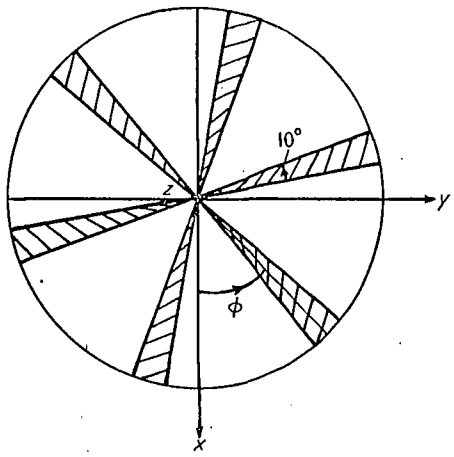

Fig. 3. The distribution of c axis directions viewed along the z axis.

direction but since this results only in an alteration in ϕ, the spectrum, and hence the linewidth, is not affected. The x-ray studies were made on the (0001) faces and thus showed the distribution produced by the rotation described above. The transition probabilities for the various transitions were calculated as a function of polar angle, using the method due to Schulz du Bois (1959), to check that no significant linewidth distortion was introduced. It was shown that at any polar angle the rates of change of transition probability with angle were so small that changes in the probability over 5 degrees (much larger than any misorientation observed) were negligible for each transition.

There is some difficulty in deriving the broadenings from the measured linewidths. In the particular instances of Gaussian or Lorentzian line shapes we may write, following Hughes and MacDonald (1961).

$$H^2 = H_0^2 + \Delta H^2 \tag{2}$$

and

$$H = H_0 + \Delta H \tag{3}$$

respectively, where H is the observed linewidth, H_0 the basic linewidth and ΔH the broadening. Here however the observed line shapes were neither Gaussian nor Lorentzian as was demonstrated by the evaluation of the parameter R (defined as the ratio of the observed linewidth to the width between points of maximum slope on the derivative trace) which lay between the values $R = 1{\cdot}175$ and $R = 1{\cdot}734$ for Gaussian and Lorentzian shapes respectively. The basic linewidths were measured where possible at $\theta = 0°$ and $\theta \doteq 90°$, where $dH/d\theta = 0$, and the values at intermediate polar angles obtained by linear interpolation; elsewhere the value for $\theta = 90°$ was used at all polar angles. As table 1 shows, the major difference between the samples was the degree of mosaic misorientation and this corresponds to the greater broadening observed for specimen A in figure 1. Substituting for $\Delta\theta$ the values of mosaic misorientation obtained from the x-ray data and using equations

(1), (2) and (3) the predicted linewidth variations for Gaussian and Lorentzian line shapes were derived. These are shown in figure 1 and the experimental points lie between them.

5. Conclusions

In vapour phase synthetic ruby the presence of mosaic imperfections, which frequently occur with angular misorientations of up to about 1° 30′, leads to anisotropic broadening of all transitions. The maximum broadening appears when $dH/d\theta$, the rate of change with polar angle of the magnetic field required for resonance, is a maximum. This occurs when θ lies between 45° and 55° and under these conditions the linewidths of the $\pm\frac{1}{2}$ to $\pm\frac{3}{2}$ transitions may be increased by up to two times above their values at $\theta = 0°$ or $\theta = 90°$. The $-\frac{1}{2}$ to $\frac{1}{2}$ transition shows a very small broadening near $\theta = 45°$ because of the smaller value of $dH/d\theta$. The results also suggest that, in nearly perfect crystals, the linewidths are more sensitive indicators of misorientation than simple x-ray techniques.

Acknowledgments

We wish to acknowledge the co-operation received from The Thermal Syndicate Ltd., who supplied the crystals on which measurements were made.

Two of us (D.A.C. and C.J.K.) wish to thank the Science Research Council for the award of maintenance grants.

References

Curtis, D. A., and Thorp, J. S., 1965, *Brit. J. Appl. Phys.*, **16**, 734–6.
Hughes, D. G., and MacDonald, D. K. C., 1961, *Proc. Phys. Soc.*, **78**, 75–80.
Scheuplein, R., and Gibbs, R., 1960, *J. Amer. Ceram. Soc.*, **43**, 458–72.
Schulz du Bois, E. O., 1959, *Bull. Syst. Tech. J.*, **38**, 271–90.
Shaltiel, D., and Low, W., 1961, *Phys. Rev.*, **124**, 1062–7.
Smith, G. W., 1964, *J. Appl. Phys.*, **35**, 1217–21.
Thorp, J. S., Sampson, D. F., and Pace, J. H., 1961, *Brit. J. Appl. Phys.*, **12**, 705–7.
Thorp, J. S., Curtis, D. A., and Mason, D. R., 1964, *Brit. J. Appl. Phys.*, **15**, 775–6.

APPENDIX 2

ANGULAR DEPENDENT LINE BROADENING TERMS

In calculation of the matrix elements of the type $\langle a|S_i S_j|a\rangle$ appearing in Eq. 5.9 allowance must be made for the mixing of states occuring at non-zero polar angles. In a system with effective spin of 3/2 the state $|a\rangle$ is represented by an expression having the form of Eq. 1.2. On expansion it is found that three of the matrix elements reduce to simple functions of eigenvectors while the rest become zero. The non-zero terms are:

$$\langle i|S_x^2|i\rangle = \left[3(a_i^2 + d_i^2) + 7(b_i^2 + c_i^2) + 4\,3(a_i c_i + b_i d_i)\right]\hbar^2/4$$

$$\langle i|S_z^2|i\rangle = \left[9(a_i^2 + d_i^2) + (b_i^2 + c_i^2)\right]\hbar^2/4$$

$$\langle i|S_x S_z + S_z S_x|i\rangle = 8\sqrt{3}(a_i b_i - c_i d_i)\hbar^2/4$$

In the tables which follow, these three terms, together with the corresponding values of $dH/d\theta$, are given for the three $\Delta M = 1$ transitions in ruby at 5° intervals of polar angle. In these tables S_x^2 represents $\{\langle a|S_x^2|a\rangle - \langle b|S_x^2|b\rangle\}^2$ etc. The eigenvalues used for these calculations were calculated separately, and are listed in Appendix 3. Values of $dH/d\theta$ are given in oersted/degree; all other quantities are in units of $\hbar^2$.

+3/2 to +1/2 Transition

	dH/dθ	S_x^2	S_z^2	S_{xz}
0	0.00	4.00	16.00	0.00
5	18.80	3.00	14.42	1.48
10	30.02	2.04	12.48	5.62
15	54.13	0.75	10.36	16.82
20	69.58	0.53	7.72	20.05
25	82.92	0.08	5.23	29.61
30	93.75	0.06	2.82	34.65
35	101.72	0.71	1.16	36.80
40	106.61	2.02	0.24	36.00
45	108.25	3.75	0.00	32.95
50	106.61	5.83	0.24	28.10
55	101.72	7.92	0.77	22.65
60	93.75	9.90	1.43	17.08
65	82.92	11.58	2.08	12.00
70	69.58	13.06	2.64	7.68
75	54.13	14.15	3.10	4.31
80	37.02	14.49	3.64	1.67
85	18.80	15.38	3.61	0.47
90	0.00	15.52	3.66	0.00

+1/2 to -1/2 Transition

	dH/dθ	S_x^2	S_z^2	S_{xz}
0	0.00	0.00	0.00	0.00
5	10.00	0.00	0.00	0.14
10	11.00	0.02	0.02	0.46
15	15.00	0.09	0.08	0.76
20	16.00	0.23	0.20	0.86
25	6.70	0.44	0.35	0.73
30	5.00	0.68	0.52	0.44
35	4.00	0.90	0.64	0.15
40	1.00	1.04	0.68	0.00
45	7.00	1.09	0.63	0.08
50	11.00	1.02	0.51	0.39
55	18.00	0.86	0.34	0.83
60	23.00	0.63	0.17	1.26
65	22.00	0.40	0.04	1.52
70	20.05	0.21	0.00	1.49
75	19.00	0.08	0.04	1.15
80	17.00	0.02	0.13	0.67
85	11.60	0.00	0.22	0.18
90	0.00	0.00	0.26	0.00

-1/2 to -3/2 Transition

	$dH/d\theta$	S_x^2	S_z^2	S_{xz}
0	0.00	4.00	16.00	0.00
5	18.80	3.94	15.82	0.49
10	30.02	3.73	15.33	1.97
15	54.13	3.38	14.50	4.46
20	69.58	2.89	13.31	8.00
25	82.92	2.26	11.78	12.46
30	93.75	1.54	9.92	17.68
35	101.72	0.83	7.86	23.14
40	106.61	0.25	5.71	28.87
45	108.25	0.00	3.66	33.24
50	106.61	0.26	1.91	36.10
55	101.72	1.17	0.67	36.57
60	93.75	2.84	0.06	34.28
65	82.92	1.08	0.09	29.63
70	69.58	7.97	0.73	22.25
75	54.13	10.85	1.78	14.28
80	30.02	13.41	2.76	6.98
85	18.80	15.14	3.54	1.85
90	0.00	15.75	3.84	0.00

APPENDIX 3

EIGENVECTORS FOR RUBY AT Q-BAND

Equation 1.2 represents the mixing of states in a system of spin S = 3/2 at non-zero polar angles. To calculate the eigenvectors, a_i etc., for ruby at Q-band, the matrix of the spin-Hamiltonian was first set up as a function of the polar angles and magnetic fields appropriate to the three transitions. Calculation of the eigenvectors from this data was carried out using the Elliott 803 computer with programme LM22 of the Elliott library. The programme calculates eigenvalues and eigenvectors, the former by solving the matrix as a quartic equation, and the latter by substituting the roots so obtained back into the matrix in turn and evaluating the cofactors of the elements in the upper line. The calculations were carried out for the three $\Delta M = 1$ transitions at 10° intervals of polar angle. The results are presented in blocks, arranged in order of polar angle with magnetic fields indicated. The format of the blocks is indicated below, where the notation for levels is consistent with that used elsewhere.

	θ	H, k.oe		
+3/2	a_1	b_1	c_1	d_1
+1/2	a_2	b_2	c_2	d_2
-1/2	a_3	b_3	c_3	d_3
-3/2	a_4	b_4	c_4	d_4

10 8.50

.9605	.2764	.0316	.0016
-.2777	.9455	.1705	.0105
.0173	-.1727	.9767	.1011
-.0004	.0071	-.1014	.9948

10 12.70

.9759	.2173	.0226	.0014
-.2197	.9607	.1716	.0113
.0156	-.1726	.9783	.1133
-.0004	.0086	-.1136	.9935

20 8.95

.8790	.4654	.1030	.0102
-.4720	.8191	.3234	-.0415
.0669	-.3342	.9181	.2024
-.0030	.0295	-.2047	.9784

20 12.85

.9131	.3991	.0824	.0083
-.4030	.8534	.3275	.0442
.0613	-.3333	.9138	.2237
-.0035	.0344	-.2255	.9736

30 9.65

.7933	.5790	.1861	.0276
-.5918	.6612	.4517	.0924
.1425	-.4719	.8157	.3027
-.0110	.0694	-.3099	.9482

30 12.30

.8292	.5341	.1642	.0247
-.5431	.6981	.4564	.0967
.1332	-.4704	.8087	.3270
-.0122	.0779	-.3327	.9379

30 14.75

.8404	.5183	.1567	.0237
-.5260	.7099	.4579	.0983
.1301	-.4699	.8056	.3366
-.0128	.0813	-.3417	.9362

40 10.60

.7116	.6463	.2703	.0536
-.6616	.4859	.5479	.1612
.2348	-.5740	.6749	.3998
-.0282	.1293	-.4138	.9007

40 12.97

.7366	.6243	.2551	.0512
-.6371	.5130	.5509	.1656
.2250	-.5726	.6671	.4201
-.0301	.1388	-.4317	.8908

40 13.50

.7408	.6204	.2524	.0508
-.6327	.5176	.5515	.1664
.2234	-.5723	.6656	.4237
-.0304	.1405	-.4349	.8889

50 11.70

.6318	.6843	.3532	.0885
-.6967	.2998	.6045	.2438
.3345	-.6307	.5010	.4892
-.0597	.2100	-.5088	.8327

50 12.43

.6387	.6799	.3492	.0879
-.6921	.3077	.6051	.2455
.3307	-.6302	.4977	.4957
-.0606	.2139	-.5141	.8284

50 12.90

.6428	.6775	.3468	.0975
-.6893	.3123	.6054	.2464
.3285	-.6299	.4957	.4996
-.0611	.2161	-.5172	.8258

60 11.55

.5418	.7043	.4390	.1330
-.7077	.0975	.6166	.3308
.4403	-.6358	.3089	.5536
-.1085	.3004	-.5758	.7526

60 12.72

.5513	.7002	.4338	.1326
-.7044	.1092	.6168	.3340
.4333	-.6351	.3021	.5625
-.1103	.3073	-.5831	.7439

60 12.78

.5518	.7000	.4336	.1326
-.7042	.1097	.6168	.3341
.4330	-.6351	.3018	.5639
-.1104	.3076	-.5835	.7435

70 10.90

.4536	.7014	.5180	.1845
-.6873	-.0983	.5863	.4173
.5376	-.5836	.1059	.5993
-.1810	.3974	-.6137	.6578

70 12.50

.4649	.6978	.5124	.1855
-.6874	-.0837	.5848	.4225
.5273	-.5834	.0951	.6104
-.1828	.4071	-.6216	.6438

70 13.65

.4715	.6956	.5091	.1859
-.6870	-.0756	.5840	.4256
.5219	-.5831	.0887	.6165
-.1837	.4127	-.6259	.6357

80 10.53

.3751	.6778	.5844	.2417
-.6407	-.2691	.5163	.5005
.6072	-.4714	-.1040	.6311
.2831	-.4960	.6193	-.5411

80 12.31

.3847	.6748	.5800	.2452
-.6446	-.2565	.5116	.5069
.5978	-.4734	-.1149	.6366
.2812	-.5047	.6234	-.5269

80 14.35

.3932	.6722	.5761	.2482
-.6474	-.2458	.5079	.5124
.5901	-.4752	-.1242	.6407
.2795	-.5117	.6282	-.5151

90 10.40

.3048	.6380	.6380	.3048
-.5764	-.4096	.4096	.5764
.6380	-.3048	-.3048	.6380
.4096	-.5764	.5764	-.4096

90 12.21

.3113	.6348	.6348	.3115
-.5825	-.4009	.4009	.5825
.6348	-.3115	-.3115	.6348
.4009	-.5825	.5825	-.4009

90 14.60

.3179	.6316	.6316	.3179
-.5879	-.3928	.3928	.5879
.6316	-.3179	-.3179	.6316
.3928	-.5879	.5879	-.3928

REFERENCES

Abragam, A. and Pryce, M.H.L. 1951. Proc. Roy. Soc. A205, 135-53

Adam, G.D., Standley, K.J. and Storey, B.E. 1963. B.J.A.P. 14, 606

Adams, I., Neilsen, J.W. and Storey, M.S. 1966. J. App. Phys. 37, 832-6

Al'tshuler, S.A. and Mineeva, R.M. 1963. Sov. Phys. Solid State 5, 1234-5

Anderson, P.W. 1959. Phys. Rev. 115, 2-13

Anderson, P.W. and Weiss, P.R. 1953. Rev. Mod. Phys. 25, 269-76

Andrew, E.R. 1958. Nuclear Magnetic Resonance (Cambridge, C.U.P.)

Andrew, E.R. and Finch, N.D. 1957. Proc. Phys. Soc. B70, 980-90

Antipin, A.A., Kamishev, A.N., Kurkin, I.N. and Shekun, L.Ya. 1967. Fiz. Tver. Tel. 9, 813-20

Arndt, R. 1965. J. App. Phys. 36, 2522-4

Artman, J.O. and Murphy, J.C. 1963. J. Chem. Phys. 38, 1544-7

Artman, J.C. and Murphy, J.C. 1964. Phys. Rev. 135, A1622-39

Barrett, C.S. 1952. Structure of Metals (New York, McGraw-Hill)

Basov, N.G. and Prokhorov, A.M. 1955. J.E.T.P. 1, 184-5

Bleaney, B. 1951. Phil. Mag. (7) 42, 441-58

Bleaney, B. and Stevens, K.W.H. 1953. Rep. Prog. Phys. 16, 108-59

Bloch, F. 1946. Phys. Rev. 70, 460-73

[illegible] 1946.

Bloch, F., Hansen, W.W. and Packard, M. 1946.

Phys. Rev. 70, 474-85

Bloembergen, N. 1956. Phys. Rev. 104, 324-7

Bloembergen, N. 1961. Science 133, 1363-4

Bloembergen, N., Purcell, E.M. and Pound, R.V. 1946.

Phys. Rev. 73, 679-712

Bloembergen, N. and Wang, S. 1954. Phys. Rev. 93, 72-83

Bond, H.E. and Harvey, K.B. 1963. J. App. Phys. 34, 440-1

Brown, G. 1967. Ph.D. Thesis, University of Durham

Brown, G., Mason, W.R. and Thorp, J.S. 1965.

J. Sci. Inst. 42, 648-9

Brown, G. and Thorp, J.S. 1967. B.J.A.P. 18, to be published

Buckmaster, H.A. and Dering, J.C. 1966. J. Sci. Inst. 43, 404-5

Burger, P. and Gunthart, H. 1962. Z.A.M.P. 13, 310-23

Carlson, E. and Dieke, G.H. 1958. J. Chem. Phys. 29, 229-30

Castle, J.G. Feldman, D.W., Klemens, P.G. and Weeks, R.A. 1963.

Phys. Rev. 130, 577-88

Chandrasekhar, S. 1943. Rev. Mod. Phys. 15, 1-89

Clark, A.F., Sands, R.H. and Kikuchi, C. 1964.

Bull. Am. Phys. Soc. 9, 36

Clement, J.R., Logan, J.K. and Gaffney, J. 1955.

Phys. Rev. 100, 733-44

Cullen, A.L. 1965. Electronics Letts. 1, 55-6

Curtis, D.A. 1964. Ph.D. Thesis, University of Durham

Curtis, D.A., Kirkby, C.J. and Thorp, J.S. 1965.
B.J.A.P. 16, 1681-5

Curtis, D.A. and Thorp, J.S. 1965. B.J.A.P. 16, 734-6

Czochralski, J. 1918. Z. Phys. Chem. 92, 219-21

Davis, C.F., Strandberg, M.W.P. and Kyhl, R.L. 1958.
Phys. Rev. 111, 1268-72

Dils, R.R., Martin, G.W. and Huggins, R.A. 1962.
App. Phys. Letts. 1, 75-6

Dodd, D.M., Wood, D.L. and Barns, R.L. 1963.
J. App. Phys. 35, 1183-6

Dodson, E.M. 1962. Analyt. Chem. 34, 966-71

Dolgopolov, D.G. and Zhogolov, D.A. 1966.
Sov. Phys. Sol. St. 8, 482-3

Donoho, P.L. 1964. Phys. Rev. 133, A1080-4

Duncan, R.C. 1965. J. App. Phys. 36, 874-5

Einstein, A. 1917. Phys. Z. 18, 121-8

Feher, E.R. 1964. Phys. Rev. 136, A145-57

Feher, G. 1957. Bell. Syst. Tech. J. 36, 449-84

Garrett, C.G.B. and Merritt, F.R. 1964. App. Phys. Letts. 4, 31-2

Gauss, C.F. 1873. Collected Works (Gottingen. Kon, Gesell.der Wiss.)

Gerlich, D. 1964. Phys. Letts. 12, 314-5

Glebashev, G.Ia. 1956. J.E.T.P. 3, 643-4

Goldsborough, J.P. and Mandel, M. 1960. Rev. Sci. Inst. 31, 1044-6

Goldschmidt, V.M. 1927. Chem. Berichte 60, 1263-96

Gordon, J.P., Zeiger, H.J. and Townes, C.H. 1954.
Phys. Rev. 99, 1264-74

Gorter, C.J. 1936. Physica 3, 503-14

Grant, W.J.C. 1964a. J. Phys. Chem. Solids, 25, 751-7

Grant, W.J.C. 1964b. Physica 30, 1433-45

Grant, W.J.C. and Strandberg, M.W.P. 1964a. Phys. Rev. 135, A715-26

Grant, W.J.C. and Strandberg, M.W.P. 1964b. Phys. Rev. 135, A727-39

Halbach, K. 1960. Phys. Rev. 119, 1230-3

Heitler, W. and Teller, E. 1936. Proc. Roy. Soc. A155, 629-39

Hemphill, R.B., Donoho, P.L. and McDonald, E.O. 1966.
Phys. Rev. 146, 329-35

Hempstead, C.F. and Bowers, K.D. 1960. Phys. Rev. 118, 131-4

Holden, A.N., Kittel, C., Merritt, F.R. and Yager, W.A. 1950.
Phys. Rev. 77, 147-8

Hoskins, R.H. and Soffner, B.H. 1964. Phys. Rev. 133, A490-3

Howarth, D.J. 1958. R.R.E. Journal 41, 7-35

Hughes, D. and MacDonald, D. 1961. Proc. Phys. Soc. 78, 75-80

Ishiguro, E., Kambe, K. and Usui, T. 1951. Physica 17, 310-18

Johnson, L.F. and Nassau, K. 1961. Proc. I.R.E. 49, 1704-6

Johnson, L.F. and Thomas, R.A. 1963. Phys. Rev. 131, 2038-40

Kambe, K. and Ollom, F. 1956. J. Phys. Soc. Japan 11, 50-2

Kaplan, J.I. 1966. J. Chem. Phys. 44, 4630-2

Kask, N.E., Kornienko, L.S., Mandel'shtam, T.S. and Prokhorov, A.F.
1964. Sov. Phys. Sol. St. 5, 1675-6

Kedzie, R.W. and Kestigian, M. 1963. App. Phys. Letts. 3, 86-7

Kikuchi, C., Lambe, J., Makhov, G. and Terhune, R.W. 1959.
J. App. Phys. 30, 1061-7

Kirkby, C.J. and Thorp, J.S. 1967. J. App. Phys. 38, 1985-6

Kittel, C. and Abrahams, E. 1953. Phys. Rev. 90, 238-9

Klein, M.P. and Mims, W.B. 1962. Bull. Am. Phys. Soc. 7, 625

Klemens, P.G. 1962. Phys. Rev. 125, 1795-8

de Klerk, D. 1965. The Construction of High-field Electromagnets
(Newport Pagnell, Newport Instruments)

Klyshko, D.N. 1964. Sov. Phys. Sol. St. 5, 2066-8

Knapp, W.J. 1943. J. Am. Ceram. Soc. 26, 48-55

Kochelaev, B.I. 1960. Sov. Phys. Doklady 5, 349-51

Koloskova, N.G. 1963. Sov. Phys. Sol. St. 4, 2292-6

Kopvillem, U.K. 1960. J.E.T.P. 11, 109-13

Kramers, H.A. 1930. Proc. Acad. Sci. Amsterdam 33, 959-72

Krebs, J.J. 1967. Phys. Rev. 155, 246-58

Kronberg, M.L. 1955. Science 122, 599-600

Kronig, R. de L. 1936. Physica 3, 1009-20

Kubo, R. and Tomita, K.J. 1954. J. Phys. Soc. Japan 9, 888-919

Kurkin, I.N. and Shekun, L.Ya. 1967. Fiz. Tver. Tel. 9, 444-8

Langford, J.I. and Wilson, A.J.C. 1963. Crystallography and Crystal Perfection (London, Academic Press)

Larson, G.H. and Jeffries, C.D. 1966a. Phys. Rev. 141, 461-78

Larson, G.H. and Jeffries, C.D. 1966b. Phys. Rev. 145, 311-24

Levingstein, H., Loicamo, G. and Nassau, K. 1963. J. App. Phys. 34, 3603-8

Likhachev, V.... 1961. Sov. Phys. Sol. St. 3, 1330-6

Linares, R.C. 1965. J. Phys. Chem. Sol. 26, 1817-20

Lorentz, H.A. 1915. Proc. Acad. Sci. Amsterdam 18, 134-50

Low, W. 1960. Paramagnetic Resonance in Solids (London, Academic Press)

Macomber, J.D. and Waugh, J.S. 1965. Phys. Rev. 140, A1494-7

Maiman, T. 1960. Nature 187, 493-4

Makhov, G., Kikuchi, C., Lambe, J. and Terhune, R.W. 1958. Phys. Rev. 109, 1399-1400

Manenkov, A.A. and Federov, V.B. 1960. J.E.T.P. 11, 751-4

Manenkov, A.A., Popova, A.A. and Khaimov-Mal'kov, V.Ya. 1963 Sov. Phys. Sol. St. 5, 1194-7

Mason, D.R. Ph.D. Thesis, University of Durham 1966.

Mason, D.R. and Thorp, J.S. 1966. Proc. Phys. Soc. 87, 49-53

Mattuck, R. and Strandberg, M.W.P. 1960. Phys. Rev. 119, 1204-7

Mims, W.B. 1965. Phys. Rev. 140, A531-5

Mims, W.B. and Gillen, R. 1966. Phys. Rev. 148, 438-443

Misra, H. 1963. Ind. J. Pure App. Phys. 1, 37-42

Mitchell, A.C.G. and Zemansky, M.W. 1934. Resonance Radiation and Excited Atoms (Cambridge, C.U.P.)

Montgomery, C.G. 1948. Techniques of Microwave Measurement (New York, McGraw-Hill)

Moroney, M.J. 1956. Facts from Figures (London, Penguin)

Nassau, K. and Broyer, A.M. 1962. J. App. Phys. 33, 3064-73

Nemanch, J. and Viehmann, W. 1967. Bull. Am. Phys. Soc. 12, 357

Orbach, R. 1961. Proc. Phys. Soc. 87, 821-6

Orbach, R. 1961. Proc. Roy. Soc. A264, 458-84

Orbach, R. and Blume, M. 1962. Phys. Rev. Letts. 8, 478-80

Pake, G.E. 1962. Paramagnetic Resonance (New York, Benjamin)

Poole, C.P. 1967. Electron Spin Resonance (New York, Interscience)

Portis, A.M. 1953. Phys. Rev. 91, 1071-8

Posener, D.W. 1959. Austral. J. Phys. 12, 184-96

Pryce, M.H.L. and Stevens, K.W.H. 1950. Proc. Phys. Soc. A63, 36-51

Ranon, U. 1964. Phys. Letts. 8, 154-5

Ranon, U. and Volterra, V. 1964. Phys. Rev. 134, A1483-5

Royce, E.B. and Bloembergen, N. 1963. Phys. Rev. 131, 1912-23

Schawlow, A.L. and Townes, C.H. 1958. Phys. Rev. 112, 1940-9

Scheuplein, R. and Gibbs, P. 1960. J. Am. Ceram. Soc. 43, 458-72

Schiff, L.I. 1955. Quantum Mechanics (New York, McGraw-Hill)

Schulz-du Bois, E.O. 1959. Bell System. Tech. J. 38, 271-96

Scott, P.L. and Jeffries, C.D. 1962. Phys. Rev. 127, 32-51

Scovil, H.E.D., Feher, G. and Seidel, H. 1957.

Phys. Rev. 105, 762-3

Shaltiel, D. and Low, W. 1961. Phys. Rev. 124, 1062-7

Sharma, S.S. 1951. Proc. Indian Acad. Sci. 33A, 245-9

Siegman, A.E. 1964. Microwave Solid State Masers (New York, McGraw-Hill)

Sil'nichenko, V.G. and Gritsenko, M.M.

Sov. Phys. Crystallography 9, 647-8

Smith, G.W. 1964. J. App. Phys. 35, 1217-21

Statz, H., Rimai, L., Weber, M.J.,de Mars, G.A. and Koster, G.F. 1961.

J. App. Phys. (Suppl.) 32, 218s-20s

Stephens, D.L. and Alford, W.J. 1964. J. Am. Ceram. Soc. 47, 81-6

Stettler, J. and Veigele, W. 1964. J. Chem. Phys. 41, 2341-6

Stoneham, A.M. 1966. Proc. Phys. Soc. 89, 909-21

Strum, P.D. Proc. I.R.E. 41, 875-89

Sturge, M.D. 1965. Chem. Phys. 43, 1826-7

Sugano, S. and Tanabe, Y. 1958. J. Phys. Soc. Japan 13, 880-99

Thilo, E., Jander, J. and Seeman, H. 1955.

Z. Anorg. u. Allgem. Chem. 279, 2-17

Thorp, J.S. 1965. Joblinglass 1, 5-7

Thorp, J.S., Curtis, D.A. and Mason, D.R. 1964. B.J.A.P. 15, 775-6

Topping, J. 1957. Errors of Observation and their Treatment (London, Chapman and Hall)

Van Bueren, H.G. 1960. Imperfections in Crystals (Amsterdam, North-Holland)

Van Vleck, J.H. 1940. Phys. Rev. 57, 426-47

Van Vleck, J.H. 1948. Phys. Rev. 74, 1168-83

Verneuil, A. 1904. Annal. Chim. Phys. 3, 20-48

Voigt, W. 1912. S. B. Bayer Akad. Wiss. 1912, 603-20

Wahlquist, H. 1961. J. Chem. Phys. 35, 1708-10

Waller, I. 1932. Z. Phys. 79, 370-88

Weber, J. 1953. Trans. I.R.E. ED-3, 1-4

Wenzel, R.F. and Kim, Y.W. 1965. Phys. Rev. 140, A1592-8

Wilson, A.J.C. 1962. Norelco Reporter 9, 55-8

Wyckoff, R.W.G. 1964. Crystal Structures (New York, Interscience)

Zaitov, M.M. and Shekun, L.Ya. 1966. J.E.T.P. Letts. 4, 228-30

Zalkin, A. and Templeton, D.H. 1964. J. Chem. Phys. 40, 501-4

Dirac, P.A.M., 1947. Quantum Mechanics, (Oxford, O.U.P.)

Mason, D.R. and Thorp, J.S. 1967. Phys. Rev. 157, 191-5

Volterra, V., Bronstein, J. and Rockni, N. 1966. App. Phys. Letts. 8, 212-3

DURHAM UNIVERSITY SCIENCE